AD-A148 253 IMPACT OF AIRCRAFT EMISSIONS ON AIR QUALITY IN THE VICINITY OF AIRPORTS V..(U) ARGONNE NATIONAL LAB IL ENERGY AND ENVIRONMENTAL SYSTEMS DIV.. K I BRUBAKER ET AL. APR 84 FAA/EE-84-14 F/G 13/2 NL

1/2

UNCLASSIFIED

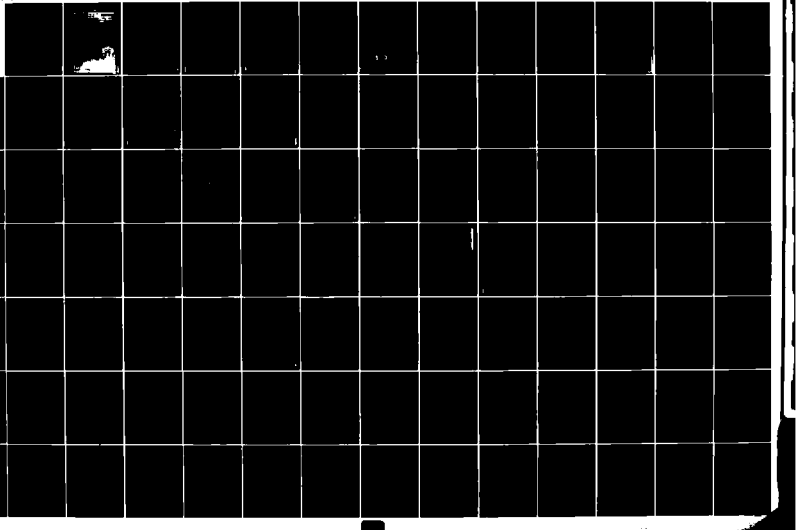

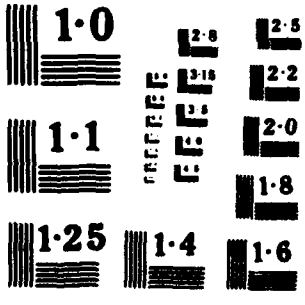
1·0
1·1
1·25
1·4
2·8
3·15
2·5
2·2
2·0
1·8
1·6

AD-A148 253

U.S. Department of Transportation
Federal Aviation Administration

Impact of Aircraft Emissions on Air Quality in the Vicinity of Airports
Volume IV: Nitrogen Oxides and Hydrocarbons

Office of Environment and Energy
Washington, D.C. 20591

United States Air Force
Engineering Services Laboratory
Tyndall Air Force Base, Florida 32403

DTIC FILE COPY

DTIC
SELECTE

Technical Report Documentation Page

1. Report No.	2. Government Accession No.	3. Recipient's Catalog No.
FAA-EE-84-14 ESL-TR-84-36	AD-A148253	

4. Title and Subtitle

Impact of Aircraft Emissions on Air Quality in the Vicinity of Airports
Volume IV: Nitrogen Dioxide and Hydrocarbons

5. Report Date
April 1984

6. Performing Organization Code

7. Author(s) Kenneth L. Brubaker, Mehul Dave, Ronald J. Wingender, Richard D. Flotard

8. Performing Organization Report No.

9. Performing Organization Name and Address
Argonne National Laboratory
Energy and Environmental Systems Division
9700 S. Cass Avenue
Argonne, Illinois 60439

10. Work Unit No. (TRAIS)

11. Contract or Grant No.
DTFA01-83-Y-10556

12. Sponsoring Agency Name and Address
U. S. Department of Transportation
Federal Aviation Administration
Office of Environment and Energy
Washington, D.C. 20591

13. Type of Report and Period Covered
Final Report
July 1980 - April 1984

14. Sponsoring Agency Code

15. Supplementary Notes This work was also supported by:
U.S. Air Force
Engineering Services Laboratory
Tyndall Air Force Base, Florida 32403

16. Abstract

This report documents the results of three related studies conducted to assess the impact of aircraft emissions of nitrogen oxides (NO_x) and hydrocarbons (Hc) on air quality. The first study consisted of a field program carried out at O'Hare International Airport and an associated model development program, the purposes of which were to assess the effect of aircraft NO_x emissions on ambient 1-hour concentrations of nitrogen dioxide (NO_2) and to provide a dispersion model suitable for the prediction of such concentrations. The second study involved the collection and laboratory analysis of samples of hydrocarbons in ambient air contaminated by jet aircraft exhaust, together with a determination of the type and relative amounts of the various hydrocarbons detected. The third study consisted of an analysis, based on available data in the literature, of the potential role of aircraft hydrocarbon emissions in the production of photochemical smog.

The results of the O'Hare field monitoring program indicate that NO_2 concentrations in aircraft plumes depend on the emission rates of both nitric oxide (NO) and NO_2 from jet engines and on the concentration of ozone (O_3) in the ambient air. The ratio of NO_2 to NO_x in jet engine emissions was estimated to be 7±2% based on field data. The ambient ozone concentration is the most important factor for plume travel times in excess of one minute, with the NO_2 emission rate most important for travel times less than one minute. The maximum plume NO_2 concentrations observed were on the order of 0.12 ppm. The maximum observed contribution of aircraft emissions to a 1-hour NO_2 concentration was 0.013 ppm. The results indicate that a photostationary state involving NO, NO_2, and O_3 exists in aircraft plumes. The 1-hour NO_2 model performed satisfactorily, although the need for a better understanding of plume rise and the rate of growth of jet aircraft takeoff plumes was clearly seen.

The hydrocarbon sampling results identified unburned fuel as the primary organic constituent of exhaust from taxiing and queuing aircraft. A detailed chemical characterization of the hydrocarbons in ambient samples as well as in a sample of jet fuel is given.

The available literature dealing with the issue of aircraft contributions to photochemical smog has been reviewed and is discussed. At present, the available information is insufficient to evaluate the effect quantitatively. The requirements for further work that would enable a quantitative evaluation to be made are discussed.

17. Key Words	18. Distribution Statement
Aircraft Emissions Dispersion Modeling Nitrogen Oxides Air Quality Impact of Aviation	This document is available to the public through the National Technical Information Service, Springfield, VA 22161

19. Security Classif. (of this report)	20. Security Classif. (of this page)	21. No. of Pages	22. Price
Unclassified	Unclassified	151	

Form DOT F 1700.7 (8-72) Reproduction of completed page authorized

ARGONNE NATIONAL LABORATORY
9700 S. Cass Avenue
Argonne, Illinois 60439

IMPACT OF AIRCRAFT EMISSIONS ON AIR QUALITY IN THE VICINITY OF AIRPORTS

VOLUME IV
NITROGEN DIOXIDE AND HYDROCARBONS

FINAL REPORT

by

Kenneth L. Brubaker, Mehul Davé, Ronald J. Wingender,
and Richard D. Flotard
Energy and Environmental Systems Division

April 1984

prepared for

U.S. Department of Transportation
Federal Aviation Administration
Office of Environment and Energy
under Interagency Agreement DTFA01-83-Y-10056

CONTENTS

TABLES

FIGURES

PREFACE

This report constitutes Volume IV in the series of reports entitled Impact of Aircraft Emissions on Air Quality in the Vicinity of Airports. Volumes III and IV in this series summarize work performed under Interagency Agreement DTFA01-83-Y-10556, between the U.S. Department of Energy/Argonne National Laboratory and the U.S. Department of Transportation/Federal Aviation Administration. This project was partially funded by the USAF, Headquarters Air Force Engineering and Services Center, Tyndall AFB, Fla. 32403 through a 1981 Memorandum of Understanding between the USAF and FAA. The project officer was Mr. Howard M. Segal, Office of Environment and Energy, FAA.

The two companion volumes are entitled:

Vol. III - Air Quality and Emission Modeling Needs

Vol. IV - Nitrogen Dioxide and Hydrocarbons

1 INTRODUCTION

For several years, the effects of aircraft on air quality have been the subject of a variety of research programs involving both field-measurement programs and computer model development, validation, and assessment work. Historically, the principal effort has gone into studies involving pollutants that are relatively inert and that may be easily measured in the field. Thus, field programs focused on pollutants such as carbon monoxide (CO), oxides of nitrogen [NO_x; by convention, the NO_x concentration is defined as the sum of the concentrations of nitrogen dioxide (NO_2) and nitric oxide (NO)], and total hydrocarbon (THC) and/or non-methane hydrocarbon (NMHC). For a historical survey of airport air-quality studies through July, 1980 and references to earlier work, see Yamartino et al., (1980a) or Segal (1981). In addition, an international conference on air quality and aviation was held in 1978. The proceedings of this conference (Sundararaman, 1978) contain many interesting papers and may be regarded as a review of the state of the art at that time. In these studies, measurements were occasionally made of both NO_x and NO, although the measurements were often made in such a way that estimation of the corresponding NO_2 concentration by difference was a rather uncertain procedure. Essentially no detailed information was obtained from these programs on the chemical composition of the hydrocarbons emitted by aircraft.

Modeling studies also reflected the emphasis on relatively inert pollutants. The bulk of the studies involved the development, refinement, validation, and utilization of models such as the Airport Vicinity Air Pollution (AVAP) model (Wang et al., 1974, 1975 and Yamartino et al., 1980a and b). To our knowledge, only one study has focused on the chemically reactive nature of the NO_x and hydrocarbon emissions (Duewer and Walton, 1978). The applicability of the AVAP model and others that, like AVAP, are based upon Gaussian plume concepts is limited to inert pollutants, or at least those that are sufficiently unreactive that they may be considered effectively inert over the relevant distances and travel times. The pollutants listed above (CO, NO_x, and THC and NMHC) fall into this category.

More recently, concern has arisen regarding the short-term effects of NO_2. The Clean Air Act amendments of 1977 required the U.S. Environmental Protection Agency (EPA) to consider a possible short-term ambient-air quality standard for NO_2. Most of the subsequent discussion has revolved about a one-hour standard ranging from 0.10 to 0.50 ppm (World Health Organization, 1977; Thuillier and Vieze, 1978). Since aircraft are known sources of NO_x, the potential effects of aircraft activity on ambient NO_2 levels over one-hour periods must be considered, and some of the factors involved are discussed by Jordan and Broderick (1978) and Bauer (1978). As indicated above, previous to this study only limited observational data existed regarding NO_2 effects specifically, and what data did exist were of limited usefulness because they were collected under conditions that were not necessarily conducive to production of high NO_2 levels and not all the relevant variables were

measured. In addition, no generally accepted mathematical model existed with which to accurately predict NO_2 effects, and, as a result, no detailed assessment that considers a variety of conditions and levels of aircraft activity could be made. Accordingly, a major component of the present program was the development of an air-quality model suitable for the prediction of NO_2 levels in the vicinity of airports and the validation of that model using data collected expressly for that purpose.

The effects of hydrocarbons in the atmosphere have been the subject of considerable interest for many years, particularly the relationship between hydrocarbons and the production of photochemical smog (Demerjian et al., 1974; USEPA, 1978a). Other effects that may relate to hydrocarbon emissions from aircraft include the production of objectionable odors and certain health effects associated with specific hydrocarbons or classes of hydrocarbon, such as the known mutagenicity of polynuclear aromatic compounds. An assessment of aircraft contributions to any of these problems must be based on knowledge of the specific chemical composition of aircraft hydrocarbon emissions, because in all cases the magnitude or even the existence of an effect depends in a sensitive way on that composition. Essentially no information on this matter was previously available, however, and the second major component of the present program was a preliminary determination of the detailed chemical composition of aircraft hydrocarbon emissions.

This report describes the results obtained in both areas of research identified above. Section 2 deals with the NO_2 field-measurement program, Section 3 with the NO_2 model development and validation program, Section 4 deals with the hydrocarbon-emission characterization program, and Section 5 summarizes what can be said at this time regarding the effects of aircraft emissions on photochemical smog formation. Appendices contain discussions of specific issues related to NO_2-NO-ozone chemistry, the averaging of wind speed and direction, and instrument response effects.

2 NITROGEN DIOXIDE FIELD-MEASUREMENT PROGRAM

As part of the effort devoted to NO_2 model development and validation, a field-measurement program was conducted at Chicago's O'Hare International Airport (ORD) by Argonne National Laboratory, Energy and Environmental Systems Division (ANL/EES). The objective of the monitoring program was to collect air quality, meteorological, and other data for the purposes of 1) assessing aircraft contributions to one-hour average NO_2 concentrations and 2) providing a data base suitable for the verification and validation of the model being concurrently developed for aircraft NO_2 effects. The purpose of this section is to provide an overall description of the field-measurement program, to describe the data processing methodology, and to present the results of the analysis.

2.1 DATA COLLECTION AND PROCESSING

2.1.1 Siting, Instrumentation, and Measurement History

The ANL/EES Air Resources Section Air Monitoring Laboratory (AML) was located at Chicago's O'Hare International Airport for approximately two and a half months in the fall of 1980. A 10-meter meterological tower was erected nearby, and a variety of instruments was employed to collect gas-phase pollutant-concentration data, meteorological data, and other relevant parameters. The AML and tower site selection was based on the following considerations:

1. Measurements were to be made downwind of aircraft take offs.

2. To avoid contaminating the aircraft exhaust plume, no significant pollution sources were to be upwind of or between the runway and the sampling site.

3. The AML and especially the meteorological tower were to be clear of aircraft takeoffs, landings, and taxiing.

4. Electrical power had to be available.

The site, as shown in Fig. 2.1, allowed sampling of plumes from aircraft taking off from runway 32R. That runway is generally used for takeoffs under westerly and northwesterly winds, and the AML was situated in a nearly optimal sampling location for those conditions. Other pollution sources include automobile traffic on the entrance road and in the Chicago metropolitan region, surrounding industries, and other airport operations, but these did did not significantly influence aircraft exhaust plumes. The site was

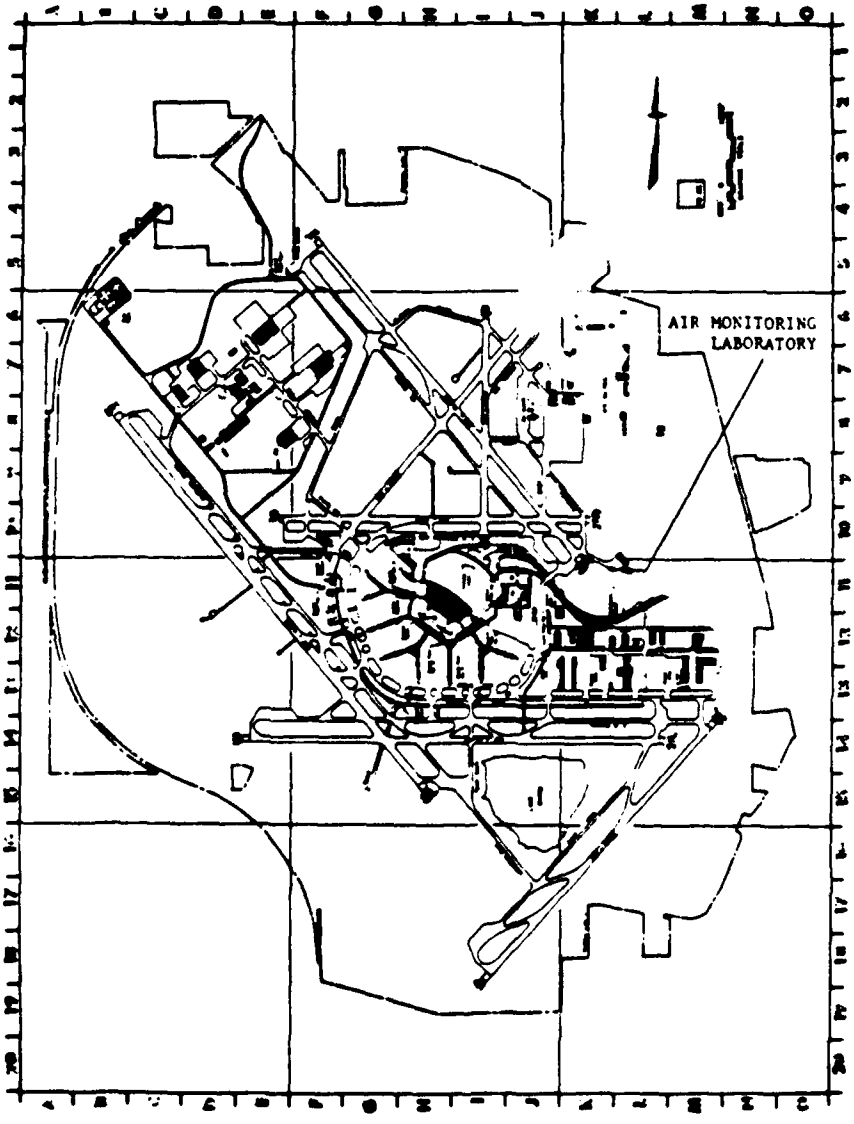

Fig. 2.1 Chicago O'Hare Runway/Taxiway Plan and Air-Monitoring-Laboratory Site

located 265 meters perpendicular to the runway axis, 165 meters from the start of 32R parallel to its axis, and 312 meters directly along a heading of 100° from the end of the runway. The latitude and longitude of the trailer site were estimated from a topographic map of the area to be 41°58'50" ± 0.4" N latitude, 87°53'16" ± 0.5" W longitude.

The 10-meter meterological tower was erected 20 meters southeast of the AML. The height of the tower and the distance from the AML were sufficient to avoid undue influence on the meterological measurements. Except for the Air Force "Alert Hanger" located 130 meters to the northeast, the surrounding topography did not contain any objects that would affect meterological measurements. The hanger undoubtedly affected meterological measurements when winds were from that direction. The area between the hanger and the sampling site was used primarily for parking snow-removal equipment, two small aircraft, and a Comet (medium-sized jet). The snow-removal equipment was occasionally turned on for maintenance but always kept stationary. The two small planes taxied out of their slots on a few occasions, and the Comet was never moved. Activity surrounding the immediate vicinity of the AML was not significant enough to influence measurements of aircraft takeoff exhaust plumes.

The air-sampling system in the AML consists of a glass 2-inch-ID intake mainfold through which outside air is drawn at a rate of approximately 400 liters/minute. The velocity of the air within the mainfold is approximately 3.3 m/s. Eight ports are provided for the extraction of samples; the first port is approximately 287 cm from the intake, and subsequent ports are spaced 28 cm apart along the manifold. Gas-phase concentrations of NO, NO_x, O_3, CO, and THC were monitored with instrumentation, described below, located within the AML. Other variables were monitored using instrumentation mounted on the meterological tower or on the top of the AML. The instruments employed are listed below.

1. A Beckman Model 950A Ozone Analyzer was used to measure the concentration of O_3 in the air. The basic operating principle is chemiluminescent gas-phase reaction of ozone with ethylene (C_2H_4). The ethylene was supplied from an external cylinder in a blend containing 10% C_2H_4 reactant and 90% CO_2 diluent. The instrument was operated in a fast-response mode, corresponding to 30 seconds to 90% response.

2. A Thermo Electron Corp. (TECO) Model 14 Chemiluminescent Analyzer was used to measure levels of NO and NO_x. The chemiluminescent reaction of NO and O_3 provides the basis of detection. However, since this instrument is equipped with only one detection system, it cannot measure NO and NO_x simultaneously. The instrument, when in "auto" mode, cycles from one substance to the other every 40 to 45 seconds. A "manual" mode may be used to continuously monitor either NO or NO_x. As a Monitor Labs Analyzer (described under item 3) capable of measuring NO and NO_x simultaneously was also in

operation, the TECO instrument was kept in NO_x "manual" mode in order to obtain continuous measurements of NO_x during most of the monitoring program.

3. A Monitor Labs (ML) Model 8440 E Chemiluminescent Analyzer was used to simultaneously measure concentrations of NO and NO_x. The chemiluminescent reaction of NO and O_3 provides the basis of operation. The instrument is equipped with a dual detection system, allowing simultaneous measurements of NO and NO_x and providing a continuous measure of NO_2 by difference. A 5-second instrumental time constant was used in order to be able to follow rapid NO and NO_x fluctuations.

A NBS-traceable NO Calibration Standard using hydrocarbon-free dry air as a diluent was used to calibrate the instrument. The primary calibration gas was further diluted using a Bendix Model 8851 Dynamic Calibration System (DCS), which also contained a permeation oven with a NO_2 permeation tube. A malfunction in the temperature control of the oven resulted in contamination of the teflon valves and tubing within the DCS with NO_2. This problem did not affect the calibration of the Monitor Labs instrument for NO, and the ML NO measurements are considered accurate. Calibration of the instrument for NO_x measurement had to be carried out by cross-calibration with the TECO NO_x instrument. This procedure is described in Sec. 2.2.2.

4. A Beckman Model 865 Nondispersive Infrared Analyzer was used to determine levels of CO in the sampled air. To determine the concentration of CO in the sample, the instrument compares infrared radiation absorbed in the sample cell containing a continuously flowing sample and in a reference cell containing a portion of the same gas with CO removed by a scrubber.

5. A modified Beckman Model 400 hydrocarbon analyzer was used to measure levels of total and nonreactive hydrocarbons (THC and NRHC). The analyzer utilizes a flame ionization detector, which functions approximately as a carbon-atom counter. The instrument was calibrated to read in ppm methane. The sensor uses a burner in which a regulated flow of sample gas passes through a flame sustained by regulated flows of hydrogen and air. The input to the analyzer was modified by addition of commercially available components to cyclically monitor total and nonreactive hydrocarbons. The instrument, however, was operated in the THC mode during most of the sampling program because the switching valve gave rise to power fluctuations that caused malfunctions in the operation of the data logger (see item 12).

6. A Columbia Research Laboratories Inc., Model SPL-103 Sound Level Meter was used to measure sound level of aircraft takeoffs. A range of 90 dB was selected so that a nearly full-scale value was obtained when an aircraft took off on runway 32R. The sound level was measured as an indicator of aircraft takeoffs.

7. An Eppley Model 50 Pyranometer was mounted on top of the AML to measure the intensity of solar radiation. The instrument was leveled horizontally and placed in a location that was free from shadows. This type

of pyranometer is sensitive to light of wavelengths ranging from the near-UV region to the near-IR region, and differs in that respect from the UV pyranometer used by others (Harvey et al. 1977, and Zafonte et al., 1977). Whereas the UV pyranometer is generally regarded as being more suitable for measurements that are to be related to atmospheric photochemistry, the broadband pyranometer that was used in this study proved to be adequate, as discussed in more detail in Sec. 2.2.1.

8. A Climet Model 011-3 wind-speed transmitter was mounted on the tower 10 meters above ground to measure wind speed.

9. A Climet Model 012-11 bivane transmitter was mounted on the tower 10 meters above ground level to monitor both horizontal and vertical components of wind direction.

10. A Climet Model 015-1 temperature probe mounted 10 meters above ground on the tower provided measurements of ambient temperature.

11. Two Climet Model 015-3 temperature probes were used to measure directly the difference between the temperature 10 meters and 1.5 meters above ground.

12. Data generated on site were recorded by a data logger consisting of a 15-channel digitizer constructed at ANL and a Cipher Data Products Model 85M-9 tape drive. Data were recorded on a 9-track 800 bpi magnetic tape at a rate of approximately one complete set of 15 measurements per second. The exact rate at which data were collected varied very slightly over a period of days about an average rate of one data sample every 0.99994429 s, as determined by time checks using WWV broadcasts. One data sample consists of a (digitized) measurement from each of the 15 channels in the data logger, collected over a period of about 35 ms. Each digitized measurement consisted of an integer ranging in value from zero to a full-scale value of approximately 255, depending on the instrument.

A measurement history of these parameters is presented in Fig. 2.2. The horizontal lines span periods of time during which the respective instruments were operating. Conversion of Julian date to calendar date may be accomplished using the charts in Fig. 2.3. The X's marked for gaseous pollutants denote calibration points for each instrument. In the case of the data logger, the X's show those times when a data tape was replaced. The two periods when no instruments are shown operating correspond to electrical power failures.

Table 2.1 shows the data logger channel number, operating range over a particular time period, full-scale voltage, and variables that are used in calculating the true physical (nondigitized) value for each measured quantity.

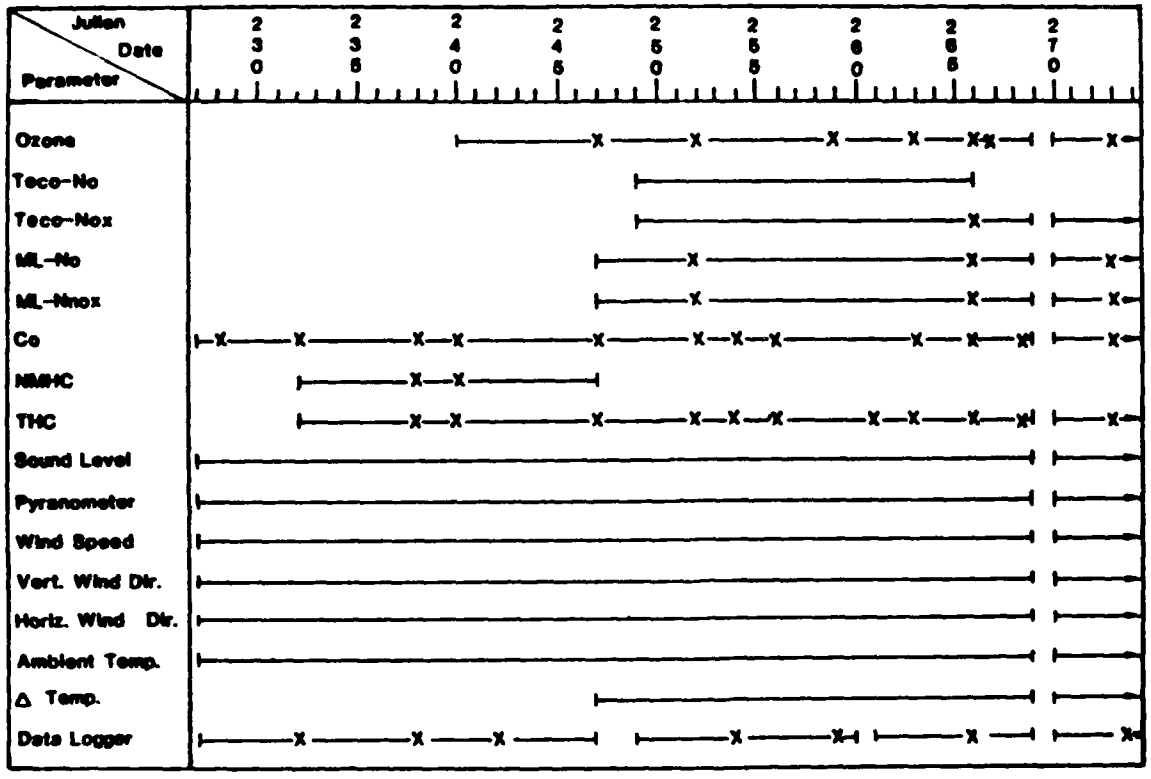

Fig. 2.2 Field-Program Measurement History

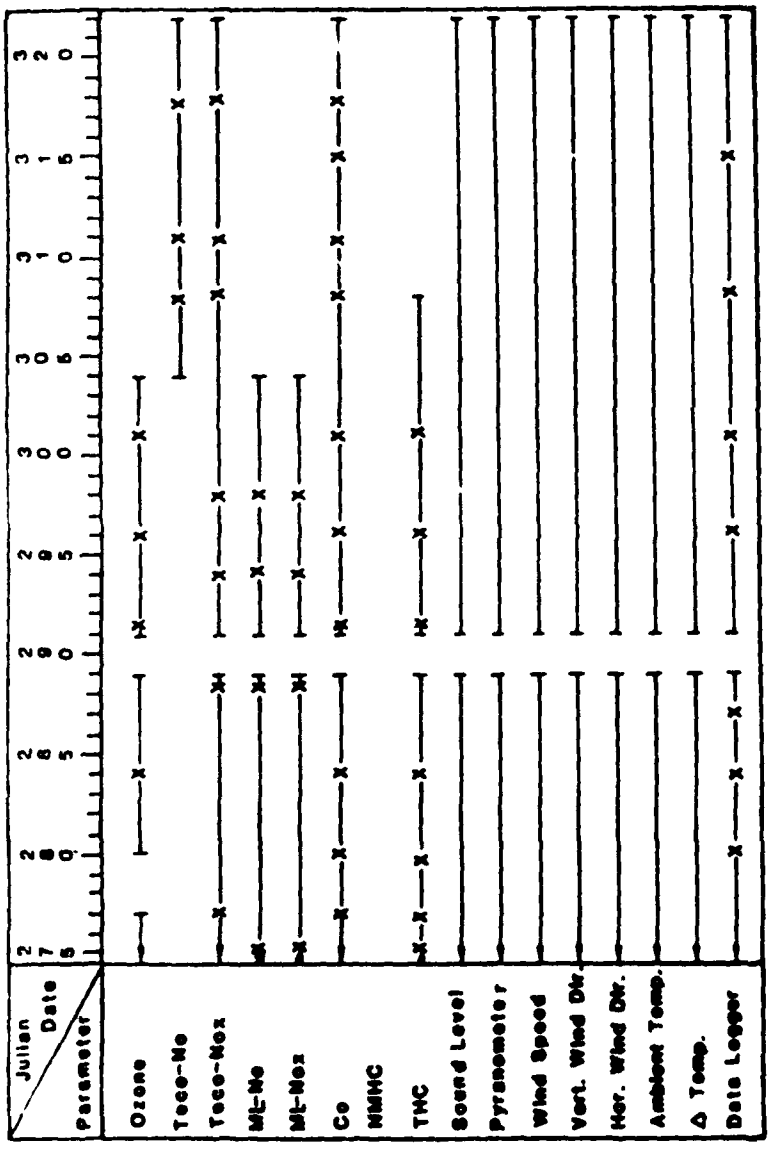

Fig. 2.2 (Cont'd)

AUGUST 1980

S	M	T	W	Th	F	S
					1 214	2 215
3 216	4 217	5 218	6 219	7 220	8 221	9 222
10 223	11 224	12 225	13 226	14 227	15 228	16 229
17 230	18 231	19 232	20 234	21 235	22 236	23 237
24 237	25 238	26 239	27 240	28 241	29 242	30 243
31 244						

SEPTEMBER 1980

S	M	T	W	Th	F	S
	1 245	2 246	3 247	4 248	5 249	6 250
7 251	8 252	9 253	10 254	11 255	12 256	13 257
14 258	15 259	16 260	17 261	18 262	19 263	20 264
21 265	22 266	23 267	24 268	25 269	26 270	27 271
28 272	29 273	30 274				

OCTOBER 1980

S	M	T	W	Th	F	S
			1 275	2 276	3 277	4 278
5 279	6 280	7 281	8 282	9 283	10 284	11 285
12 286	13 287	14 288	15 289	16 290	17 291	18 292
19 293	20 294	21 295	22 296	23 297	24 298	25 299
26 300	27 301	28 302	29 303	30 304	31 305	

NOVEMBER 1980

S	M	T	W	Th	F	S
						1 306
2 307	3 308	4 309	5 310	6 311	7 312	8 313
9 314	10 315	11 316	12 317	13 318	14 319	15 320
16 321	17 322	18 323	19 324	20 325	21 326	22 327
23 328	24 329	25 330	26 331	27 332	28 333	29 334
30 335						

Fig. 2.3 Julian Date/Calendar Date Correspondence

Table 2.1 Instrument Ranges and Data Conversion Parameters

Parameter	Channel Number	Range	Time Period[a]	Full-Scale Voltage	X_1	X_2	X_3	Z
Ozone	2	250 ppb	240:1400-298:1100	5.0 V	255	250	0	ppb
		100 ppb	298:1100-304:1210	5.0 V	255	100	0	ppb
TECO NO/NO_x	3 and 4	500 ppb	249:1345-273:1150	10.0 V	255	500	0	ppb
		1000 ppb	273:1310-275:1330	10.0 V	255	1000	0	ppb
		5000 ppb	275:1330-304:1345	10.0 V	255	5000	0	ppb
		1000 ppb	304:1345-322:1240	10.0 V	255	1000	0	ppb
ML NO/NO_x	15 and 14	500 ppb	247:1230-275:1451	10.0 V	255	500	0	ppb
		2000 ppb	275:1615-304:1247	10.0 V	255	2000	0	ppb
CO	5	33.33 ppm	227:1425-322:1225	5.0 V	255	33.33	0	ppm
THC/NMHC	6 and 7	10 ppm	232:1345-240:1125	1.0 V	255	10	0	ppm
		20 ppm	240:1227-273:1216	1.0 V	255	20	0	ppm
		200 ppm	273:1216-275:0920	1.0 V	255	200	0	ppm
		50 ppm	275:0945-301:1343	1.0 V	255	50	0	ppm
Sound Level	13	-10 to ± 90 dB	227:1245-322:1220	10.0 V	255	100	-10	dB
Solar Intensity	8	0-989 watts/m^2	227:1245-322:1220	1.0 V	255	989	0	watts/m^2
Wind Speed	9	0-49 m/s	227:1245-322:1220	0.973 V	248	49	0	m/s
Vertical Wind Direction	11	-60° to + 60°	227:1245-322:1220	0.973 V	248	120	-60	DEG
Horizontal Wind Direction	10	0° to 360°	227:1245-322:1220	0.968 V	b	b	b	b
Temperature	12	-30°C to +50°C	227:1245-322:1220	1.0 V	255	80	-30	°C
Delta Temperature	7	-6°C to +12°C	227:1245-322:1220	0.973 V	248	18	-6	°C

[a]Julian Date: Central Daylight Time.

[b]Use Equations 2.2 and 2.3 to compute horizontal wind direction.

The value of a measured parameter in physical units was computed from the raw digitized measurement using Eq. 2.1.

$$\text{Value in Z units} = \left(\frac{J}{X_1}\right)X_2 + X_3 \qquad (2.1)$$

where:

J = an adjusted raw data value,
Z = physical units of given quantity,
X_1 = digitized full-scale value,
X_2 = physical full-scale value, and
X_3 = baseline adjustment.

Values of Z, X_1, X_2, and X_3 for each instrument are given in Table 2.1. The adjusted raw data value J corresponding to a particular measurement was obtained from the actual raw data value I, which takes on integer values between zero and 255 inclusive, as follows. Values I = 0 or 255 were discarded as being ambiguous, since a value of zero results from any monitoring instrument output less than that which gives rise to a digitized value I = 1, and a value of 255 results from any output in excess of full scale. In other words, values I = 0 or 255 represent only upper and lower bounds, respectively, to the "true" value. An exception was made in the case of ozone, for which a value I = 0 was allowed on the argument that since the investigation dealt with NO_x sources, the ozone level in a plume may indeed be expected to be small in most instances. Also, since the digitizer in effect truncates to the nearest integer rather than rounding off, the same digitized value I will be produced from any input voltage in the range from the threshold for value I to the threshold for value I + 1, and when converted to physical units represents a lower bound to the true value. For example, when the instrument was operated in the 0-2 ppm range, the digitization resolution of the Monitor Labs NO/NO_x data is 2000/255 = 7.8 ppb. The direct use of the value I itself therefore results in a systematic underestimate of the measured value of the physical quantity being considered. In the NO/NO_x example, each measurement would be underestimated by an amount ranging from zero to 7.8 ppb. The loss of resolution due to the digitization process will be referred to as the digitization error. An approximate correction for this effect was made by adding 0.5 to the raw value I, on the assumption that the input voltages that give rise to the value I are approximately uniformly distributed over the corresponding range and using J = I + 0.5 gives the corresponding statistically expected value and reduces the digitization error by up to half. This procedure was used in processing all digitized data. In addition, for TECO-NO_x, ML-NO, ML-NO_x, and O_3 measurements, a further correction is made for instrument-response-time effects and for relative time lags between the responses of these four instruments to changes in airstream concentrations. These corrections were found to be necessary in order to obtain maximum resolution and to insure that, in the later analysis, concentrations being

compared or used together corresponded as closely as possible to simultaneous measurements on the same air parcel. The experiments and procedures by which these corrections were made are described in Sec. 2.1.2.

Equation 2.1 allows calculation of all parameters except horizontal wind direction (HWD). HWD may be calculated using Eqs. 2.2 and 2.3:

$$X = (2.0833 \cdot \frac{I}{247}) - 1.0 \qquad (2.2)$$

$$ANGLE = 248.15 + X(260.64 + X(7.2956 - 4.9252X)) \qquad (2.3)$$

where I = raw data value of HWD.

If ANGLE $\geq$ 360.0, subtract 360.0.

Computations of gaseous-pollutant concentrations using Eq. 2.1 provide estimates uncorrected for the calibration of each instrument. All gas-phase-concentration monitoring instruments were calibrated every 3-4 days using the following general procedure:

A. Replace in-line filters and adjust appropriate flows.

B. Set recorder zero.

C. Set instrument zero.

D. Set instrument span.

E. Record start time of a data recording period and place instrument into sample position.

F. Record stop time of the data recording period.

G. Record final recorder zero.

H. Record final instrument zero.

I. Record final instrument span.

In addition, primary multipoint calibrations were carried out for the TECO NO_x and O_3 instruments prior to or early in the measurement program. The results showed both instruments to be performing properly, with a linear response over the ranges of interest. The NO_2-NO converter in the TECO NO_x instrument was found to be 98% efficient.

As a further check on the performance of the instrumentation, a Quality Assurance Performance Audit was performed by a local consulting firm on Sept. 23, 1980, on the Beckman O_3 and the Monitor Labs NO/NO_x instruments. The findings of this audit indicated that the O_3 and the ML NO instruments were performing satisfactorily, but the ML NO_x measurements were in error due to the calibration difficulties mentioned earlier. There was no evidence that the instrument itself was malfunctioning, and the measurements are considered to be of satisfactory accuracy after calibration by cross-comparison with the TECO NO_x measurements.

The bivane used for wind-direction measurements was calibrated, and the vertical component measurement was found to be linear between the instrument limits of ± 60°. The horizontal-component measurements were not quite linear, and the calibration data were fit with a third-degree polynominal in order to insure accurate measurements (see Eq. 2.3). No calibration was required for measurements of wind speed, ambient temperature, solar intensity, or sound intensity.

2.1.2 System Characterization

The major objective of the field-measurement program was to acquire data that could be used to validate the NO_2 model being developed. The approach taken in the model is to describe individual takeoff plumes and base one-hour average predictions on the individual takeoff events for that hour. The data, therefore, were collected at a rapid enough rate, about one complete set of measurements per second, that individual plume profiles would be well determined. The entire time required for the passage of a plume is on the order of 30 seconds and up, depending on the distance of the monitoring site from the aircraft. The instrumentation used to measure such profiles must either have a rapid enough response time to accurately follow a typical concentration variation of zero to half a part per million and back again over 30 seconds, or the data must be corrected for the finite instrument response time for an accurate determination of plume shape and size. A general discussion of the effects of instrument response and of ways of correcting for those effects is given in Appendix 3.

Manufacturer's specifications in the various instrument manuals give some indication as to the various response times. However, such specifications usually refer to the electronic response only, and it was felt desirable to have independent measurements of the response of the instruments within the total sampling system of the Air Monitoring Laboratory. Accordingly, a set of experiments was conducted on Oct. 13, 1980, to characterize the response of the NO, NO_x, and O_3 instruments.

The experimental setup was as shown in Fig. 2.4. A quantity of NO was introduced into the intake of the sampling manifold on an intermittent basis so as to simulate a series of approximately rectangular pulses. Both NO and NO_x measurements were affected directly; the O_3 measurements are also affected, since ambient O_3 reacts with part of the NO injected, as discussed

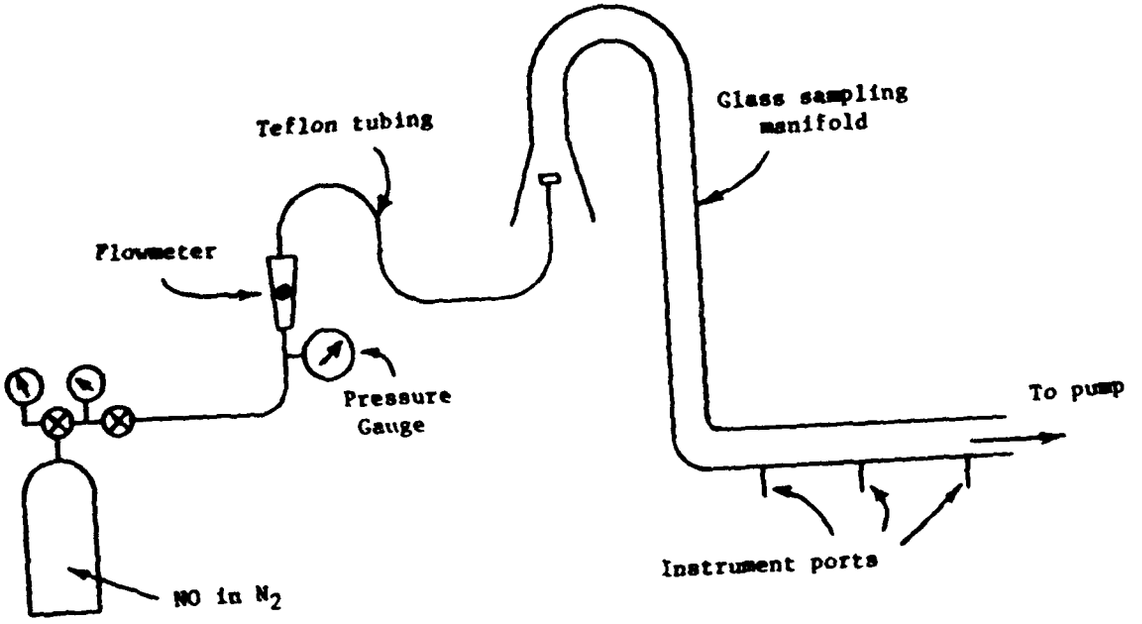

Fig. 2.4 Instrument-Response Experimental Setup

in Sec. 3.1.3. The responses of the TECO NO_x, ML NO/NO_x, and O_3 instruments were recorded at a rate of 10 sets of measurements per second on magnetic tape using the data logger; the ML NO/NO_x and O_3 instrument responses were also followed using strip-chart recorders. A total of seven experiments were carried o t, of which four gave useful data. In the other three experiments, fluctuations in the wind velocity caused unacceptably large fluctuations in the amount of NO being drawn into the intake. The problem was solved by pushing the NO source further into the intake so that the amount drawn in would be less susceptible to wind variations. The strip charts from experiment no. 7 are reproduced in Fig. 2.5.

The data were analyzed to obtain response times by numerical least-squares fitting of a theoretical response curve to the individual instrument responses as recorded on magnetic tape. Each instrument was assumed to respond in an exponential manner to its respective input signal. The input signal was assumed to be a diffuse step input, i.e., a step that has diffused somewhat so that the front is not infinitely sharp. Under these assumptions, a theoretical instrument-response curve y(t) can be evaluated (see Appendix 3) for a diffuse step increase:

$$y(t) = y_o + \frac{y_\infty}{2}\left[1 + \mathrm{erf}(\zeta) - \mathrm{erfc}(\alpha - \zeta)\exp(\alpha^2 - 2\alpha\zeta)\right] \qquad (2.4)$$

and a diffuse step decrease:

$$y(t) = y_o + \frac{y_{-\infty}}{2}\left[1 - \mathrm{erf}(\zeta) + \mathrm{erfc}(\alpha - \zeta)\exp(\alpha^2 - 2\alpha\zeta)\right] \qquad (2.5)$$

in which y_o is a baseline value, y_∞ and $y_{-\infty}$ are asymptotic values, and α and ζ are defined by:

$$\alpha = \frac{\sigma}{\sqrt{2}\,\tau} \qquad (2.6)$$

$$\zeta = \frac{t - t_o}{\sqrt{2}\,\sigma} \qquad (2.7)$$

In these equations, σ denotes the parameter that characterizes the diffuseness of the step, τ denotes the instrument response time, and t_o denotes the arrival time of the front or step. The functions erf and erfc denote the standard error function and the complementary error function:

$$\mathrm{erf}(x) = \frac{2}{\sqrt{\pi}}\int_0^x e^{-t^2}\,dt$$

and

$$\mathrm{erfc}(x) = 1 - \mathrm{erf}(x)$$

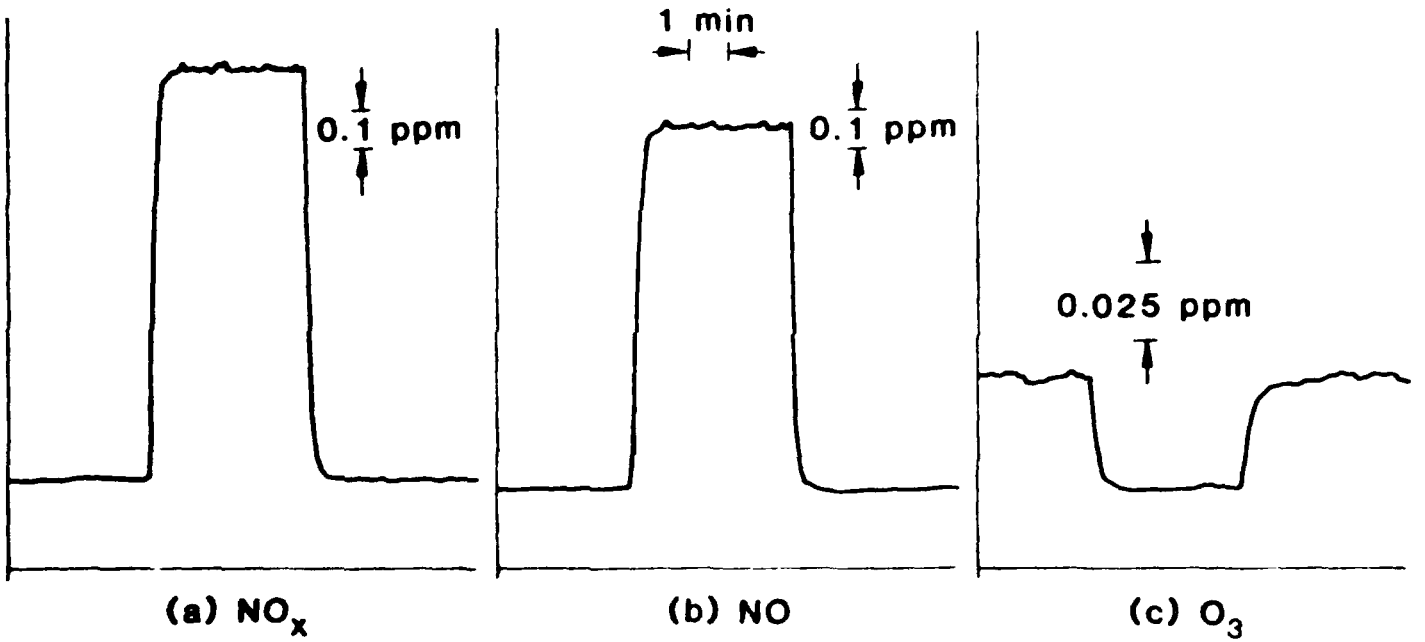

Fig. 2.5 Instrument Response Data for Experiment Seven

The five parameters y_o, $y_{t=\infty}$, σ, τ, and t_o were all considered unknown and determined simultaneously for each instrument in each experiment. The step-increase and step-decrease phases of each experiment were considered independently. The residuals from each fit were examined visually; no systematic trends were observed, and it was concluded that Eqs. 2.4 and 2.5 adequately represent the observed behavior.

Selected results from these experiments are given in Table 2.2. The values of response time and arrival time represent averages over the various experiments; values for the baseline and asymptotic concentrations as well as the diffuseness parameter σ are not given, since they reflect the manner in which the experiments were carried out rather than any significant property of the sampling system or instrumentation. It is interesting to notice that in most cases the measured response time was noticeably longer than the manufacturer's specification, the single exception being the ozone instrument for step-decrease experiments. It is also interesting to notice that the response times for step-increase cases are all higher than those for step-decrease cases. In each instrument, the sample stream is mixed with another gas mixture containing a substance that reacts chemically with the species to be detected, the reaction being such that light is emitted and detected. It is thought that the difference in response times between increase and decrease cases may reflect details of the gas mixing and detection processes. Differences in arrival times reflect primarily differences in sample flow rates and sampling tube lengths. Differences due to the finite air velocity in the manifold are estimated to be much less than one second.

The data analysis required that measurements of NO_x, NO, and O_3 be as nearly simultaneous as possible, and the significant differences in arrival times observed in the response experiments just discussed indicate that correction for these effects is required in the subsequent analysis. In order to examine the possibility that the relative time lags between the NO_x, NO, and O_3 instruments varied over the duration of the measurement program, an alternative procedure was adopted for their determination and was utilized to determine time lags for several different periods of time scattered throughout the measurement history. The alternative procedure involved the computation of the square of the correlation coefficient (R^2) between the TECO NO_x measurements and the other three measurements (ML NO_x, ML NO, and O_3) for a variety of different time lags. The results were plotted as a function of time lag and the optimal time lag was taken to be that which maximized the value of R^2. The time lags determined in this way were found to be constant over the entire measurement program and are given in Table 2.3 along with typical R^2 values. Values are somewhat different from those given in Table 2.2, which were determined in an entirely different manner, but not dramatically so. The ML NO/NO_x lags are somewhat larger than found earlier, but the ML NO–ML NO_x time lag of 0.7 second reproduces the earlier value, and the ozone time lag is within the previous experimental error. The values given in Table 2.3 were used in the basic data processing.

Table 2.2 Selected Instrument-Response-Parameter Values[a]

Parameter		Monitor Labs NO_x	Monitor Labs NO	TECO NO_x	Ozone
Response Time τ (s)	Up	6.87 ± 0.16	6.82 ± 0.16	3.53 ± 0.27	14.03 ± 2.67
	Down	6.50 ± 0.13	5.99 ± 0.12	2.79 ± 0.17	9.36 ± 0.46
	Total	6.67 ± 0.24	6.41 ± 0.44	3.16 ± 0.43	11.70 ± 3.02
	Specs.[b]	5.0	5.0	2.2	13.0
Arrival Time t_o[c] (s)	Up	4.92 ± 0.08	4.20 ± 0.08	-	3.26 ± 1.06
	Down	4.89 ± 0.07	4.13 ± 0.06	-	2.27 ± 0.48
	Total	4.91 ± 0.08	4.17 ± 0.08	-	2.77 ± 0.96

[a]Values given are averages over four experiments involving a step increase (the "Up" values), over four experiments involving a step decrease (the "Down" values), and over all eight experiments, combining both step increase and decrease results (the "Total" values). Indicated uncertainties represent one standard deviation.

[b]Manufacturer specified value. TECO NO_x value for manual mode.

[c]With respect to the TECO NO_x arrival time; the values cited are in fact values of the difference $t_o - t_o$ (TECO NO_x).

Table 2.3 Relative Instrument Time Lags[a] as Determined by Time-Sequence Analysis

Monitoring Instrument	Optional Time Lag (seconds)	R^2
TECO NO_x	-	-
Monitor Labs NO_x	6.0	0.9
Monitor Labs NO	5.3	0.9
Beckman O_3	3.25	0.45

[a]Values given with respect to the TECO NO_x instrument.

The correction of the measured data for instrument response was made using Eq. 2.8 (see Appendix 3 for the derivation) using the response times given in Table 2.2. Equation 2.8 involves the assumption of exponential response, an assumption which is adequate in view of the lack of any systematic trends in the residuals of the numerical fits to the response experiment data.

$$x_k = \left(\frac{\tau}{\delta t}\right)[y_k - y_{k-1}\exp(-\delta t/\tau)] \qquad (2.8)$$

In this equation, x_k denotes the corrected response at time instant k, y_k and y_{k-1} denote the instrument response at times k and k-1, respectively, δt represents the sampling interval (nominally one second), and τ represents the instrument response time.

As indicated earlier, a malfunction in the Dynamic Calibration System (DCS) made the calibration of the Monitor Labs NO_x measurements highly uncertain. The calibration of the TECO instrument was not affected, since it contains only one detection chamber and was always calibrated in the NO mode, the NO_2-NO conversion having been checked and found to be satisfactory, as discussed in Sec. 2.1.1. Similarly, the calibration of the Monitor Labs NO channel was not affected. In order to make use of the ML NO_x data, the ML NO_x channel was cross-calibrated against the TECO NO_x data taken simultaneously. Since the TECO data could be calibrated, this procedure allowed the Monitor Labs data to also be calibrated, although this procedure does not yield results that are as accurate as would have been obtained with a properly functioning DCS. It is fair to say, however, that the redundancy built into the monitoring program by having two NO_x instruments allowed a potentially serious and program-threatening problem to be reduced to an annoyance.

The procedure used for the cross-calibration was essentially the same time-sequence analysis method used to determine the relative instrument time lags, except that the slope and intercept as well as the R^2 value was of interest. A new cross-calibration had to be run each time either instrument was calibrated. Table 2.4 contains the results of the cross-calibration for each calibration period. A total of 13 joint calibration periods (JCPs) were identified; these are periods during which the calibration of both instruments and the instrument settings (mode, range, etc.) remain unchanged. The regression period is that period of time within the JCP selected for regression analysis. All times are Central Daylight Times. The regression results, number of points used, instrument ranges and calibration periods are presented. The regression analysis was carried out using raw data from both instruments, so that the cross-calibration slope and intercept could be used to convert a ML NO_x raw datum to an effective TECO NO_x datum.

The analysis had to be carried out differently for JCPs 1-4 than for the rest because during those times, the TECO instrument was operated in "automatic" mode. In this mode, the instrument automatically cycles between

Table 2.4 Monitor Labs NO_x -- TECO NO_x Cross-Calibration Results

Joint	Calibration Period		Regression Period		No. Points	Slope	Intercept	R^2	Range (ppm)		Calibr. Period	
	Start	Stop	Start	Stop					ML	TECO	ML	TECO
1[a]	249:1345	252:1140	250:1200	251:1200	144	0.983	-2.199	0.992	0.5	0.5	1	1
2[a]	252:1400	266:1145	252:1400	253:1400	144	1.088	5.044	0.974	0.5	0.5	2	1
			257:2400	258:2400	136	1.035	-2.380	0.935				
			264:2400	265:2400	144	0.911	10.073	0.958				
					424	1.101	4.245	0.956				
3[a]	266:1350	270:1138	268:0000	269:1000	203	1.190	-2.255	0.997	0.5	0.5	3	2
4[a]	270:1138	273:0815	270:1200	271:2400	216	0.630	-3.037	0.997	0.5	1.0	3	2
5	273:0840	273:1150	273:0840	273:1150	11,390	0.515	0.543	0.912	0.5	1.0	3	2
6	273:1400	275:1327	273:1400	274:0700	61,190	0.515	-0.343	0.976	0.5	1.0	4	3
7,8	275:1327	275:1445	NOT USED						0.5	5.0	4	3
9	275:1615	277:1235	276:0600	276:2200	18,287	0.202	0.299	0.697	2.0	5.0	5	3
10	277:1543	289:0842	284:1000	284:1600	5,233	0.286	-1.308	0.919	2.0	5.0	5	4
11	289:1315	294:1221	291:2000	291:2200	2,693	0.386	-0.393	0.938	2.0	5.0	6	5
			293:1100	293:1300								
12	294:1413	298:0845	294:1800	294:2000	7,726	0.409	-0.017	0.934	2.0	5.0	7	6
			295:1400	295:1745								
13	298:1216	304:1247	298:1700	298:1900	5,786	0.372	-0.056	0.942	2.0	5.0	8	7
			303:1400	303:1600								

[a]TECO NO_x/NO instrument operated in automatic mode.

NO and NO_x approximately every 45 seconds. The cycle time is not constant, however, and may range up to 60 seconds. During the time when NO is being measured, the NO_x output-channel voltage is held fixed at the last value it had prior to the switch to NO, and vice-versa. It proved to be impossible to reliably identify the NO_x periods from the raw data, and the regression against ML NO_x data was therefore carried out with values that represented raw digital data averaged over a 10-minute period. Other averaging times were examined, but 10 minutes proved to be optimal in that it was long enough to average out the NO/NO_x cycling of the TECO instrument but short enough to preserve enough variation in the data to allow the analysis to be made with reasonable accuracy. No correction for relative lag times was made in these runs.

In JCPs 5-13, the TECO instrument was operated in the manual mode and provided continuous measurements of NO_x. Cross-calibration analyses involved the comparison of each pair of raw data values, and the relative time lag was determined simultaneously by running comparisons using different lag times and selecting the results that correspond to the maximum R^2 value. In all cases, the slope of the regression was maximized at the same time lag that maximized the R^2 value.

Figures 2.6 through 2.9 exemplify the wealth of data that were collected in the field-measurement program and the effects of the various processing steps. Figure 2.6 shows pseudo-stripcharts generated from the raw digitized data for Oct. 29, 1980 (Julian day 303); the raw data have been averaged over two-minute periods for purposes of display but not corrected nor changed to physical units. From top to bottom, the four plots shown represent ML-NO, ML-NO_x, ozone, and TECO-NO_x measurements, respectively. Displays of this type as well as similar presentations for the CO, total hydrocarbon, solar intensity, wind direction, temperature, and sound intensity data, were generated for each day of the program and proved to be invaluable in identifying periods during which peaks due to aircraft activity could be found as well as in obtaining a feeling for the overall performance of the system and in identifying periods during which either malfunctions or some other interesting external phenomenon occurred.

Figure 2.7 shows the period from 1400 to 1600 hours CDT on day 303 in more detail, and represents a plot of three-second rather than two-minute averages of the raw data. Several aircraft peaks may clearly be seen in all of the NO or NO_x plots, and the depletion of the ozone level within each aircraft plume is clearly demonstrated. Figure 2.8 displays the raw data for the period 303:1454:35 to 303:1455:55 (a total elapsed time of 80 seconds), during which the passage of a single aircraft plume was observed. The ozone depletion is clearly seen, and the effect of the relative instrument time lags can also be clearly seen by comparing the corresponding positions of various points in the different curves. For example, the TECO NO_x peak occurs significantly earlier than either ML peak or the ozone minimum. In addition, the TECO NO_x peak seems to contain significantly more structure than the ML NO or NO_x peaks, which in turn have more structure than the ozone curve. This is

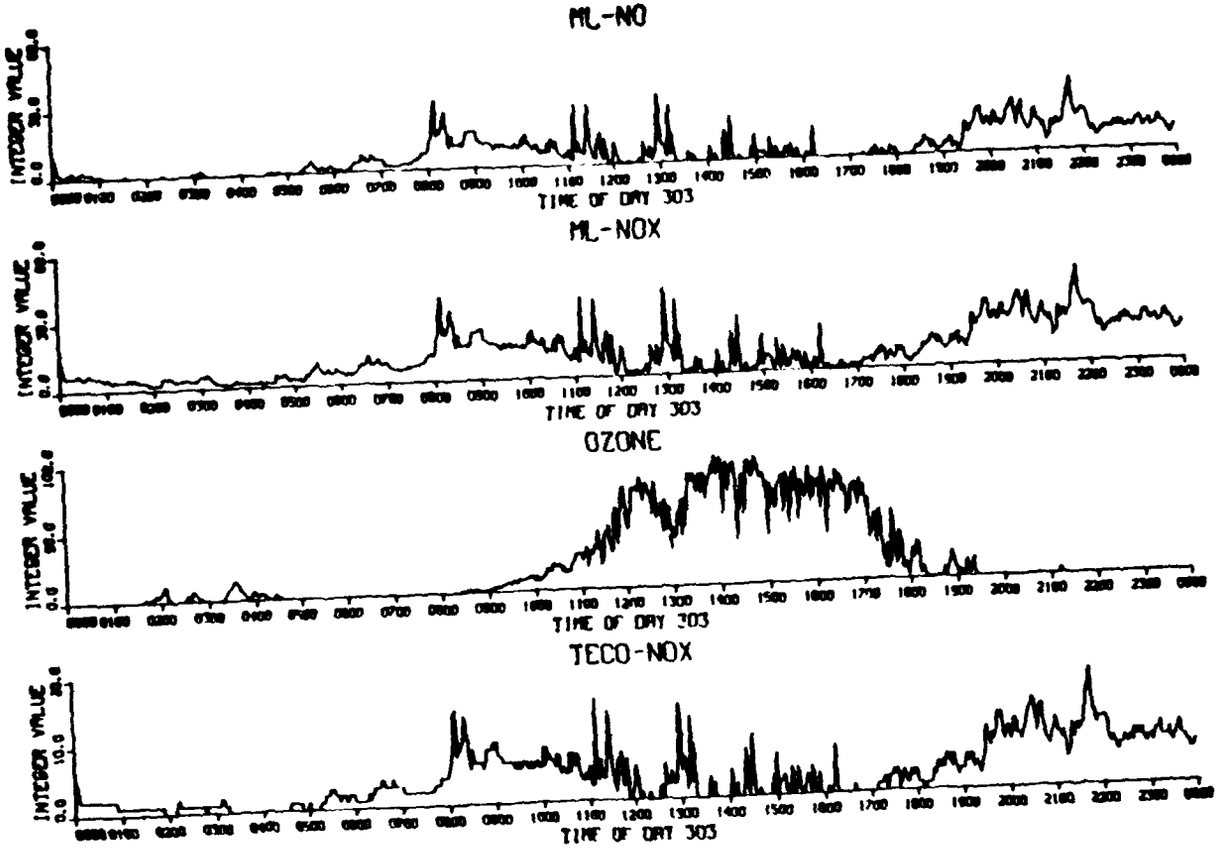

Fig. 2.6 Julian Day 303, Two-Minute Average Data

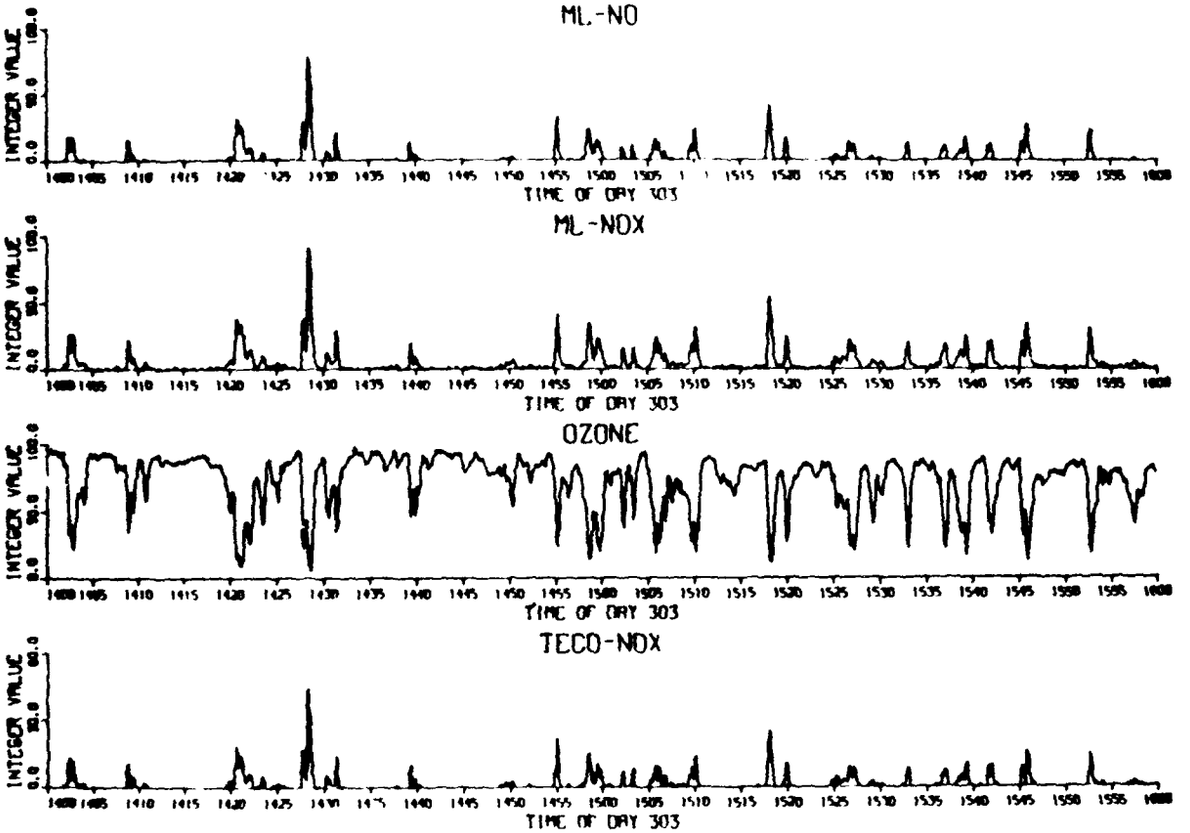

Fig. 2.7 Julian Day 303, 1400-1600 Hours, Three-Second Average Data

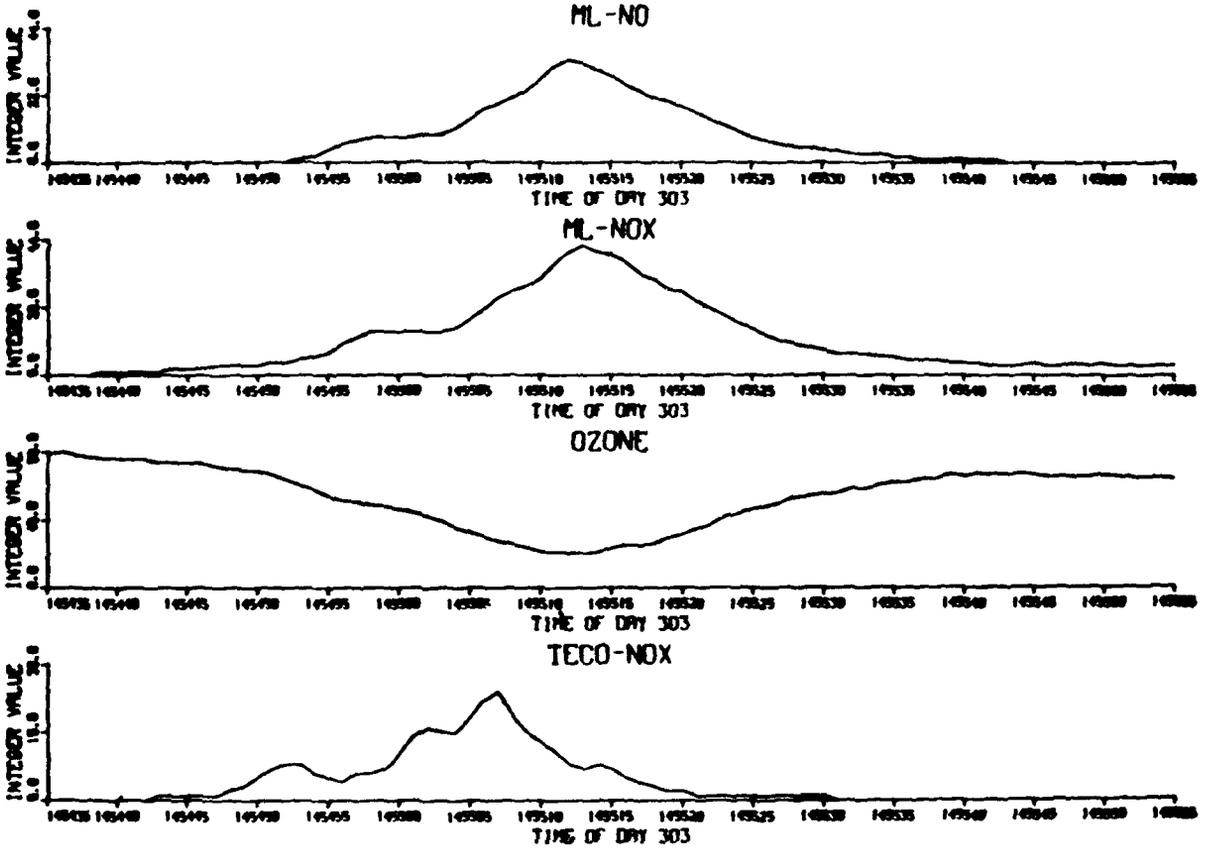

Fig. 2.8 Julian Day 303, 1454:35-1455:55 Raw Data

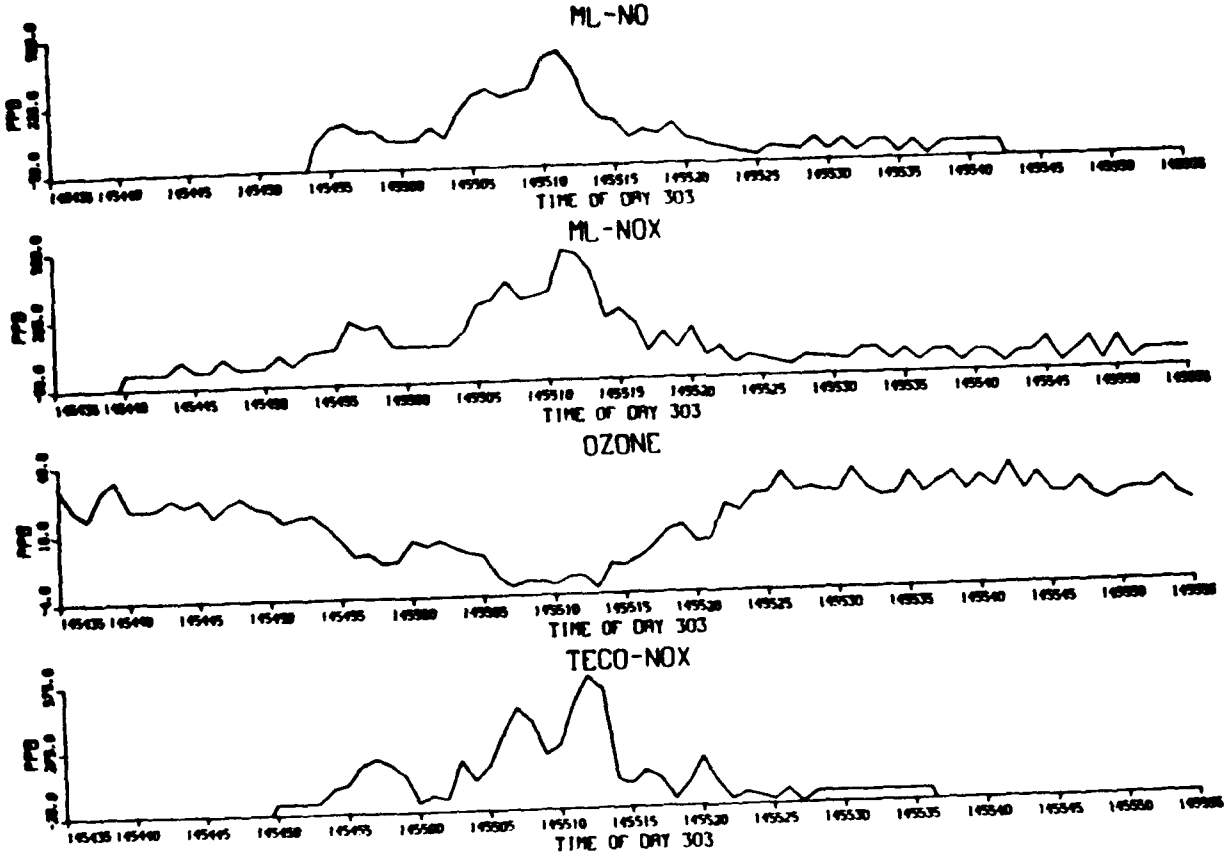

Fig. 2.9 Julian Day 303, 1454:35 - 1455:55 Data After Processing

due to differences in instrument response, the TECO instrument having the shortest response time and the ozone instrument having the longest, as was shown in Table 2.2. Finally, Fig. 2.9 shows the same period of time as Fig. 2.8 but displays the processed data after conversion to physical units. The structures in the various curves are now seen to correspond closely, illustrating the effect of the time-lag and instrument-response corrections. During all data processing, the ML-NO_x data were used to define the basic time points, and the data from the other instruments were shifted accordingly. Thus, in Fig. 2.9 the main TECO peak occurs at 1455:13 rather than at the uncorrected time of 1455:07 as displayed in the raw data in Fig. 2.8.

2.2 DATA ANALYSIS AND RESULTS

2.2.1 Ambient Photostationary State and Pyranometer Calibration

One of the basic assumptions made in the development of the NO_2 model is that the ambient NO, NO_2, and O_3 concentrations satisfy the photostationary state relation (Leighton, 1961):

$$\frac{[NO][O_3]}{[NO_2]} = \frac{k_A}{k_B} \tag{2.9}$$

where [] denotes the concentration (number density) of the bracketed chemical species, k_A is the rate coefficient for NO_2 photodissociation and k_B is the rate coefficient for the reactions between NO and O_3 to produce NO_2. A more detailed discussion of the chemistry, including a derivation of Eq. 2.9, may be found in Sec. 3.1.3. The first task in analyzing the field data was to determine the extent to which the measured ambient concentrations satisfied Eq. 2.9.

The available data are not sufficient to allow a rigorous test of the validity of Eq. 2.9; in particular, direct continuous measurements of k_A, which depends upon the ambient near-UV light intensity, were not made. This type of measurement is by no means routine, although in recent years several research groups have reported on the design, construction, and use of devices for the direct determination of k_A (Burch et al., 1974; Jackson et al., 1975; Stedman et al., 1975; Harvey et al., 1977; Zafonte et al., 1977; Bahe et al., 1980). In most of these studies, direct measurements of k_A were correlated with simultaneous UV radiation measurements made with pyranometers sensitive only to near-UV wavelengths. The results indicate that UV-pyranometer data are a useful surrogate for direct k_A measurements and that the development of empirical relationships that enable k_A to be estimated from a pyranometer measurement of light intensity is entirely feasible. In order to test the consistency of the measurements with Eq. 2.9, the tentative assumption was made that Eq. 2.9 is valid and an empirical relationship was developed between the pyranometer data and the apparent values of k_A.

If one assumes that Eq. 2.9 is valid, measurements of the ambient concentrations of NO, NO_2, and O_3 may be combined with the known value of k_B to provide an estimate of the value of k_A, which will be termed the apparent NO_2 photolysis rate. Denoting this estimate by $\tilde{k}_A$ to distinguish it from the value k_A that a direct measurement would yield, one finds that $\tilde{k}_A$ is given by:

$$\tilde{k}_A = k_B \frac{[NO][O_3]}{[NO_2]} \tag{2.10}$$

This quantity may be evaluated on a continuous basis from data collected during the field program, although individual values obtained in this way are subject to significant random errors arising from a combination of the digitization error associated with each concentration measurement and the fact that in order to have measurable quantities of all three substances present at the same time, all three concentrations must be rather small.

The method whereby the consistency of the ambient data with Eq. 2.9 was checked was to examine the relationship between $\tilde{k}_A$ and the corresponding pyranometer data. Five time periods, one on each of five separate days, were identified for analysis. The periods chosen were such that (1) no aircraft plumes were included and (2) a wide range of ambient lighting conditions were covered. Table 2.5 lists the periods chosen along with a brief description of the lighting conditions. These five periods were subdivided into 30-second intervals, and median values of $\tilde{k}_A$ and the solar radiation intensity as measured by the pyranometer within each interval were determined. A total of 3120 out of the possible 3240 intervals yielded a valid median for $\tilde{k}_A$.

Figure 2.10 shows the results in the form of a plot, with the vertical axis specifying the $\tilde{k}_A$ value and the horizontal axis the pyranometer reading. A high degree of correlation between $\tilde{k}_A$ and solar intensity is obvious. The apparent photolysis rate approaches zero with the solar intensity, and increases monotonically as the solar intensity increases. The relationship between the two is clearly nonlinear; this feature is in accord with other, similar results obtained using UV pyranometers and is due mainly to the cosine response curve of the Eppley instrument (Harvey et al., 1977; Zafonte et al., 1977). It should be noted, however, that in the only other published study known to us to use a device sensitive to a broad range of wavelengths, a linear relationship was found over the entire range of solar intensities and photolysis rates examined (Bahe et al., 1980). These investigators comment that a nonlinear relationship had been expected and attribute the linearity of their results to the fact that data from all seasons of the year and a great variety of weather conditions were included. In addition, an early version of the direct-measurement device designed by Stedman and coworkers also produced a linear relationship when correlated against an Eppley UV pyranometer (Jackson et al., 1975). Harvey et al. (1977) comment that curvature in the type of plot under consideration is expected when the sky is clear, but that one effect of clouds is to diffuse the available sunlight more evenly over the sky and thereby reduce the significance of the

Table 2.5 Ambient-Photostationary-State Analysis Periods

Period	Date:Times(CDT)	Solar Zenith Angle (degrees) Min	Max	Sky Conditions
1	256:1400-1800	41.4	78.6	intermittent clouds
2	259:1100-1700	39.2	68.6	cloudy
3	262:1100-1700	40.4	69.6	clear
4	263:1100-1900	40.8	92.0[a]	clear to 1500, intermittent clouds after 1500
5	264:1100-1300	41.2	55.3	intermittent clouds

[a]After sunset, during civil twilight.

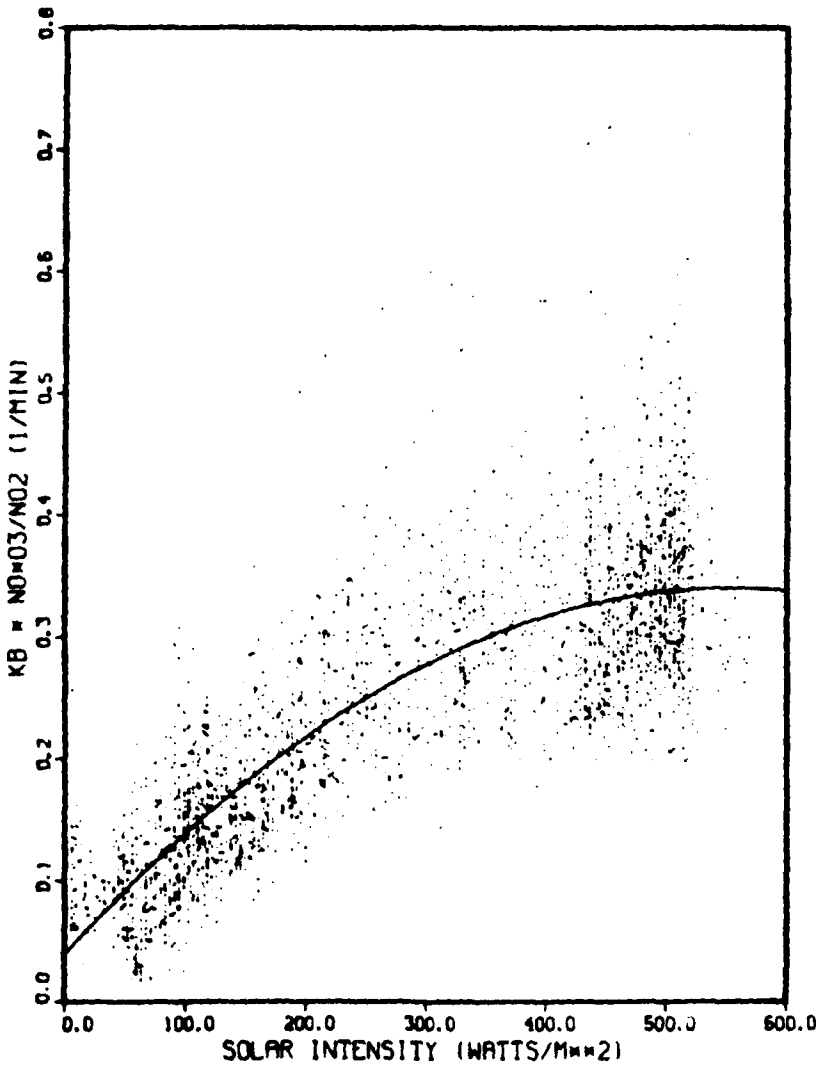

Fig. 2.10 Effective NO_2 Photolysis-Rate Coefficient Versus Solar Intensity

directional nature of the instrument response. Although an effort was made to include a variety of conditions in our study, the one day that was largely overcast (Julian day 259; Sept. 15) did not give rise to solar intensities in the upper part of the range but rather contributed mainly to the lower part of the curve in Fig. 2.10. The observed curvature is therefore considered to be in agreement with the results of other researchers.

The numerical values of $\tilde{k}_A$ in Fig. 2.10 tend to be somewhat lower than direct measurements of k_A at similar solar zenith angles, although not dramatically so. This difference may be due to any of several factors, including higher aerosol concentrations at the monitoring site than at other sites at which measurements have been made or possibly an otherwise undetected systematic bias in the concentration measurements. It seems unlikely that an actual deviation from the photostationary state would contribute to this effect, since such deviations are expected to be in the opposite direction (Bilger, 1978; Kewley, 1980). In view of the uncertainties and experimental difficulties involved, however, the general agreement of the results shown in Fig. 2.10 with expectations and with the results of other researchers is considered satisfactory. We also conclude that our data are consistent with the assumption that Eq. 2.9 is valid. Finally, this analysis also provides a valuable indication that the measurement system and data-reduction procedures are performing in a satisfactory manner.

An empirical relationship between $\tilde{k}_A$ and the pyranometer readings was developed in order that estimates of the NO_2 photolysis rate could be made, in subsequent analyses, from the solar radiation data. The solid line shown in Fig. 2.10 is the result of that fit, which was produced using a standard nonlinear least-squares regression algorithm assuming that a quadratic fit is adequate. The equation developed in this way is:

$$k_A = 3.9153 \times 10^{-3} + 1.0884 \times 10^{-3} P - 9.86136 \times 10^{-7} P^2 \qquad (2.11)$$

where $\tilde{k}_A$ is given in min^{-1} and P denotes the total solar-radiation intensity in $watts/m^2$ as measured by the pyranometer. In all subsequent work, $\tilde{k}_A$ as computed from Eq. 2.11 was used as an estimate of k_A.

2.2.2 Aircraft-Plume Photostationary-State Verification

A other basic assumption made in the NO_2-model development work is that the photostationary-state relation in Eq. 2.9 is valid at all points and at all times within an aircraft exhaust plume. Following the ambient-data analysis and the development of Eq. 2.11 as discussed in the previous section, the validity of Eq. 2.9 within aircraft plumes was examined.

Two approaches were adopted for this analysis. In the first approach, the deviations of measured values of Φ, defined as (see Sec. 3.1.3 for a discussion and definition of K):

$$\Phi = \frac{NO \cdot O_3}{K \cdot NO_2} \qquad (2.12)$$

from the value of unity that would obtain if the photostationary state relation were valid were computed, and their variation as the NO_x concentration increases was examined. Low NO_x concentrations generally correspond to ambient air and higher NO_x concentrations to points within plumes, with the highest concentrations corresponding to plume peak levels. Any systematic tendency for Φ to be higher or lower than unity, and in particular any systematic trend with increasing NO_x levels, would indicate a possible deviation within aircraft plumes from a photostationary state. On the other hand, if no significant variations from unity are observed, then it may be concluded that the data are consistent with the photostationary-state assumption. In order to carry out this approach, seven periods of heavy aircraft activity were identified, one on each of seven *different* days. In each of these periods, the passage of aircraft plumes was the dominant source of variability of the NO_x concentration. The periods were arbitrarily divided into two groups, as shown in Table 2.6. Values of the quantity Φ were computed for all points in these periods for which the NO_2 concentration was greater than or equal to 1.67 ppb, which value corresponds to a difference of one unit in the raw integer data for NO and NO_x. Without this test, points for which the digitized NO and NO_x concentrations are equal and which give rise to NO_2 values that are totally without significance cause an appreciable distortion of the results.

In order to examine the effect of increasing NO_x levels, the values of Φ were aggregated into bins corresponding to 50-ppb-wide NO_x-concentration intervals. Thus, interval No. 1 corresponds to NO_x concentrations in the range 0-50 ppb, interval No. 2 to the range 50-100 ppb, and so on. The distributions of the values of Φ within these intervals were highly skewed, primarily because of errors in estimating the NO_2 concentration, and the median value rather than the arithmetic mean was used as an indicator of the average value of Φ in each interval in the subsequent analysis. The median is a much more robust measure of the "center" of a distribution and is much less sensitive to measurement errors that give rise to outliers. The average of the median values of Φ, denoted by $\langle \Phi_{MEDIAN} \rangle$, was computed for each of the two groups, the contribution from each interval being weighted by the number of values in the interval. The value of $\langle \Phi_{MEDIAN} \rangle$ obtained in this way depended primarily on the values for the lower intervals (low NO_x concentrations) because of the relatively large number of points in those intervals. The values of $\langle \Phi_{MEDIAN} \rangle$ for the two groups of data are given in Table 2.6. Finally, the difference $\Phi_{MEDIAN} - \langle \Phi_{MEDIAN} \rangle$ was plotted against interval number (or NO_x concentration), with the results shown in Fig. 2.11.

Several features of the results shown in Fig. 2.11 are of interest. First, for small NO_x concentrations the points cluster near zero, as expected since the ambient atmosphere is on average in a photostationary state, at least for the conditions examined in this study. The Group 1 points seem to behave better in this regard than the Group 2 points, and the agreement of the

Table 2.6 Plume-Photostationary-State Analysis Periods

	Group	
	1	2
Julian date:time interval (CDT)	284:1000-1800	293:1000-1700
300:1100-2000	294:1500-1700	
303:1100-1500	295:1400-1700	
	299:0800-1700	
No. valid points	15499	10157
$\langle \Phi_{MEDIAN} \rangle$	1.094	1.404

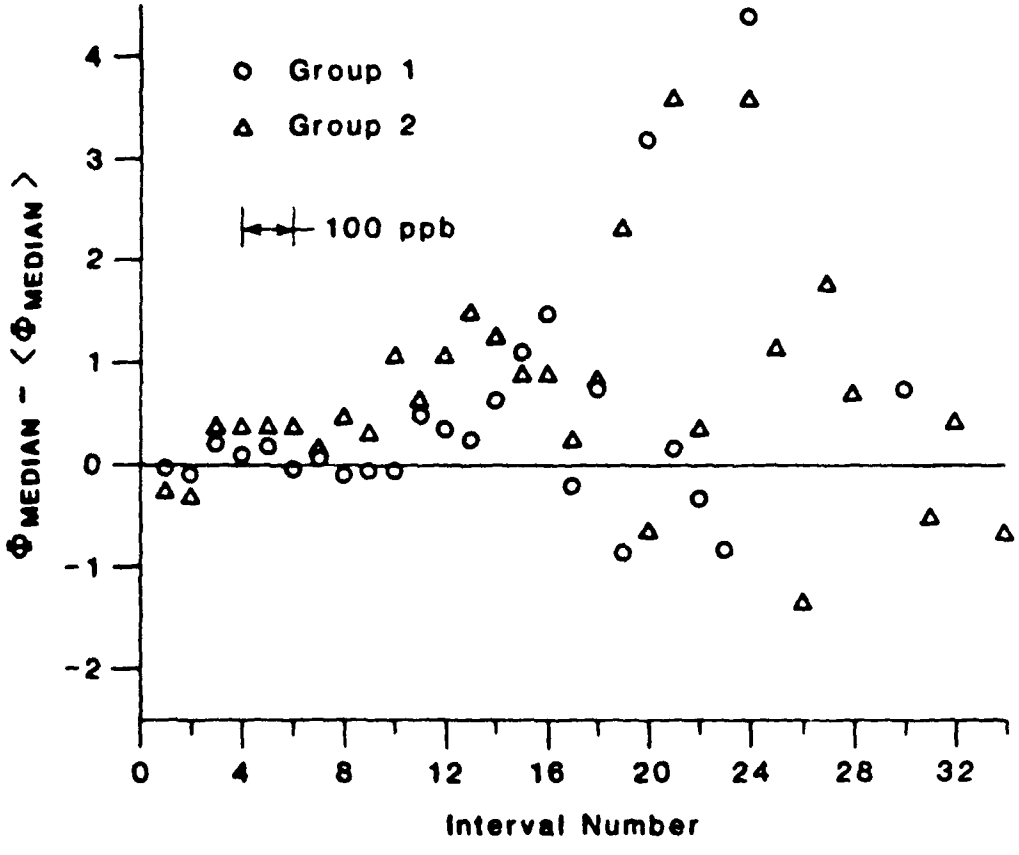

Fig. 2.11 Aircraft-Plume Photostationary-State Check

$\langle \Phi_{MEDIAN} \rangle$ value in Table 2.6 with the expected value of 1.0 is also better for Group 1. Second, there is some tendency for Φ_{MEDIAN} to be greater than $\langle \Phi_{MEDIAN} \rangle$ for intervals in the range 10-24, although the scatter is such that this tendency does not appear to be statistically significant. Finally, at the high end (24-34) there is no obvious tendency for deviation from a photostationary state, although these points correspond to a much smaller number of values of Φ than the points corresponding to lower NO_x concentrations. On the whole, this analysis reveals no significant departure from photostationary-state conditions either within or outside of aircraft plumes.

The second method of analysis makes use of data for 50 plumes selected for detailed analysis in the model-verification phase of the program. The data for these plumes are discussed more completely in Sec. 3.1.6; it suffices here to say that data for peak NO, NO_x, and O_3 concentrations are available, where "peak" implies an average over the three consecutive points at the position (or time) of maximum NO_x concentration. If Eq. 2.9 holds, the ratio NO/NO_2 is given by:

$$\frac{[NO]}{[NO_2]} = \frac{K}{[O_3]} \tag{2.13}$$

By definition, $[NO_x] = [NO] + [NO_2]$; Eq. 2.13 implies therefore that the ratio $[NO]/[NO_x]$ is given by:

$$\frac{[NO]}{[NO_x]} = \frac{K}{[O_3] + K} \tag{2.14}$$

if the photostationary state relation is valid. The quantity D, defined as $([NO]_p/[NO_x]_p) - K/([O_3]_p + K)$, was computed for each plume for which the calculation yielded meaningful results; the subscript p denotes peak value. Plumes for which $[NO]_p > [NO_x]_p$ or for which $[O_3]_p < 0.0$ (i.e., for which $[O_3]_p$ is below detectability) were discarded from this analysis. In all, 20 Boeing 727 plumes and 6 McDonnell-Douglas DC-10 plumes were used. If the plume is in a photostationary state, D is expected to be zero. The average value of D ($\bar{D}$) for the 727 plumes was found to be 0.063, with a standard deviation of 0.140, and for the DC-10 plumes, $\bar{D} = 0.012$ with a standard deviation of 0.097. In neither case was a significant departure from photostationary conditions observed.

The general conclusion reached from these analyses is that the observational data is consistent with and supports the assumption of photostationary state conditions within aircraft plumes. The use of such an assumption in the development of a model for estimating NO_2 levels within such plumes is therefore justified.

2.2.3 Estimation of NO_2/NO_x Emission Ratios

As mentioned in the previous section, a number of individual aircraft plumes were singled out for use in the model-verification phase of the program. The data for these plumes may also be used to estimate the NO_2/NO_x emission ratios, as follows. The NO_2/NO_x emission ratio is given by:

$$\frac{[NO_2]_e}{[NO_x]_e} = 1 - \frac{[NO]_e}{[NO_x]_e} \tag{2.15}$$

from the definition of NO_x. The peak observed concentration of NO_x within a plume is given by:

$$[NO_x]_p = f[NO_x]_e + (1 - f)[NO_x]_a \tag{2.16}$$

where f is the peak volume mixing ratio of aircraft exhaust gas (i.e., the fractional contribution of exhaust to the volume of gas whose composition was measured) and the subscripts p, e, and a denote peak observed, exhaust, and ambient concentrations, respectively. The ratio $[NO_x]_p/[NO_x]_a$ is therefore given by:

$$\frac{[NO_x]_p}{[NO_x]_a} = f\left\{\frac{[NO_x]_e}{[NO_x]_a} - 1\right\} + 1 \tag{2.17}$$

On the assumption that $[NO_x]_e \gg [NO_x]_a$, which is certainly valid in this case, $[NO_x]_p$ is given to good approximation by:

$$[NO_x]_p = f[NO_x]_e + [NO_x]_a \tag{2.18}$$

Also, assuming that aircraft do not emit ozone, $[O_3]_p$ would be given by:

$$[O_3]_p = (1 - f)[O_3]_a \tag{2.19}$$

if no chemical reaction with NO occurred, and $[NO]_p$ under the same assumption would be given by:

$$[NO]_p = f[NO]_e + [NO]_a \tag{2.20}$$

The stoichiometry of the chemical reaction between NO and O_3 is such that for every molecule of O_3 that disappears, one molecule of NO also vanishes (and one molecule of NO_2 appears, so that the NO_x concentration is unaffected). If

the concentration changes of O_3 and NO are denoted by ξ, ξ may be evaluated using:

$$\xi = (1 - f)[O_3]_a - [O_3]_p \tag{2.21}$$

or, assuming $f \ll 1$, from:

$$\xi = [O_3]_a - [O_3]_p \tag{2.22}$$

The assumption regarding f must be made to allow ξ to be evaluated from measured ozone concentrations, since no independent measurement of f or $[NO_x]_e$ is available for the plumes used in this analysis. The effect of the reaction is to reduce [NO] by the amount ξ, so that the observed concentration is given by:

$$[NO]_p = f[NO]_e + [NO]_a - \xi \tag{2.23}$$

Combining Eqs. 2.18, 2.22, and 2.23, the ratio $[NO]_e/[NO_x]_e$ may be evaluated in terms of measured quantities:

$$\frac{[NO]_e}{[NO_x]_e} = \frac{f[NO]_e}{f[NO_x]_e} = \frac{[NO]_p - [NO]_a + [O_3]_a - [O_3]_p}{[NO_x]_p - [NO_x]_a} \tag{2.24}$$

The data for the individual plumes used in the analysis include estimated travel times from emission to passage over the monitoring site. Including only plumes having travel times estimated at 100 seconds or less, the mean value $\bar{R}$ of the quantity $R = [NO]_e/[NO_x]_e$ was computed to be 0.935 + 0.097 (1σ) for 21 Boeing 727 plumes, and 0.932 + 0.024 (1σ) for 15 McDonnell-Douglas DC-10 plumes. If travel times less than or equal to 60 seconds are considered, $\bar{R}(727)$ becomes 0.896 (12 values) with a standard deviation of 0.100, and $\bar{R}$(DC-10) is essentially unchanged at 0.935 (9 values, $\sigma = 0.023$). There is no obvious physical explanation for the difference in the two values of $\bar{R}(727)$, and they are not statistically different given the above standard deviations. The conclusion is that the NO/NO_x emission ratio is essentially the same for 727 and DC-10 aircraft, having a value of approximately 0.93, and therefore that the NO_2/NO_x emission ratio is 0.07, or 7%, for these aircraft.

2.2.4 Relative Significance of Direct NO_2 Emissions and Chemical Conversion of NO

The individual plume measurements also allow the evaluation of the relative importance of direct emissions and NO to NO_2 conversion as contributing factors to peak (ground-level) NO_2 concentations. As discussed in the preceding sections, the quantity ξ is the NO concentration decrease due to chemical reaction and is also therefore the NO_2 concentration increase due to chemical reaction. Since ξ may be estimated by $[O_3]_a - [O_3]_p$, the fraction f_r of the peak measured NO_2 concentration that is due to chemical reaction may be estimated by:

$$f_r = \frac{[O_3]_a - [O_3]_p}{[NO_2]_p} \tag{2.25}$$

Figure 2.12 shows a plot ot values of f_r for individual 727 and DC-10 plumes against estimated travel time. In that figure, circles represent 727 plumes and triangles DC-10 plumes. Filled symbols designate points for which $[O_3]_p$ was greater than or equal to zero, and open symbols designate points for which $[O_3]_p$ was less than zero due to measurement errors for very low concentrations. In the latter cases, f_r was estimated by the ratio $[O_3]_a/[NO_2]_p$.

A clear trend towards increasing importance of chemical processes with increasing travel time is apparent in the figure. After 40 seconds travel time, chemical reaction is responsible for only about 30% of the observed NO_2 at the peak, but after 80 seconds chemical reaction contributes about 70%. Extrapolating the trend, it appears that, after about 120 seconds, between 90 and 100% of the NO_2 would be due to chemical processes. Although there are insufficient data beyond about 100 seconds to clearly show what happens, it is expected that f_r would, on the average, approach the limiting value of 1.0. It should be pointed out that, in general, the relative contributions from chemical reaction should increase with increasing ambient ozone level for a given travel time. The ambient ozone concentrations corresponding to the plumes used in this analysis ranged approximately between 20 and 40 ppb, values that are generally considered rather low. It is also worth noting that there is no obvious difference between the 727 and DC-10 plumes in this regard.

2.2.5 One-Hour NO_x and NO_2 Dosages

Thirty-two one-hour periods of aircraft activity were identified for use in the verification of model one-hour predictions. These data are described more fully in Sec. 3.2.2. It seems appropriate, however, to include here a brief discussion of the results independently of the operation of the model.

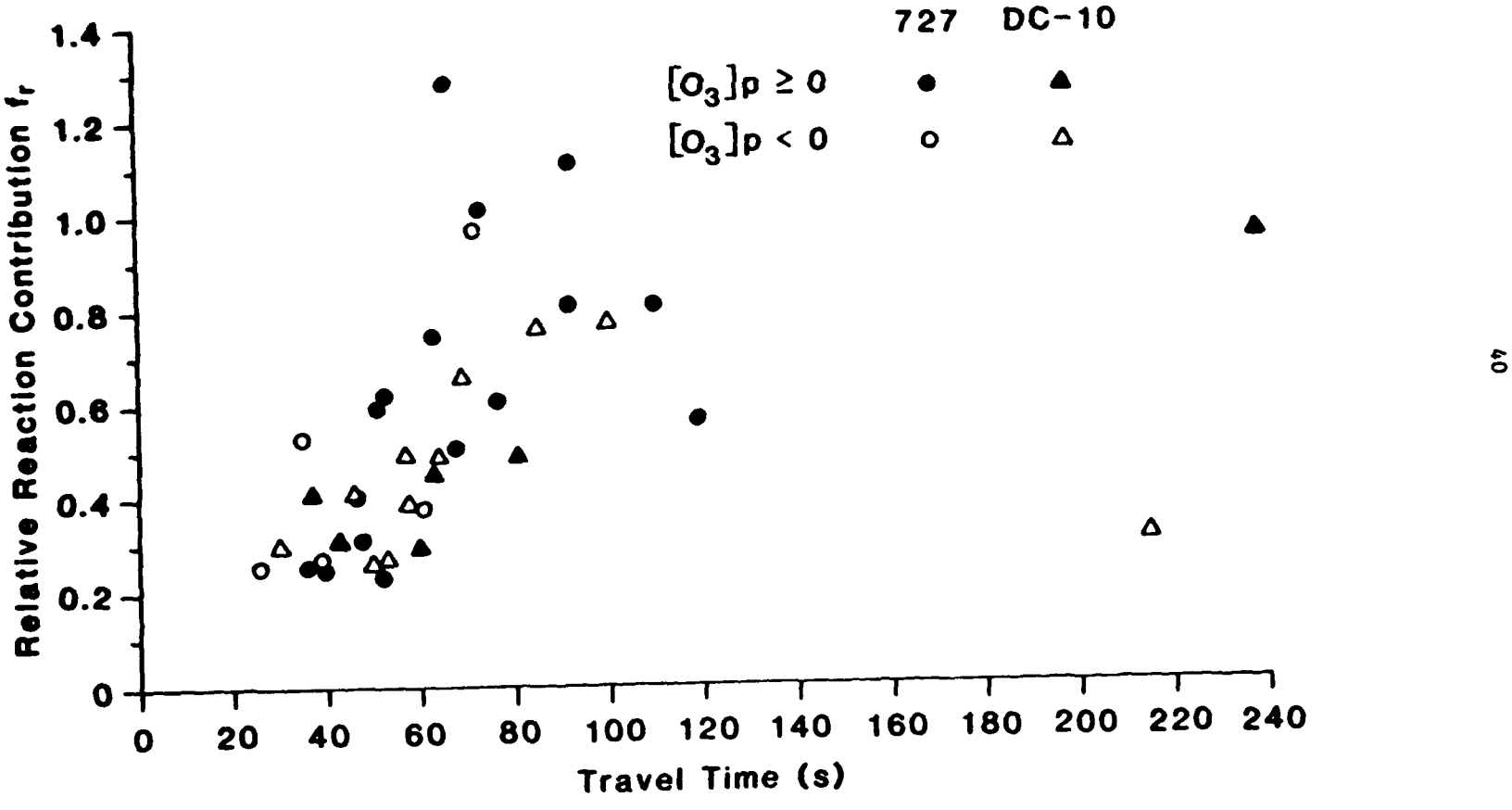

Fig. 2.12 Relative Importance of NO + O_3 Reaction in Aircraft Plumes

The periods selected for analysis were chosen primarily on the basis of a visual examination of the daily reconstituted strip charts. Considerations included the relative constancy of wind speed and direction, solar intensity, and ambient ozone level, in addition to level of aircraft activity. The number of takeoff events in any given one-hour period varied from a minimum of [illegible] to a maximum of 35. For each period, the total dose of NO_x and NO was computed by summing the products of the NO_x and NO concentrations and the basic time interval (one second) over all points in the period. The total NO_2 dose was then estimated by difference. Finally, the corresponding aircraft-related dosages were computed by subtracting estimated ambient background [illegible] from the totals.

Figure 2.13 shows the observed aircraft-related one-hour NO_x dosages plotted against the aircraft activity level measured by the number of takeoffs per hour. Figure 2.14 shows the corresponding NO_2 dosages plotted in a similar manner, with the additional feature that the open circles denote periods for which the average ozone concentration was greater than 24 ppb, and the filled circles denote periods for which the ozone concentration was less than 24 ppb, the average ozone concentration over all 32 periods.

The results shown in Figs. 2.13 and 2.14 indicate a linear relationship between the one-hour NO_x and NO_2 dosages and the number of takeoffs per hour. No attempt was made to stratify these results according to meteorological conditions or ambient concentration levels, with the exception noted in the previous paragraph. In addition, it must be pointed out that these results refer to one specific monitoring location near one particular runway. The runway used here is not as a rule used by the very largest aircraft; in particular, it is not generally used for takeoff by Boeing 747s, which have the highest NO_x emission rates. In point of fact, the most common aircraft observed to use runway 32R were 727s, DC-9s and DC-10s. The results shown in the figures would be expected to differ somewhat for other monitoring sites, including those near other runways.

Examination of Fig. 2.14 reveals a slight dependence of the results on the ozone level. Most filled circles lie below the solid line, which represents an overall best fit, as discussed in the next paragraph, while most open circles lie above it. The dependence exhibited in Fig. 2.14 is not very pronounced, due probably to the relatively low ambient-ozone levels observed during these periods in combination with the relatively short travel times that are involved and the correspondingly small contribution from the NO + O_3 reaction compared with direct NO_2 emissions (see Sec. 2.2.4 above). It is expected that the higher the ozone level, the greater the slope of the $D(NO_2)$-versus-aircraft-activity regression line would be, with the limiting value being the slope of the $D(NO_x)$-versus-aircraft-activity regression line.

The solid lines shown on the two figures represent the linear least-squares regression fits to the data and are represented by the following equations:

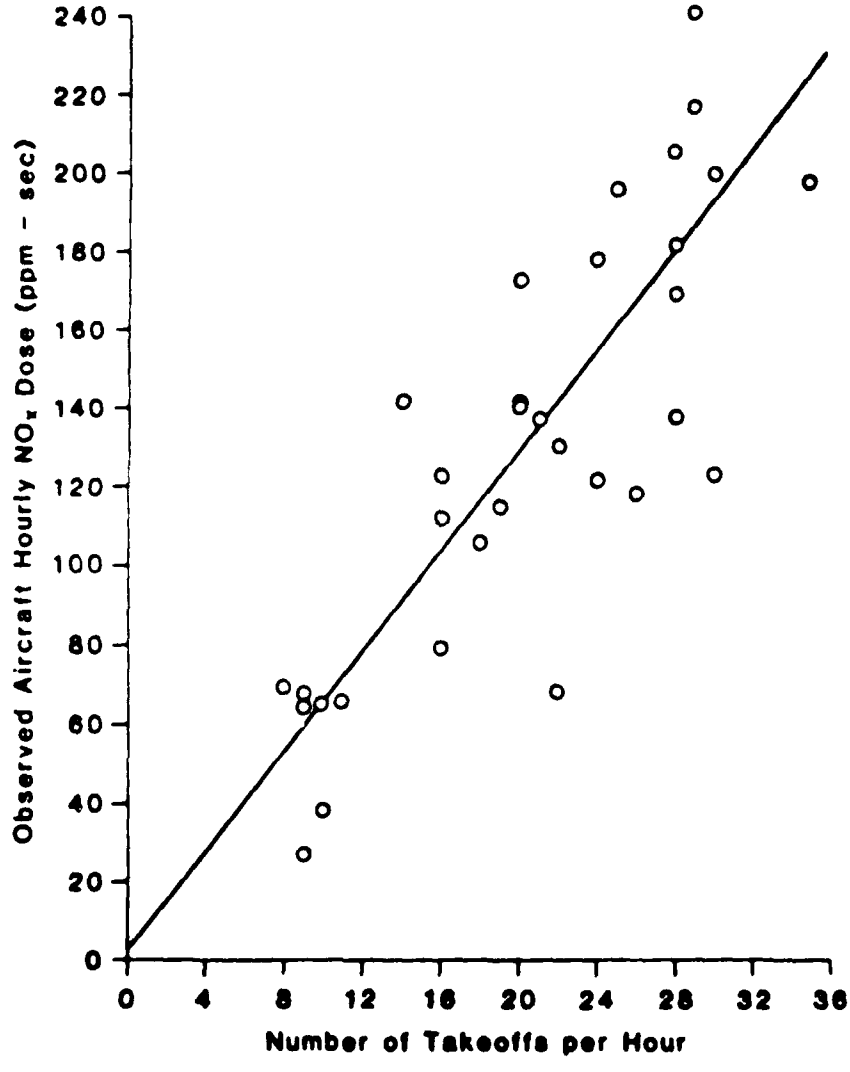

Fig. 2.13 Aircraft NO_x Dose Versus Number of Takeoffs

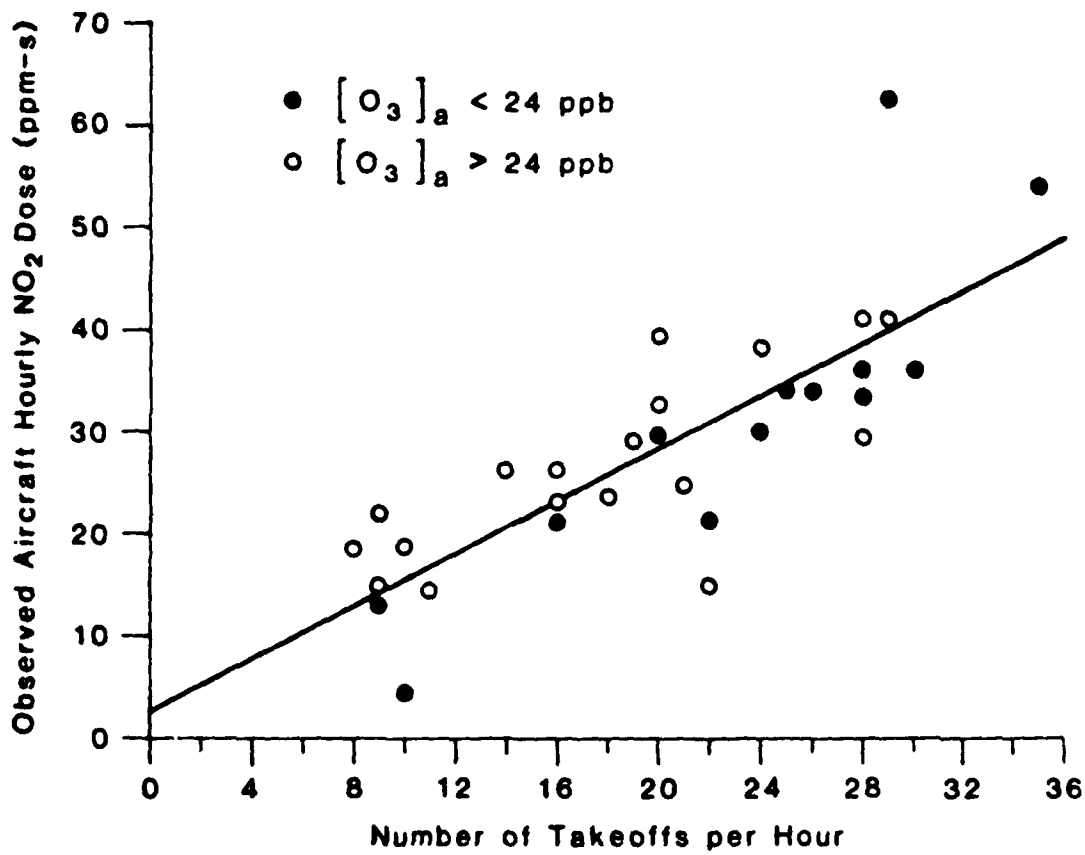

Fig. 2.14 Aircraft NO_2 Dose Versus Number of Takeoffs

$$D(NO_x) = (3.367 + 6.309A) \text{ ppm-s} \quad (2.26)$$

$$D(NO_2) = (2.761 + 1.284A) \text{ ppm-s} \quad (2.27)$$

in which $D(NO_x)$ and $D(NO_2)$ denote one-hour dosages of NO_x and NO_2, respectively, and A denotes the aircraft activity in takeoffs per hour. The intercepts are not statistically different from the expected values of zero. It is interesting and relevant to note that even at the highest level of activity, 35 takeoffs per hour, the corresponding one-hour average values of the NO_x and NO_2 concentrations (given by $D(NO_x)/3600$ and $D(NO_2)/3600$, respectively, and estimated from Eqs. 2.26 and 2.27) are only 12 ppb and 13 ppb. Thus, the actual contributions of aircraft to NO_x and NO_2 levels are fairly low in the cases examined here.

3 NITROGEN DIOXIDE MODEL DEVELOPMENT

3.1 BASIC MODEL DESIGN AND FORMULATION

The first and most important stage in the development of an air quality simulation model is the identification of an appropriate mathematical formulation. In this stage, design decisions are made that critically affect the applicability and practicability of the final computer code, and it is important to identify the physical and chemical factors that must be accurately simulated in the model in order to then incorporate suitable and mutually compatible treatments of them into the model. A fairly comprehensive discussion of the general elements that comprise an air-quality simulation model and the circumstances under which they require accurate treatment may be found in the Workbook for Comparison of Air Quality Models (USEPA, 1978b). The purpose of this section is to outline the important factors relating to the prediction of one-hour average NO_2 concentrations arising from aircraft activity at airports and to describe and justify the specific design decisions that have been made as part of the development of a model for making such predictions.

3.1.1 Treatment of Source Emission Characteristics

The emissions characteristics of the sources in question are inevitably among the most important factors to consider. With regard to NO_2 effects, the actual emission composition and the intermittent nature of the emissions are particularly relevant. Table 3.1, reproduced from Yamartino, et al. (1980b), shows the NO_x emission rates of various aircraft engines in different modes of operation. As can clearly be seen, NO_x emission rates are very much higher during takeoff than during other modes. It therefore seems entirely justifiable in the initial development to focus attention on takeoff operations only, and this is the approach adopted here. Emissions that occur when an aircraft is airborne (during approach and climbout) are, in any event, expected to have a negligible effect at ground level.

The emission rates given in Table 3.1 are those of total NO_x emissions, expressed as if the total were NO_2. However, emission measurements made on three common jet engines indicate that the NO_2/NO_x emission ratio is typically four to eight percent by volume (Pratt and Whitney, 1972, cited by Yamartino, et al., 1980a. Our results indicated 7%; see Sec. 2.2.3.). Thus, most of the NO_x emissions are actually NO rather than NO_2. If NO_2 and NO were chemically inert substances, the design of an appropriate air-quality model would be considerably simplified and could be carried out along traditional lines. However, both NO_2 and NO undergo rapid chemical reactions that, in effect, convert one species into the other and that must be taken into account in the formulation of the model. The existence of a reaction that converts NO into NO_2 is clearly significant in that such a reaction provides an alternative

Table 3.1 NO_x Emission Rates (lb/hr as NO_2) of Aircraft Engines[a]

Engine Manufacturer and Model	Taxi/ Idle	Landing	Takeoff	Approach	Climbout
Pratt and Whitney, JT9D-7	5.73	123.14	474.60	35.25	282.30
Pratt and Whitney, JT3D-7	2.23	34.29	126.40	16.35	78.60
Rolls Royce, RB-211-22B	5.31	129.31	504.10	32.26	301.90
General Electric, CF6-50C	3.02	171.29	670.95	52.80	462.20
General Electric, CF6-6D	4.88	121.77	467.50	41.54	309.20
Pratt and Whitney, JT8D-17	3.91	53.94	202.06	19.39	123.40
Rolls Royce, RDa7	0.29	2.31	8.51	0.57	5.55
Garrett AiResearch, TPE731-2	0.54	8.05	29.80	3.59	7.18
Pratt and Whitney, PT6A-27	0.28	1.25	3.32	1.80	2.80
General Electric, 700-2D	0.82	4.26	14.60	1.65	9.98
AVCO Lycoming, TIO540 J2B2	0.01	0.05	0.09	0.13	0.05

[a]All emission rates except those for landing are from Pace (1977). The landing emission rates are computed by assuming that the landing operation consists of 60% idle, 24% takeoff thrust (i.e., thrust reversers), and 16% approach thrust (to account for the spool down/up/down cycle).

mechanism to direct emission by which aircraft operations can affect atmospheric NO_2 concentrations. A discussion of the relevant chemistry is given in Sec. 3.1.3; it is sufficient here to point out that the conversion of NO to NO_2 is a nonlinear process in which the rate of conversion at a particular point in a plume depends upon the product of the NO and O_3 concentrations at that point. This type of behavior significantly complicates the mathematical formulation of a model unless simplifying assumptions can be made. Some possible assumptions will be discussed below. In general, the presence of nonlinear chemical processes implies that all NO_x sources that contribute significantly to NO_2 levels at the same time at a given receptor must be treated simultaneously. It is incorrect in principle to calculate the effects of different sources separately and then to estimate the total effect by adding them, as is commonly done in air-quality models for inert substances. The implication is that if the exhaust plume from an aircraft takeoff event overlaps or interacts with the plume from another source, including a previous takeoff event, both must be considered simultaneously. Fortunately, data taken at Washington National Airport indicate that individual takeoff plumes may in fact be considered independently, at least in the vicinity of the airport, since they are sufficiently far apart that they do not interact with each other over the distances of interest here (Yamartino, et al., 1980a). The basic approach to be used in the model is therefore to treat takeoff events on an individual basis and to predict one-hour average NO_2 concentrations in terms of these individual contributions. Under sufficiently low wind-speed conditions and sufficiently high aircraft takeoff activity, the assumption of noninteracting plumes may become invalid. In addition, the presence of a significant contribution from some other source, located either on or off the airport grounds, must generally be taken into account. In this work it is assumed that, with the exception of the takeoff plumes themselves, the trace-chemical composition of the ambient atmosphere is homogeneous in space and constant in time, at least over the one-hour period for which a prediction is to be made.

3.1.2 Treatment of Initial Jet-Plume Effects

The problem of describing the behavior of a jet takeoff-exhaust plume in the atmosphere is in some sense equivalent to that of describing the mean trajectory and evolution in size of a hot, turbulent, fluid jet emitted parallel to and some distance above a solid, plane surface into another turbulent fluid medium whose turbulence properties depend on the height above the surface and whose mean flow speed and direction bear no special relation to that of the initial jet. The evolution of such a turbulent, fluid jet is not well understood theoretically nor is it well-characterized on an observational basis. One characteristic of any fluid jet, however, is that the initial energy imparted to the fluid is eventually dissipated, and the motion and rate of growth of a jet plume in the atmosphere becomes controlled by ambient turbulence at or near the point at which the rate of dissipation of energy in the jet has decreased nearly to ambient levels. The basic philosophy adopted

in this work regarding the treatment of the dynamic effects of the initial jet velocity may be summarized by saying that (1) no attempt is made to simulate in detail the behavior of the jet plume near the engine, where the plume velocity is significantly different from the ambient wind velocity and where turbulent effects are poorly known, and (2) the model is required to describe the transport and dispersion of exhaust emissions only after that point at which ambient turbulence and meteorological conditions become the controlling factors. Specifically, the model describes the emission of a plume by a moving jet aircraft during takeoff in terms of an equivalent but dynamically passive emission at an effective (moving) source point and with an effective initial spatial distribution. The effective source location and size are determined from the initial jet-exhaust velocity and thermal content using available empirical estimates of the rate of energy dissipation in a simpler turbulent jet and the trajectory followed by a simple jet injected into a flowing medium.

The physical situation is sketched in Fig. 3.1, which shows schematically a snapshot of an exhaust plume from a single moving jet engine taken from above and looking down on the plume. The ambient wind direction is taken to be at an angle θ to the takeoff direction and, following the customary convention, the coordinate axes are defined along and perpendicular to the wind velocity. The effective source location and effective initial crosswind standard deviation σ_{yo} are shown, as are the relative orientations of the various velocities involved in the problem. In reality, at least three additional factors affect the location of the source point and the effective initial standard deviation. The first is that most commercial aircraft use more than one jet engine and therefore emit more than one exhaust plume. These plumes interact with each other, complicating the picture even further from the point of view of the dynamics of plume turbulence, and the relative vertical and horizontal separations of the engines contribute to the effective initial exhaust distribution. The second factor is that a moving aircraft generates a turbulent wake that exists over a dimension comparable to the wingspan of the aircraft. This additional turbulence also contributes to the initial spread. The third factor is that when a jet is injected into a fluid moving at an angle to the initial jet velocity, the motion of the fringes of the jet is affected by the motion of the medium earlier than the motion of the jet core is, resulting in a distortion of the shape of the jet cross-section and the possible generation of vortices (Abramovich, 1963). The distribution may become somewhat flattened on the upwind side of the jet and somewhat elongated, particularly near the top, on the downwind side. The effect is qualitatively similar to that of wind shear on elevated plumes and results in an additional enhancement of the effective crosswind spread.

Empirical descriptions of the trajectory of the center of mass of a jet emitted into a crosswind and of the rate of dissipation of turbulent energy as a function of position along that trajectory are required in order to estimate the position of the effective source point. No theoretical or experimental results seem to exist for this specific situation, and it is necessary to make the simplifying assumption that the energy dissipation rate is independent of

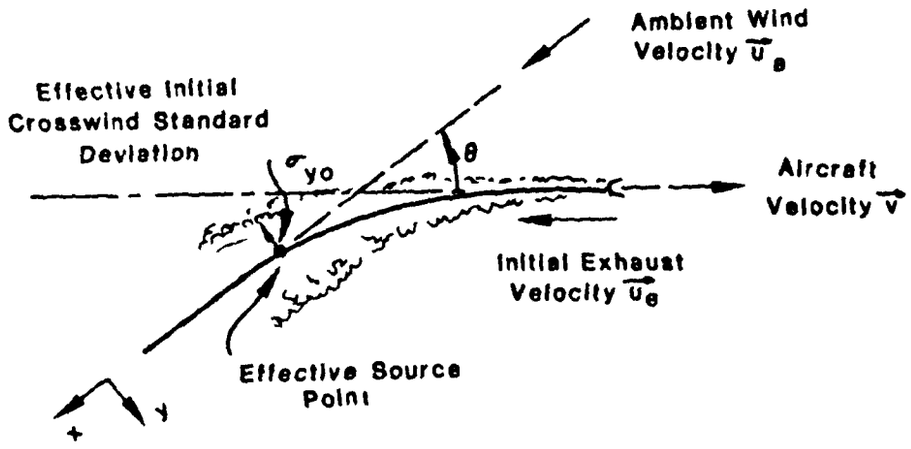

Fig. 3.1 Schematic of Jet Exhaust Plume

the shape of the trajectory. This assumption is unlikely to be strictly valid, although its validity presumably increases as the angle θ approaches zero. With the assumption, available empirical results can be used.

Abramovich (1963) summarizes the experimental results available at the time on the trajectory of a circular jet in a moving medium, and of the empirical equations given, the one most applicable to the present problem is:

$$\frac{x}{d} = \left(\frac{q_{o1}}{q_{o2}}\right)^{1.3} \left(\frac{y}{d}\right)^3 + \left(\frac{y}{d}\right)\cot\theta \tag{3.1}$$

in which d denotes the initial jet diameter and q_{o1} and q_{o2} denote the dynamic pressures in the ambient flow and in the initial jet, respectively, and are given by:

$$q_{o1} = \rho_a \frac{u_a^2}{2} \quad \text{and} \quad q_{o2} = \rho_e \frac{(u_e - v)^2}{2}$$

where ambient and exhaust densities are denoted by ρ_a and ρ_e. The origin of the coordinate system has been taken at the jet origin and the sign of the variable y in Eq. 3.1 is opposite to that shown in Fig. 3.1. The ambient wind speed is denoted by u_a, the aircraft speed by v, and the jet exhaust velocity relative to the aircraft by u_e.

Briggs (1969, 1975), in discussion of the plume rise of neutrally buoyant vertical jets in a cross-wind, gives a variety of expressions including his theoretical result (Briggs, 1975, Eq. 45, rewritten for comparison with Eq. 3.1):

$$\frac{x}{d} = \frac{4\beta^2}{3}\left(\frac{q_{o1}}{q_{o2}}\right)\left(\frac{y}{d}\right)^3 \tag{3.2}$$

Both expressions indicate that x is proportional to y^3 for $\theta = 90°$, but differ in the value of the proportionality constant. In Eq. 3.2, β is given by $0.4 + 1.2u_a/(u_e-v)$. For the case $\rho_e = \rho_a$, $u_a = 5$ m/sec, $u_e = 230$ m/sec, $v = 0$, and $\theta = 90°$, Eq. 3.1 gives $(y/d) = 0.0362(x/d)^{1/3}$ while Eq. 3.2 gives $(y/d) = 0.0485\ (x/d)^{1/3}$. Thus the predicted values of y using the two equations differ by a constant factor, $0.0352/0.0485 = 0.75$ in this case. An uncertainty of this magnitude is not unreasonable, and the plume trajectory given by Eq. 3.1 was initially chosen for use in this work simply because the dependence on the angle θ is explicitly given.

The evolution of an axisymmetric, neutrally buoyant jet emitted into an effectively infinite unbounded space containing a coflowing or stationary fluid has received considerable experimental and theoretical attention (see Abramovich, 1963; Hinze, 1975; and Tennekes and Lumley, 1972, for discussions). Tennekes and Lumley give the following expressions for the peak

excess velocity u_J in such a jet and the standard deviation σ in the cross-flow direction of the jet velocity distribution:

$$\frac{u_J}{u_{Jo}} = 6.4\left(\frac{d}{s}\right) \text{ and } \sigma = 0.067s$$

in which s denotes the distance from the jet origin measured along the trajectory (which is straight along the symmetry axis in this simple case), and u_{Jo} is the initial excess velocity above the ambient flow velocity. The factor 0.067 in the expression for σ may be interpreted as the tangent of half the angle ϕ subtended by the length 2σ at a distance s from the origin; the corresponding value of ϕ is 7.6°. If instead an angle of ϕ = 9°-12° (Tank and Hodder, 1978) is used, the factor is in the range 0.079-0.105. The above expressions for u_J/u_{Jo} and σ, in combination with the plume trajectory, Eq. 3.1, and an expression for the energy dissipation rate as a function of u_J and σ, allow the estimation of the effective source point and initial spread. According to Tennekes and Lumley (1972; see also Briggs, 1975), the energy-dissipation rate ε_J within a circular jet may be written as:

$$\varepsilon_J = A\frac{u_J^3}{\sigma} \tag{3.3}$$

in which A is a dimensionless coefficient of order unity. Substitution for u_J and σ in terms of s gives:

$$\varepsilon_J = \frac{2.6 \times 10^2 \, A}{\tan(\phi/2)}\left(\frac{u_{Jo}^3}{d}\right)\left(\frac{s}{d}\right)^{-4} \tag{3.4}$$

The effective source point is defined as that point on the plume trajectory at which $\varepsilon_J = B\varepsilon_a$, where ε_a denotes the ambient turbulent energy dissipation rate and B is a coefficient in the range 1 to 10. If the distance along the plume trajectory from the jet engine to the effective source point is denoted by s', then s' may be evaluated in terms of ε_a and the characteristics of the jet engine:

$$\frac{s'}{d} = 4\left(\frac{A}{B}\right)^{1/4}\left[\frac{1}{\varepsilon_a \tan(\phi/2)}\left(\frac{u_{Jo}^3}{d}\right)\right]^{1/4} \tag{3.5}$$

The initial exhaust velocity of the jet may be written in terms of the thrust F produced by the engine and the exhaust density ρ_e:

$$u_e = \frac{2}{d}\left(\frac{F}{\pi\rho_e}\right)^{1/2} \tag{3.6}$$

and u_{Jo} is given by:

$$u_{Jo} = |u_e - v - u_a\cos\phi| \tag{3.7}$$

Taking $\phi = 10.5°$ and A/B = 1 and collecting constants in Eq. 3.5, the expression for s'/d becomes:

$$\frac{s'}{d} = 7.3\left[\frac{1}{\varepsilon_a}\left(\frac{u_{Jo}^3}{d}\right)\right]^{1/4} \tag{3.8}$$

with the value of the coefficient 7.3 uncertain by perhaps plus or minus 50%.

Thus, by virtue of Eqs. 3.1 and 3.8, the plume trajectory and the location on it of the effective source point may be estimated for a single jet. Referring to Fig. 3.2, which is simply Fig. 3.1 redrawn to shown distance and angle relationships more clearly, it can be seen that once the distances x' and y' are determined from the distance s' and the known path of the plume, the distances $l_\parallel$ and $l_\perp$ may be found from:

$$\begin{aligned} l_\parallel &= x'\cos\theta + y'\sin\theta \\ l_\perp &= x'\sin\theta - y'\cos\theta \end{aligned} \tag{3.9}$$

In Fig. 3.2, the effective source location is identified by a black dot. A mathematical inconvenience arises at this point in that analytic expressions for x' and y' in terms of s' and θ cannot be found, and these distances are determined using an appropriate numerical procedure in the computer code.

Use has been made throughout this discussion of empirical results relating to a circular jet in an unbounded medium. No account has been taken of the effects of the ground surface. Abramovich (1963) gives some information about these effects, but very recently a paper by Davis and Winarto (1980) has appeared that contains the result of an experimental investigation into precisely the effects in question. The results described in that paper indicate that the treatment of the effective source location is reasonably valid. Particularly interesting results are given for the relative rates of vertical and horizontal spreading of the plume. In unbounded space, an initially axisymmetric jet in a stationary or coflowing medium remains axisymmetric, there being nothing to disrupt this symmetry. The results of Davis and Winarto indicate, however, that the ratio of the horizontal and vertical spreading rates approaches a limiting value of about 8.5 at large distances from the jet nozzle. This observation may have very significant implications for the estimation of the effective initial-plume standard deviations σ_{yo} and σ_{zo}.

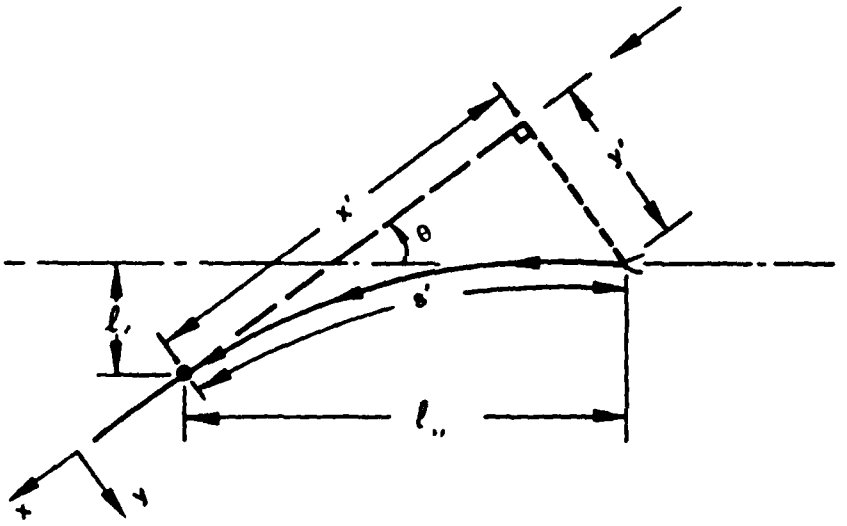

Fig. 3.2 Jet Exhaust-Plume Geometry

No mention has been made thus far of the plume rise in takeoff plumes. This effect is certainly significant; however, no measurements were initially available with which to estimate the rise of such a plume. The approach adopted in this work to simulate takeoff plume rise is discussed in Sec. 3.1.6.

3.1.3 Treatment of Chemistry

As indicated earlier, both NO_2 and NO undergo rapid chemical reactions in the atmosphere and, in particular, NO may be converted to NO_2, thereby making all of the NO_x emissions relevant to the problem at hand rather than just that small fraction that is actually NO_2. Several factors affect the choice of a suitable treatment of these processes, including the details of the chemistry involved; the rates of the various reactions; the availability of data on specific reaction rates, emissions, and other quantities; the desired model accuracy; and the practicality of alternative approaches. Before considering alternative treatments, a brief discussion of the important chemical facts is in order.

The principal chemical reactions that govern ambient NO_2 concentrations are (Seinfeld, 1977; Demerjian et al., 1974):

$$NO_2 \xrightarrow{h\nu} NO + O \qquad (A')$$

$$O + O_2 + M \longrightarrow O_3 + M \qquad (A'')$$

$$NO + O_3 \longrightarrow NO_2 + O_2 \qquad (B)$$

Reaction A'' is very fast, due to the high ambient concentration of molecular oxygen in the atmosphere, and as a result reactions A' and A'' may be combined into a net reaction A:

$$NO_2 + O_2 \xrightarrow{h\nu} NO + O_3 \qquad (A)$$

the rate of which is the same as the rate of NO_2 photolysis, reaction A'. The hν denotes the presence of light of suitable wavelength. The rate of reaction A (i.e., the change in NO_2 concentration per unit time due to reaction A) is given by the expression $k_A[NO_2]$, where k_A is the rate coefficient and $[NO_2]$ denotes the number density or concentration of NO_2. Similarly, the rate of reaction B is given by the expression $k_B[NO][O_3]$. The rates of these reactions depend therefore on the concentrations and on the values of rate coefficients, which in turn depend on ambient conditions. The coefficient k_A depends on the light intensity in the wavelength range $\lambda \leq 420$ nm, which leads to photodissociation, and is mainly a function of altitude and solar angle. The possible values of k_A at ground level range from 0 to approximately 0.60 min^{-1} for an overhead sun (Calvert, 1976). The coefficient k_B is a function of temperature, and is given by:

$$k_B = 2.3 \times 10^{-12} \exp(-1450/T) \text{ cm}^3 \text{ sec}^{-1}$$

or, for a total atmospheric pressure P (atmospheres), by:

$$k_B = 1.01 \times 10^6 \left(\frac{P}{T}\right) \exp(-1450/T) \text{ ppm}^{-1} \text{min}^{-1}$$

(Hudson and Reed, 1979; Hampson, 1980), T being the temperature in degrees Kelvin. At 25°C and a total pressure of one atmosphere, $k_B = 26.2$ ppm^{-1} min^{-1}. Figure 3.3 exhibits the temperature dependence of k_B in the form of a plot of log k_B versus 1000/T for a total pressure of one atmosphere.

Mention should be made of the effect of hydrocarbons on the NO_2 concentrations. As is well known, the presence of certain types of hydrocarbons leads to the production of significant amounts of ozone and a corresponding conversion of NO to NO_2 over periods of time on the order of an hour or more (Demerjian et al., 1974; Finlayson-Pitts and Pitts, 1977); see also Sec. 5 of this report. In the discussion to follow, we will be concerned only with estimating NO_2 concentrations in the immediate vicinity of an airport, at distances for which the travel time is typically much less than one hour. The effect of the presence of hydrocarbons will therefore be ignored in the formulation of the model.

Mention should also be made of the effect of other reactive species present in the atmosphere. Nitric oxide may be converted to NO_2 by reaction with, for example, atomic oxygen, NO itself (in the presence of molecular oxygen), and free radical species such as HO_2 and RO_2, where R denotes an organic component. Reaction of NO with HO_2 and RO_2 is known to be important in the generation of photochemical smog (Demerjian et al., 1974). Nitrogen dioxide may also be converted to other substances by reaction with O_3 and free radicals, primarily OH, HO_2, and organic oxygenated radicals. An examination of the relevant rate constants, in combination with concentration estimates, indicates, however, that reactions A and B are the two most important reactions for typical urban atmospheric conditions, although the significance of reaction A clearly decreases with the light intensity and vanishes at night. Other reactions, thought to proceed by heterogeneous mechanisms, may be significant over time scales of an hour or more, particularly at night.

As a result of the relative rapidity of reactions A and B, an approximate "photostationary state" (Leighton, 1961) may exist in which the net effects of these reactions balance each other; note that they are essentially the reverse of each other. Equating the two rate expression yields the photostationary-state relation:

$$\frac{[NO][O_3]}{[NO_2]} = \frac{k_A}{k_B} \equiv K \qquad (3.10)$$

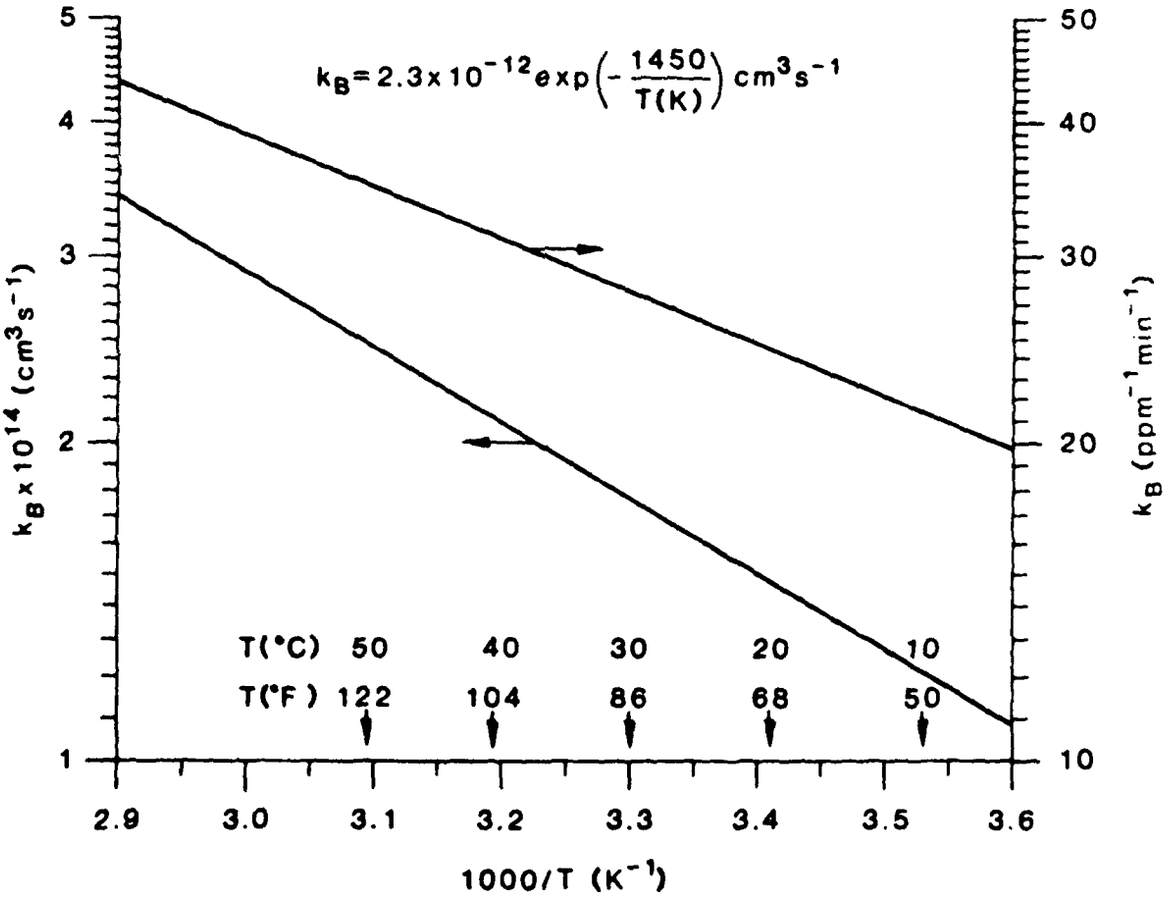

Fig. 3.3 Temperature Dependence of NO + O_3 Reaction-Rate Coefficient

Under certain conditions, to be discussed below, Eq. 3.10 can be used as the basis for predicting NO_2 concentrations, given information regarding the NO_x source strength and ambient dispersion rates and concentrations of NO_2, NO, and O_3 (Peters and Richards, 1977). The utilization of Eq. 3.10 will be designated as the "photostationary-state" approach.

For some purposes, a simpler approach may be adopted in which the effects of reaction A are ignored. This approach, the "ozone-limiting" method, can be shown to be a special case of the photostationary-state approach and to represent an overestimate or upper bound to the true NO_2 concentration within a plume. The ozone-limiting method consists of estimating the NO_2 concentration as the sum of a contribution from direct NO_2 emissions, a background level, and a contribution from NO conversion equal to the smaller of the ambient O_3 concentration and the NO concentration from the source in question, estimated as if no chemical processes were operating. This procedure amounts to assuming that k_A is zero and k_B is infinitely large, with the ratio K equal to zero. Since this method is easy to apply and is guaranteed to produce an upper bound to the NO_2 concentration, it may be considered suitable for many purposes. A complication arises in the case of continuous releases, in which the treatment of the dispersion of the plume becomes important. The approach adopted here, that of treating individual takeoff events, avoids this complication.

The photostationary-state approach is not always appropriate in principle. In particular, the rates of reactions A and B may not be fast enough to establish and maintain a composition satisfying Eq. 3.10 if perturbations that cause deviations from that composition are present and act with sufficient rapidity. Such perturbations might include rapid variations in the ambient light intensity and, hence, in the value of k_A, and rapid mixing with air of a different composition. It is possible to develop criteria for identifying such cases, based on the chemical "relaxation time" (τ) of the photostationary state and the characteristic time scales involved in the perturbation considered. For example, the NO_2 concentration at a point in a plume divided by the rate of change of the NO_2 concentration due to a rapid dispersion or mixing process provides an indication of the dispersion time scale. If that time scale is comparable to or larger than τ, the composition would not be expected to satsify Eq. 3.10. Conversely, perturbations having time scales much less than τ would indeed alter the concentrations of NO_2, NO, and O_3 at each point, but those concentrations would be expected to satisfy Eq. 3.10 very nearly because in that case the chemical reactions proceed rapidly enough to maintain the photostationary state. An expression for τ in terms of the rate coefficients k_A and k_B and the steady-state NO and O_3 concentrations may be derived; this derivation is carried out in Appendix I as part of a discussion of the exact analytic expressions for the NO_2, NO, and O_3 concentrations as functions of time in a spatially homogeneous system. The expression is:

$$\tau = \frac{1}{k_A + k_B\left([NO]_{ss} + [O_3]_{ss}\right)} \qquad (3.11)$$

in which the subscript ss denotes "stationary state". Plots of τ versus $[NO]_{ss} + [O_3]_{ss}$ for various values of k_A are given in Fig. 3.4. In that figure, k_B is taken to be 24.0 ppm^{-1} min^{-1}, corresponding to a temperature of about 19°C (66°F). As can be seen from the figure, the relaxation time for a perhaps typical mid-plume situation, in which $[NO]_{ss}$ is 0.2-0.3 ppm and $[O_3]_{ss}$ is very small by comparison, is on the order of 10 seconds. Based on this estimate, it is expected that the photostationary-state expression, Eq. 3.10, should be very nearly satisfied within the takeoff plume of an aircraft, the characteristic dispersion time scale being much smaller than this. As discussed in Sec. 2.2.2, our results verify this expectation.

Observational support for the use of Eq. 3.10 in a model is also provided by measurements made in plumes from fossil-fuel-fired power plants (Hegg, et al., 1976, 1977; White, 1977; Bowen and Stearns, 1977). These studies all indicate that reactions A and B are sufficient to explain the observed concentrations and that the rate of conversion of NO to NO_2 within a plume as a whole is governed by the rate at which the plume disperses and entrains ambient air containing ozone. The latter conclusion implies that the chemistry is fast enough to maintain a photostationary state, so that the process limiting the conversion rate is plume dispersion. Nitrogen oxide chemistry within power-plant plumes has been simulated in smog chamber experiments by Spicer and co-workers (Spicer, et al., 1981 and Sverdrup, et al., 1982). Equation 3.10 has also been verified directly in smog-chamber experiments (O'Brien, 1974) and in polluted urban atmospheres (Calvert, 1976; Stedman and Jackson, 1975). Our ambient concentration measurements are also consistent with Eq. 3.10, as discussed in Sec. 2.2.1. The work of Eastman and Stedman (1980) may be consulted for a demonstration of the dynamic response of ambient O_3 levels to a variation in light intensity due to a partial solar eclipse (see also Babe et al., 1980).

It is interesting to note that systematic departures from the photostationary-state relation have also been observed (Ritter et al., 1979, and Kelly et al., 1980). These observations were made in "clean" rural sites in northern (lower) Michigan and in Colorado, and reactions involving peroxy radicals such as HO_2 and RO_2 are suggested as a possible reason for the departures from Eq. 3.10.

The arguments and evidence just presented, as well as the results obtained in this program, indicate that the photostationary-state approach is suitable for use in a model for predicting NO_2 levels within aircraft takeoff plumes, and it has been adopted. It is also necessary to assume that the ambient NO_2, NO, and O_3 concentrations satisfy Eq. 3.10; as indicated above, this assumption is supported by observations made in urban areas but not in clean rural areas. Even in very clean areas, however, the assumption of an ambient photostationary state is very unlikely to lead to significant error in predicting aircraft impacts on NO_2 levels since, because of the relatively high plume concentrations of NO, a stationary state is expected within the plume even if it does not hold in the ambient air. The assumption is

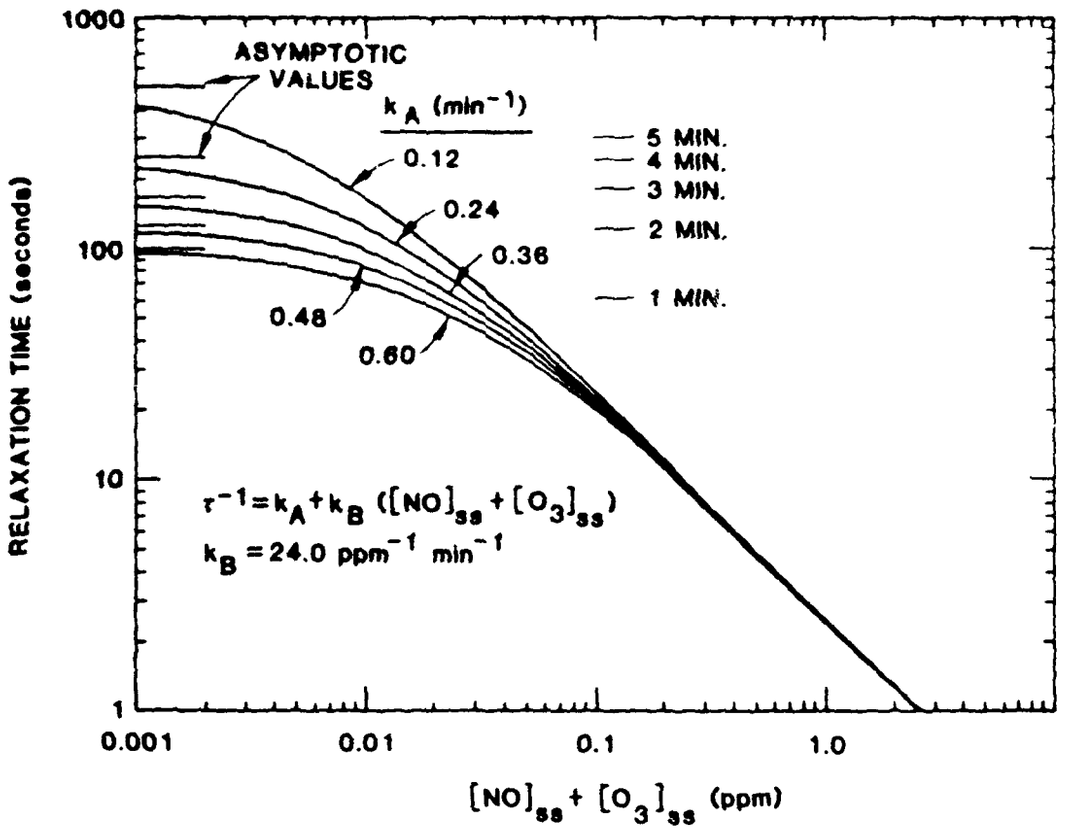

Fig. 3.4 NO_2-NO-O_3 Photostationary State Relaxation Time

necessary, however, in order to avoid certain mathematical inconsistencies in the model.

In order to utilize Eq. 3.10 to predict NO_2 concentrations within a plume, one needs to be able to predict the concentrations of NO_2, NO, and O_3 assuming that no reactions take place, i.e., as if these substances were chemically inert. If the volume mixing ratio of jet exhaust gas at a point in the plume is denoted by f, then the concentration of some inert substance X at that point is given by:

$$[X] = f[X]_e + (1-f)[X]_a \tag{3.12}$$

where subscripts e and a denote exhaust and ambient concentrations, respectively. The mixing ratio f is defined as the fraction of a small volume of gas, located at the point in question, that is exhaust gas, so that 1 - f is the fraction that is entrained ambient air. If the NO_2, NO, and O_3 concentrations predicted using Eq. 3.12 are denoted by $[NO_2]_o$, $[NO]_o$, and $[O_3]_o$, the application of the photostationary-state relation amounts to correcting these concentrations for the effects of reactions A and B. This correction is accomplished using:

$$[NO_2]_{ss} = [NO_2]_o + \xi_{ss} \tag{3.13a}$$

$$[NO]_{ss} = [NO]_o - \xi_{ss} \tag{3.13b}$$

$$[O_3]_{ss} = [O_3]_o - \xi_{ss} \tag{3.13c}$$

with ξ_{ss} given by (see Appendix 1 for a derivation):

$$\xi_{ss} = \frac{1}{2}\left\{a + K - \left[b^2 + K\,4[NO_2]_o + 2a + K\right]^{1/2}\right\} \tag{3.14a}$$

with

$$a = [NO]_o + [O_3]_o \tag{3.14b}$$

$$b = [NO]_o - [O_3]_o \tag{3.14c}$$

The corrected concentrations are the predicted concentrations, using this approach. The ozone-limiting approach amounts to setting K = 0 in Eq. 3.14a, which then becomes simply:

$$\xi_{ol} = (a - |b|)/2 \tag{3.15}$$

Thus, the ozone-limiting approach is a special case of the photostationary-state approach and the two are equivalent at night, when $k_A = 0$.

The formulation of a general approach to time-dependent models, such as is required here, has been given by Lamb and Seinfeld (1973) and was adopted in slightly modified form in this program. The basic equation for the prediction of the concentration of an inert substance was taken to be:

$$C(\vec{x},t) = \int_{-\infty}^{t} dt' \int_{-\infty}^{\infty} d\vec{x}' C(\vec{x}',t') P(\vec{x},t;\ \vec{x}',t') \tag{3.18}$$

in which $C(\vec{x},t)$ denotes the concentration at position $\vec{x}(= x,y,z)$ at time t, $C(\vec{x}',t')dt'$ the concentration increase at position $\vec{x}'$ due to emissions over the time interval from t' to t' + dt', and $P(\vec{x},t;\ \vec{x}',t')dx'$ the fractional contribution to $C(\vec{x},t)$ from material located in volume element $d\vec{x}'$ at position $\vec{x}'$ at time t'. $P(\vec{x},t;\ \vec{x}',t')$ is essentially a normalized distribution function that describes the transport and dispersion processes that cause an emission at $(\vec{x}',t')$ to affect concentrations at $(\vec{x},t)$; P is usually referred to as the transport kernel. The first basic assumption adopted in this formulation is that the transport kernel is Gaussian and depends only on the travel time t-t':

$$P(\vec{x},t;\vec{x}',t') = F_p(x,x';t-t')G_p(y,y';t-t')S_p(z,z';t-t') \tag{3.19}$$

with

$$F_p(x,x';t-t') = \frac{1}{(2\pi)^{1/2}\sigma_x} \exp\left[-\frac{1}{2}\left(\frac{x-x'-\bar{u}(t-t')}{\sigma_x}\right)^2\right] \tag{3.20}$$

$$G_p(x,x';t-t') = \frac{1}{(2\pi)^{1/2}\sigma_y} \exp\left[-\frac{1}{2}\left(\frac{y-y'}{\sigma_y}\right)^2\right] \tag{3.21}$$

$$S_p(z,z';t-t') = \frac{1}{(2\pi)^{1/2}\sigma_z}\left\{\exp\left[-\frac{1}{2}\left(\frac{z-z'}{\sigma_z}\right)^2\right] + \exp\left[-\frac{1}{2}\left(\frac{z+z'}{\sigma_z}\right)^2\right]\right\} \tag{3.22}$$

In these expressions, σ_x, σ_y, and σ_z are functions of the travel time t-t', $\bar{u}$ denotes the mean wind speed over the travel time, and perfect reflection at ground level has been assumed in Eq. 3.22. The x-axis is taken in the direction of the mean wind-velocity vector, and the wind velocity is implicitly assumed to be homogeneous in the region between source and observer. Furthermore, the dispersion coefficients σ_x and σ_y are assumed to be equal for all travel times, and will be denoted by σ_h, the horizontal dispersion coefficient. It can be seen by an examination of Eqs. 3.19-3.22 that the transport kernel has the form of a Gaussian puff, which is released at $(\vec{x}',t')$ and contributes to the concentration at $(\vec{x},t)$.

The second basic assumption is that the effective initial source distribution is also Gaussian:

3.1.4 Treatment of Transport and Dispersion

In order to be compatible with the treatment of chemical effects discussed in the previous section, the treatment of transport and dispersion used in the NO_x model was required to predict the "initial" concentrations of NO, NO_2, and O_3, i.e., those which would exist within the plume if no chemical reactions took place. These concentrations were denoted $[NO]_o$, $[NO_2]_o$, and $[O_3]_o$ in the previous section. The effects of chemistry are then handled by the photostationary-state method, and the predicted "true" concentrations are those obtained using Eqs. 3.13 and 3.14. In order for this approach to be valid, however, the initial concentrations must be predicted for a particular instant in time and for a particular location at that instant; in other words, the model must be capable of describing individual true, physical plumes and not simply time-averaged concentrations from one or more plumes.

To see why this requirement arises, consider a simple example in which for a time interval $\Delta t/2$ constant initial concentration values of x_{o1}, y_{o1}, and z_{o1} are predicted (with x denoting $[NO_2]$, y denoting [NO], and z denoting $[O_3]$) and for the next time interval $\Delta t/2$ different constant initial values x_{o2}, y_{o2}, and z_{o2} are predicted. When the photostationary-state procedure described in the previous section is applied separately to these two time intervals, two different values of ξ_{ss}, denoted by ξ_1 and ξ_2, are produced and the predicted NO_x concentrations, including chemical effects, are given by $x_{o1} + \xi_1$ and $x_{o2} + \xi_2$. If, however, only the average initial concentrations over the entire interval Δt, denoted $\tilde{x}_o$, $\tilde{y}_o$, and $\tilde{z}_o$, are predicted by the transport and dispersion algorithm, and if these values are inserted into Eq. 3.14 to produce the corresponding value of ξ (denoted by $\tilde{\xi}$), the predicted NO_2 concentration value $\tilde{x}$ would be given by

$$\tilde{x} = \tilde{x}_o + \tilde{\xi} = \frac{1}{2}(x_{o1} + x_{o2}) + \tilde{\xi} \tag{3.16}$$

The true average NO_2 concentration over the entire time interval Δt is given by:

$$\bar{x} = \frac{1}{2}(x_1 + x_2) = \frac{1}{2}(x_{o1} + x_{o2}) + \frac{1}{2}(\xi_1 + \xi_2) \tag{3.17}$$

Comparison of these two equations shows that, while the initial (pre-chemical-reaction) concentrations may be averaged to obtain the correct average no-chemistry value, the correction for the effects of chemistry are not the same in the two cases because ξ is not a linear function of the initial concentration values. In other words, since $\tilde{\xi}$ is not equal to $(\xi_1 + \xi_2)/2$, $\tilde{x}$ is not equal to $\bar{x}$. In general, in order to predict the true average NO_2 concentration, separate predictions must be made at a (possibly large) number of times and then averaged. This is especially the case when emissions occur only intermittently and large fluctuations in the initial concentrations occur at the location for which predictions are to be made. This is precisely the situation with regard to air wait effects from takeoff events, although it is also the case for continuous plumes because of the meandering of such plumes.

The formulation of a general approach to time-dependent models, such as is required here, has been given by Lamb and Seinfeld (1973) and was adopted in slightly modified form in this program. The basic equation for the prediction of the concentration of an inert substance was taken to be:

$$C(\vec{x},t) = \int_{-\infty}^{t} dt' \int_{-\infty}^{\infty} d\vec{x}' C(\vec{x}',t') P(\vec{x},t;\ \vec{x}',t') \tag{3.18}$$

in which $C(\vec{x},t)$ denotes the concentration at position $\vec{x}(= x,y,z)$ at time t, $C(\vec{x}',t')dt'$ the concentration increase at position $\vec{x}'$ due to emissions over the time interval from t' to t' + dt', and $P(\vec{x},t;\ \vec{x}',t')dx'$ the fractional contribution to $C(\vec{x},t)$ from material located in volume element $d\vec{x}'$ at position $\vec{x}'$ at time t'. $P(\vec{x},t;\ \vec{x}',t')$ is essentially a normalized distribution function that describes the transport and dispersion processes that cause an emission at $(\vec{x}',t')$ to affect concentrations at $(\vec{x},t)$; P is usually referred to as the transport kernel. The first basic assumption adopted in this formulation is that the transport kernel is Gaussian and depends only on the travel time t-t':

$$P(\vec{x},t;\vec{x}',t') = F_p(x,x';t-t')G_p(y,y';t-t')S_p(z,z';t-t') \tag{3.19}$$

with

$$F_p(x,x';t-t') = \frac{1}{(2\pi)^{1/2}\sigma_x} \exp\ -\left[\frac{1}{2}\left(\frac{x-x'-\bar{u}(t-t')}{\sigma_x}\right)^2\right] \tag{3.20}$$

$$G_p(x,x';t-t') = \frac{1}{(2\pi)^{1/2}\sigma_y} \exp\left[-\frac{1}{2}\left(\frac{y-y'}{\sigma_y}\right)^2\right] \tag{3.21}$$

$$S_p(z,z';t-t') = \frac{1}{(2\pi)^{1/2}\sigma_z}\left\{\exp\left[-\frac{1}{2}\left(\frac{z-z'}{\sigma_z}\right)^2\right] + \exp\left[-\frac{1}{2}\left(\frac{z+z'}{\sigma_z}\right)^2\right]\right\} \tag{3.22}$$

In these expressions, σ_x, σ_y, and σ_z are functions of the travel time t-t', $\bar{u}$ denotes the mean wind speed over the travel time, and perfect reflection at ground level has been assumed in Eq. 3.22. The x-axis is taken in the direction of the mean wind-velocity vector, and the wind velocity is implicitly assumed to be homogeneous in the region between source and observer. Furthermore, the dispersion coefficients σ_x and σ_y are assumed to be equal for all travel times, and will be denoted by σ_h, the horizontal dispersion coefficient. It can be seen by an examination of Eqs. 3.19-3.22 that the transport kernel has the form of a Gaussian puff, which is released at $(\vec{x}',t')$ and contributes to the concentration at $(\vec{x},t)$.

The second basic assumption is that the effective initial source distribution is also Gaussian:

$$C(\vec{x}',t') = Q(t')F_o(x',x_o)G_o(y',y_o)S_o(z',z_o) \tag{3.23}$$

with

$$F_o(x',x_o) = \frac{1}{(2\pi)^{1/2}\sigma_{ho}} \exp\left[-\frac{1}{2}\left(\frac{x'-x_o}{\sigma_{ho}}\right)^2\right] \tag{3.24}$$

$$G_o(x',x_o) = \frac{1}{(2\pi)^{1/2}\sigma_{ho}} \exp\left[-\frac{1}{2}\left(\frac{y'-y_o}{\sigma_{ho}}\right)^2\right] \tag{3.25}$$

$$S_o(z',z_o) = \frac{1}{(2\pi)^{1/2}\sigma_{zo}} \left\{\exp\left[-\frac{1}{2}\left(\frac{z'-z_o}{\sigma_{zo}}\right)^2\right] + \exp\left[-\frac{1}{2}\left(\frac{z'+z_o}{\sigma_{zo}}\right)^2\right]\right\} \tag{3.26}$$

In these equations, $Q(t')$ denotes the emission rate and σ_{ho} and σ_{zo} the initial values of the dispersion coefficients (specifying the initial plume size); x_o, y_o, and z_o specify the position of the effective source point (see Figs. 3.1 and 3.2) at the time t'. By allowing the effective source position (x_o,y_o) to be a function of time t', the formulation can handle moving sources such as aircraft during takeoff. The vertical effective source coordinate z_o is allowed to be a function of travel time in order to simulate plume rise.

In the case of aircraft takeoff events, the time dependence of the emission rate was taken to be

$$Q(t') = \begin{cases} 0 \text{ for } t' < t_o \\ Q \text{ a constant for } t_o \le t' \le t_o + T \\ 0 \text{ for } t' > t_o + T \end{cases} \tag{3.27}$$

in which t_o is the time at which takeoff roll begins and T is the total time required for takeoff.

If Eqs. 3.19-3.26 are inserted into Eq. 3.18, the integral over $d\vec{x}$ may be done analytically with the following result:

$$C(\vec{x},t) = \int_{t_o}^{t} Q(t')F(x,x_o;t,t')G(y,y_o;t,t')S(z,z_o;t-t')dt' \tag{3.28}$$

with

$$F(x,x_o;t,t') = \frac{1}{(2\pi)^{1/2}\Sigma_h} \exp\left[-\frac{1}{2}\left(\frac{x-x_o-\bar{u}(t-t')}{\Sigma_h}\right)^2\right] \tag{3.29}$$

$$G(y,y_o;t,t') = \frac{1}{(2\pi)^{1/2}\Sigma_h} \exp\left[-\frac{1}{2}\left(\frac{y-y_o}{\Sigma_h}\right)^2\right] \tag{3.30}$$

$$S(z,z_o;t,t') = \frac{1}{(2\pi)^{1/2}\Sigma_z}\left\{\exp\left[-\frac{1}{2}\left(\frac{z-z_o}{\Sigma_z}\right)^2\right] + \exp\left[-\frac{1}{2}\left(\frac{z+z_o}{\Sigma_z}\right)^2\right]\right\} \tag{3.31}$$

where the "total" dispersion coefficients Σ_h and Σ_z are given by:

$$\Sigma_h^2 = \sigma_{ho}^2 + \sigma_h^2(t-t') \tag{3.32a}$$

$$\Sigma_z^2 = \sigma_{zo}^2 + \sigma_z^2(t-t') \tag{3.32b}$$

Everything in the integrand of Eq. 3.28 is assumed to be known, and although the integral cannot in general be evaluated analytically to give an explicit formula for $C(\vec{x},t)$, it can be evaluated numerically for any particular $(\vec{x},t)$.

It is worth pointing out that a perhaps more commonly used alternative to direct numerical integration for the evaluation of Eq. 3.28 is to divide the time interval $t-t_o$ into N segments of length Δt and approximate the integral by a sum over segments:

$$C(\vec{x},t) \cong Q\Delta t \sum_{i=1}^{N} F(t_i)G(t_i)S(t_i) \tag{3.33}$$

with

$$F(t_i) = F(x,x_o(t_i);t,t_i) \tag{3.34a}$$

$$G(t_i) = G(y,y_o(t_i);t,t_i) \tag{3.34b}$$

$$S(t_i) = S(z,z_o(t_i);t,t_i) \tag{3.34c}$$

and in which the times t_i are given by:

$$t_i = t_o + (i - \tfrac{1}{2})\Delta t \tag{3.35}$$

The fact that Q is taken to be constant has been used to factor the quantity $Q\Delta t$ out of the summation. Equations 3.33-3.35 constitute the traditional Gaussian-puff approach to this type of problem, $Q\Delta t$ being the mass of pollutant in each puff and t_i the emission times.

The approach actually used to evaluate Eq. 3.28 was a direct numerical integration method, a slightly modified version of an adaptive Simpson's rule

technique developed by Linz (1972). The primary reasons why this approach, rather than the Gaussian-puff procedure described in the previous paragraph, was chosen were that the numerical procedure allows better control over the errors introduced and, due to its adaptive nature, the Linz method promised to be more efficient. No comparison of methods was made, however, and all that can be said is that the chosen method performed quite satisfactorily.

3.1.5 Adjustment of Model Parameters

Specific values of the various coefficients and parameters that appear in the preceding formulation are required before the model can actually be run, and the manner in which they were determined is described in this section and the next one. This section deals with parameters that relate to the determination of the size and motion of the effective source, and the next section deals with the description of dispersion and plume rise. The specification of all parameters relating to the plume chemistry was described in Sec. 3.1.3.

Table 3.2 shows the numerical values of various takeoff parameters for specific aircraft. The physical dimensions, engine positions, and average takeoff distances, speeds, and masses were provided by the Great Lakes Office of the Federal Aviation Administration. The mean accelerations and takeoff times given in the table were computed from these data; in the model, the acceleration for a given aircraft type was assumed constant over the entire takeoff roll. The takeoff time corresponds to the quantity T in Eq. 3.27. The thrust per engine, used in the computation of the effective source point, was obtained from the mass and the acceleration using the relation:

$$\text{Thrust per engine} = \frac{(\text{mass}) \times (\text{acceleration})}{\text{number of engines}} \tag{3.36}$$

The engine positions were used to estimate the contributions to the initial plume size due to the fact that the engines are not all located at the same point. An examination of a large number of individual plumes provided no clear evidence that the separate plumes from the different engines on the various aircraft needed to be treated separately, although occasionally it appeared that a plume consisted of two nearly superimposed components. It was concluded that, for the purposes of modeling aircraft takeoff plumes, it is entirely adequate to assume only one plume per aircraft. It was felt, however, that the initial spread of that plume would be due in part to the separation of its components, and for a given aircraft type, the initial values of the dispersion coefficients σ_{ho} and σ_{zo} were estimated from:

$$\sigma_{ho}^2 = \sigma_{ho}^2(\text{turb}) + S_h^2 \tag{3.37a}$$

and

Table 3.2 Aircraft Takeoff Parameters

Aircraft Type	Emission Height (m)	S_z[a] (m)	S_h[a] (m)	Acceleration (m/s^2)	Takeoff Time (s)	Number of Engines (n)	Engine Diameter (m)	Thrust per Engine (N)	Total NO_x Emission Rate (gm/s)
747	2.37	0.24	17.19	1.547	54.9	4	1.08	97100	239.2
L-1011	3.45	1.09	8.67	1.853	41.7	3	1.00	89600	190.5
DC-10	4.92	3.19	7.69	1.792	44.5	3	1.15	90800	176.7
707	2.20	0.29	13.27	1.465	52.7	4	0.88	38100	63.7
DC-8	2.96	0.30	11.10	1.594	48.4	4	1.35	42200	63.7
727	4.68	1.10	2.32	1.767	42.2	3	0.75	39000	76.4
737	1.51	0.00	4.83	2.019	36.9	2	0.85	41900	50.9
DC-9	3.41	0.00	2.72	1.706	39.2	2	1.05	38700	50.9

[a]Computed using Eqs. 3.38a and 3.38b.

$$\sigma_{zo}^2 = \sigma_{zo}^2(\text{turb}) + S_z^2 \tag{3.37b}$$

in which (turb) denotes the contribution from turbulent dispersion within each individual component, and S_h and S_z are the values given in Table 3.2, which were in turn computed from:

$$S_h^2 = \frac{1}{n} \sum_{i=1}^{n} d_i^2 \tag{3.38a}$$

and

$$S_z^2 = \frac{1}{n} \sum_{i=1}^{n} (z_i - \bar{z})^2 \tag{3.38b}$$

The quantity d_i is the distance of engine i from the axis of the aircraft, z_i is the height above ground, $\bar{z}$ (the emission height in Table 3.1) is the average of the z_i, and n is the number of engines. The quantities σ_{ho}(turb) and σ_{zo}(turb) were taken to be 16 m and 8 m, respectively, and are independent of aircraft type. An attempt was made to estimate σ_{ho}(turb) and σ_{zo}(turb) from measurements by extrapolating back to zero travel time, but the measurements were inadequate for this purpose. The results of a brief sensitivity examination indicated that model predictions are relatively insensitive to changes in the values of these parameters.

The total NO_x emission rates given in Table 3.1 were computed from Table 3.1 together with the aircraft type-engine type correspondence given by Yamartino et al., (1980a,b).

The location of the effective source point with respect to the moving aircraft was discussed in general terms in Sec. 3.1.2. An examination of plumes observed when the wind was from the southwest and of the corresponding predicted plume trajectories indicated that the best qualitative agreement with observations occurred when the effective source point was located on the runway axis behind the aircraft at a distance given by Eq. 3.23 -- in other words, when the $(y/d)^3$ term in Eq. 3.16 is ignored. Relatively few plumes were observed, however, and no attempt was made to determine the optimum description quantitatively. For the purpose of this study, Eq. 3.8 was used to estimate the distance of the effective source point behind the aircraft, using engine diameters d given in Table 3.2 and assuming an ambient energy dissipation rate of 0.125 m^2/s^3, a value that is typical for neutral atmospheric stability.

The effective source point accelerates with the aircraft. In the computer code, the source point trajectory was computed prior to any dispersion calculations and positions $(x_o(t'),y_o(t'))$ at half-second time intervals stored in an array for reference. The initial emission height was taken to be equal to $\bar{z}$, although, as mentioned earlier, the effective emission

height was allowed to be a function of travel time in order to simulate plume rise.

3.1.6 Determination of Dispersion Coefficients and Plume Rise

The dispersion coefficients σ_h and σ_z and the height above ground of the plume center are important quantities in that model predictions are sensitive to changes in them. Because of the necessity of adopting a time-dependent modeling approach, it is also necessary to be able to estimate plume dispersion and plume rise as functions of travel time rather than of travel distance, as is usually done. Furthermore, since the approach does not assume a continuous release and corresponding steady state, the more common dispersion-coefficient formulas used in dispersion modeling are of no use. What is required is a description of the dispersion of puffs, i.e., short-period releases of material into the atmosphere, and in particular a description of the dispersion of particles relative to their center of mass.

A useful summary of what is known about atmospheric relative diffusion is provided by Gifford (1977). Based on the discussion of Gifford, it had been expected prior to the analysis of the data that σ_h and σ_z would vary approximately as the travel time raised to the 1.2 power, and a preliminary version of the model incorporated this behavior along with the assumption of no plume rise. Initial comparisons of preliminary model predictions with observations indicated, however, that these assumptions were in error and required modification. In order to determine the necessary changes, 50 individual plumes (29 727 plumes and 21 DC-10 plumes) were identified for analysis and were, in effect, used to determine the dependence on travel time of σ_h and σ_z, as well as of the height of the plume (z_0). Tables 3.3 and 3.4 present the data for these 50 plumes.

The data presented in these tables consist of the vector mean wind speed u and vector mean wind direction θ, the ambient temperature T, the estimated NO_2 photolysis rate $\tilde{k}_A$ obtained from pyranometer measurements using Eq. 2.11, ambient NO_x and O_3 concentrations, peak plume concentrations of NO, NO_x, NO_2, and O_3, the contribution from the aircraft plume to the NO_x and NO_2 dosage, the estimated travel time of the plume between release and passage over the monitoring site, and the observed effective plume width σ_h at the monitoring site. A brief explanation of how these quantities were determined is in order.

Appendix 2 contains a discussion of the different methods of averaging wind speed and direction and contains formulas with which various quantities may be computed from a set of observed wind-velocity vectors. Since wind speed and direction were measured at only one location, near the monitoring site, the determination of travel time and of the vector mean wind velocity involves some degree of approximation. In practice, after determining the arrival time of a given plume, a back trajectory was computed using the wind speed and direction measurements for each second prior to the arrival time.

Table 3.3 727 Analysis Plumes[a]

Plume No.	u (m/s)	θ (deg.)	T (°C)	$\bar{k}_e$ (min^{-1})	$[NO_x]_a$ (ppb)	$[O_3]^a$ (ppb)	Peak Concentration (ppb) NO	NO_x	NO_2	O_3	Dose (ppm-s) NO_x	NO_2	t (s)	σ_h' (m)
1	2.44	321.7	10.0	0.338	1.7	32.4	50	54	3	8	1.515	0.303	600	22.5
2	2.29	340.7	10.8	0.338	1.7	32.8	89	76	-	6	3.061	0.940	600	36.1
3	4.07	294.8	10.7	0.339	2.9	31.2	56	81	25	11	4.482	1.923	110	117.6
4	2.89	286.2	10.7	0.339	2.4	32.2	71	119	48	5	6.516	2.387	119	56.4
5	7.46	241.4	26.0	0.319	13.1	19.2	219	294	75	-	6.395	3.223	26	175.8
6	6.58	264.8	26.4	0.328	24.2	22.5	259	348	88	0	5.159	1.982	36	44.1
7	6.08	265.2	14.4	0.283	9.1	16.3	205	265	60	1	2.497	0.619	39	27.7
8	5.64	261.0	15.0	0.298	13.9	21.9	249	330	81	2	2.793	0.469	40	22.5
9	5.94	276.9	15.2	0.301	14.9	21.5	253	322	69	0	6.434	1.774	48	54.8
10	5.98	281.3	16.0	0.315	14.1	2.6	308	392	84	7	4.765	0.705	52	26.1
11	6.71	295.0	16.3	0.318	15.4	32.0	206	259	53	5	6.247	1.265	68	84.5
12	5.31	290.4	16.5	0.318	4.0	31.1	106	149	43	5	1.700	0.502	77	55.2
13	5.72	298.1	16.4	0.319	10.6	35.0	78	87	9	6	1.851	0.480	89	97.2
14	6.85	288.4	16.6	0.320	2.5	33.0	155	204	49	3	2.038	0.384	53	51.0
15	5.81	298.9	17.8	0.323	14.7	35.9	129	172	43	1	3.327	0.656	92	64.6
16	6.83	312.3	18.0	0.336	12.1	41.0	72	93	21	6	0.842	-	207	57.4
17	6.91	297.5	18.0	0.259	16.8	39.4	159	192	33	6	5.309	0.343	73	98.1
18	6.36	314.5	17.9	0.211	14.5	29.6	145	170	25	-	4.427	0.281	314	83.2
19	8.18	309.5	17.8	0.212	20.0	37.3	79	98	19	6	1.447	-	128	85.6
20	5.75	298.9	17.4	0.200	34.0	38.1	70	98	28	7	-	-	92	28.0
21	7.07	298.1	17.5	0.131	20.0	37.8	215	254	39	-	2.590	0.222	72	57.9
22	7.82	288.6	18.0	0.298	18.9	36.5	152	173	21	7	1.207	-	47	24.3
23	6.67	291.6	17.7	0.323	13.2	35.8	201	215	15	5	2.657	0.252	60	29.6
24	5.93	287.9	18.0	0.299	14.7	34.7	446	437	92	-	5.034	0.245	61	17.8
25	8.29	292.9	17.7	0.270	3.5	30.8	214	263	49	2	5.640	1.044	51	76.5
26	8.04	298.9	17.9	0.288	33.1	38.3	176	202	26	5	1.849	0.501	66	50.0
27	6.73	281.7	18.0	0.295	8.8	33.6	181	254	73	4	3.242	0.701	46	61.2
28	7.27	295.3	18.1	0.283	4.0	33.5	109	150	41	3	2.632	0.578	63	88.6
29	7.27	271.0	18.3	0.280	7.4	37.9	228	300	72	-	1.969	0.501	35	16.6

[a]See text for explanation of symbols and headings.

[b]A dash (-) indicates a negative value.

Table 3.4 DC-10 Analysis Plumes[a]

Plume No.	u (m s)	θ (deg.)	T (°C)	K_A (min^{-1})	$[NO_x]_a$ ppb	$[O_3]^a$ ppb	Peak Concentration (ppb) NO	NO_x	NO_2	O_3	Dose: ppm-sec NO_x	NO_2	t (s)	σ_h (m)
1	2.20	316.8	9.9	0.338	1.7	32.8	152	62	-	14	1.004	0.384	600	30.1
2	2.35	2.5	11.7	0.337	1.7	35.9	35	33	-	18	1.260	0.820	600	64.2
3	6.49	267.2	14.2	0.289	14.4	21.9	306	351	46	3	4.187	1.017	37	30.2
4	6.70	263.3	14.6	0.296	6.8	23.9	460	541	80	-	5.671	1.423	35	26.8
5	7.31	288.4	15.4	0.307	15.1	24.0	724	816	92	-	12.731	1.657	50	42.0
6	7.54	293.6	16.7	0.320	22.1	36.1	655	747	92	-	14.774	1.814	58	70.8
7	6.52	290.8	16.9	0.321	4.9	37.3	882	1005	123	1	14.025	1.548	60	32.1
8	6.63	314.8	17.2	0.324	16.0	36.3	94	106	12	6	1.565	-	318	81.3
9	8.14	298.1	17.7	0.326	29.1	37.0	550	632	82	0	22.646	3.110	63	140.3
10	6.11	301.8	17.9	0.330	4.8	39.2	387	438	51	-	8.396	1.448	100	61.6
11	6.60	313.0	17.6	0.251	20.9	36.1	218	256	37	1	8.846	1.214	238	144.2
12	8.49	299.2	17.7	0.205	43.2	37.9	633	711	77	-	7.195	0.768	64	70.3
13	7.04	296.9	17.8	0.167	20.0	38.8	434	493	59	-	11.011	-	69	62.0
14	7.75	303.2	17.6	0.146	19.6	41.6	613	668	55	-	9.962	0.330	85	39.7
15	8.85	289.5	18.1	0.199	11.7	32.3	724	828	104	0	16.468	1.644	43	56.2
16	8.07	293.6	18.1	0.204	36.7	29.7	782	891	109	-	14.977	1.830	53	60.3
17	8.17	302.8	17.8	0.264	20.0	36.4	556	628	72	1	13.685	0.848	81	68.9
18	8.74	291.6	17.5	0.227	7.6	31.9	505	583	78	-	9.314	1.303	46	48.3
19	7.44	293.2	18.3	0.280	12.5	37.8	783	860	77	-	17.005	2.316	57	41.9
20	3.63	305.9	4.6	0.304	29.7	22.8	718	792	74	-	30.508	4.193	215	102.8
21	3.74	340.4	6.0	0.314	8.6	31.8	712	780	67	1	22.206	3.450	600	35.3

[a]See text for explanation of symbols and headings.

[b]A dash (-) indicates a negative value.

The trajectory was continued until either it intersected the runway axis or 600 seconds had elapsed. The estimated travel time is simply either the time from the beginning of the back trajectory to the intersection with the runway axis or 600 seconds. The vector mean wind speed and direction for the given plume were computed from the set of one-second speed and direction values that comprise the trajectory according to the formulas in Appendix 2. Figures 3.5 and 3.6 illustrate the results of these computations for two of the 50 analysis plumes, 727 plume no. 4 and DC-10 plume no. 11, respectively. In those figures, the circled cross indicates the location of the monitoring site and the small arrow denotes the mean wind velocity vector determined from the trajectory.

The observed effective plume width σ_h' at the monitoring site was computed by the following technique. The arrival time of the plume was first computed as a concentration-weighted time average over the period during which the NO_x concentration was greater than one-tenth of the peak value:

$$t_{arr} = \frac{\Sigma w_i t_i}{\Sigma w_i} \tag{3.39}$$

where

$$w_i = \max \begin{cases} [NO_x]_i - ([NO_x]_{max}/10) \\ 0 \end{cases} \tag{3.40}$$

The observed variance in arrival time corresponding to the mean defined by Eq. 3.39 is defined by:

$$\sigma_t^2 = \frac{\Sigma w_i (t_i - t_{arr})^2}{\Sigma w_i} \tag{3.41}$$

and the corresponding effective plume width is given by

$$\sigma_h' = 1.188\ u\sigma_t \tag{3.42}$$

In Eq. 3.42, u denotes the vector mean wind speed and the factor 1.188 corrects the value of σ_t for the fact that only concentrations greater than $[NO_x]_{max}/10$ were considered and, therefore, a slightly low estimate of σ_t is obtained. The factor 1.188 is simply the ratio of the true standard deviation of a Gaussian distribution to the value obtained by integrating only over the region of the distribution in which the value is greater than one-tenth of the maximum:

$$1.188 = \left[\sigma^2 \Big/ \int_{-\delta}^{\delta} \frac{x^2}{\sqrt{2\pi}\sigma} \exp\left[-\frac{1}{2}\left(\frac{x}{\sigma}\right)^2 \right] dx \right]^{1/2} \tag{3.43}$$

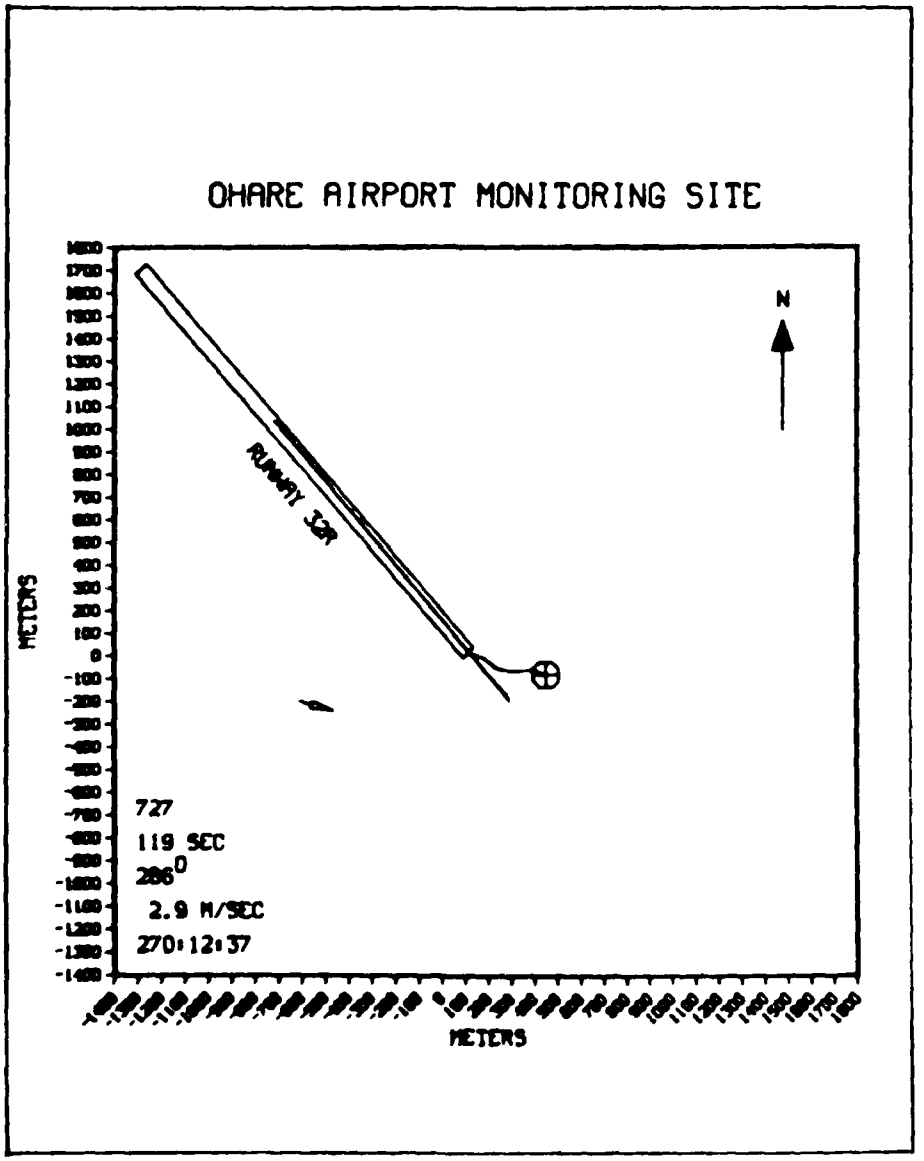

Fig. 3.5 Back Trajectory for 727 Plume No. 4

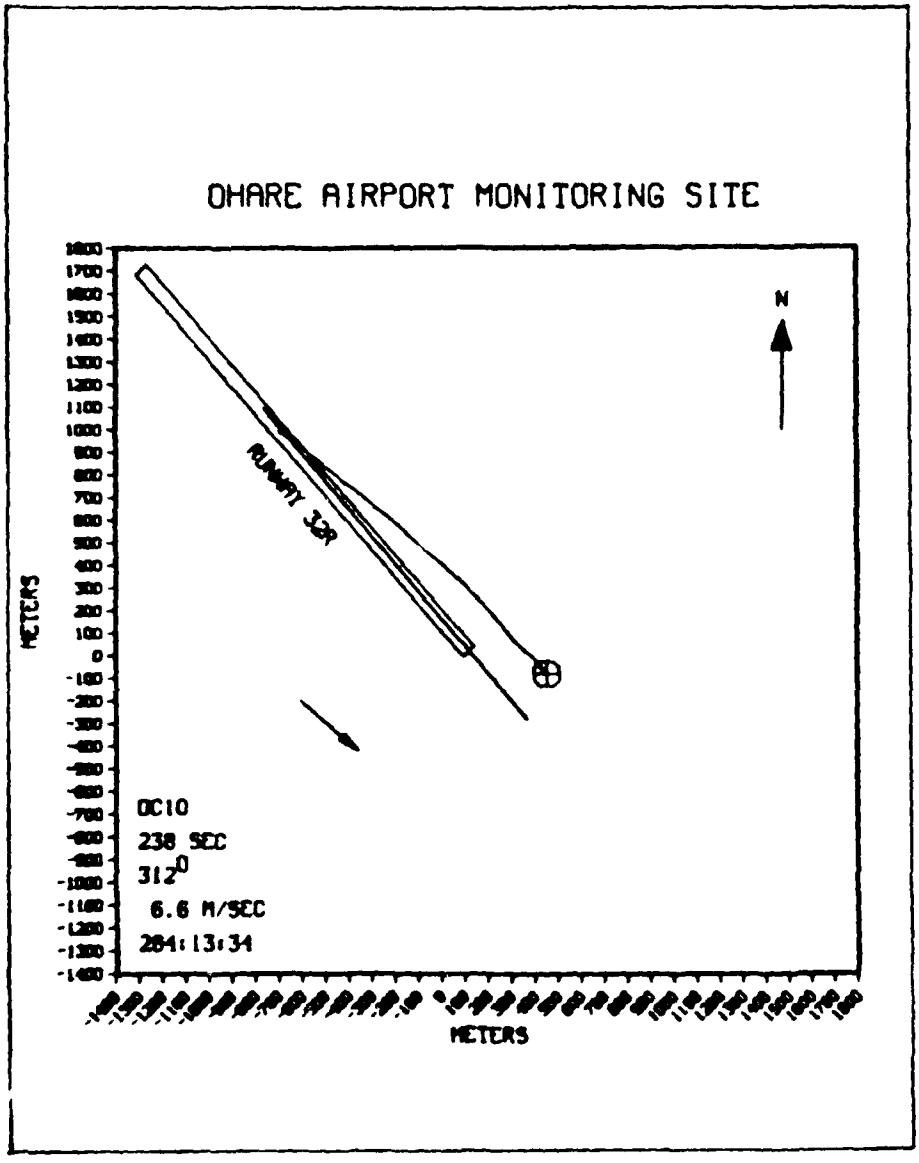

Fig. 3.6 Back Trajectory for DC-10 Plume No. 11

where $\delta = 2.146\sigma_h$ is the distance on either side of the peak at which the distribution drops to one-tenth of the peak value. The quantity σ_t computed from Eq. 3.41 is an estimate of the integral in the above expression.

In Tables 3.3 and 3.4, the temperature and NO_2 photolysis rate require no further explanation. The ambient NO_x and O_3 concentrations were estimated as averages over the values on either side of the plume. The peak of a plume was defined as the time of maximum NO_x concentration, and the peak concentrations represent averages over three successive points centered on the peak.

The NO_x and NO_2 dosages due to the aircraft plume were estimated as the differences between the total dosages over a period of time spanning the passage of the plume and the dosages that would have resulted from the ambient concentrations alone over the same time period.

It should also be noted that for modeling purposes, the coordinates of the endpoints of runway 32R were, in meters: initial (124.7, 18.8), final (-1978.5, 2566.1). In the same coordinate system the coordinates, in meters, of the monitoring site were (456.1, -80.5). The first number of each pair corresponds to the x-coordinate, and the second to the y-coordinate. The origin was chosen arbitrarily, and the x- and y-axes were taken along the east and north directions, respectively. Based upon observations, aircraft were assumed to begin takeoff at a point 40 meters from the initial end of the runway.

Determination of $\sigma_h(t)$. The concentration profile across an aircraft plume is expected to be Gaussian on the average, and if horizontal profiles are examined for various heights above ground, the shapes as given by the standard deviations at the different heights are expected to be approximately the same. Assuming no dependence of σ_h on altitude, it should be possible to extract information about σ_h from the observed shapes of the peaks measured at a stationary location as the plumes pass by. This approach was adopted in this work.

An observed peak shape represents a section through the plume at an angle that generally differs from 90° and also represents the superposition of contributions from a conceptually large number of puffs having slightly different travel times. For these reasons, the observed standard deviation for a particular peak does not directly correspond to σ_h. The angle at which an aircraft plume passes a monitoring site is well defined in a model that assumes a uniform wind field, but in observational practice is poorly defined and difficult to measure because of turbulent fluctuations in the wind, especially those larger eddies that give rise to significant meandering. Several instances may be found in the analysis plume data of Tables 3.3 and 3.4 in which the back trajectory computed from wind measurements at the monitoring site did not intersect the runway (the 600-second-travel-time cases). In these cases it is presumed that the wind measurements simply did not reflect well enough the wind variation that actually took place along the

[illegible] In any event, lacking good information about the angle of attack of the plume, it was decided simply to examine the time dependence of the observed plume widths without correction for this effect. Figure 3.7 shows a plot of σ_h versus travel time, where σ_h was estimated from σ_θ using:

$$\sigma_h = x\sigma_\theta \sqrt{1 + \left(\frac{\sigma_{h_0}}{x\sigma_\theta}\right)^2} \qquad (3.44)$$

where σ_{h_0} is the aircraft specific standard deviation due to engine placement discussed in sec. 2.1.2. Also shown on the figure is the corresponding regression line, which corresponds to a time dependence given by:

$$\sigma_h = at^b \qquad (3.45)$$

with $b = 0.5698$. The coefficient a was determined not by regression analysis from Fig. 3.7 but rather by running a specialized version of the model using various values of a and selecting as the optimum value that which gave the best agreement with the observed standard deviations. In this way the model was 'tuned' to reproduce observed plume widths. The value of a that resulted from this analysis was 1.38, with a standard deviation of 0.54. The values 1.38 and .5698 for coefficient and exponent, respectively, were then fixed in the model and the corresponding time dependencies of σ_z and the plume height were investigated.

During the preparation of this report, an alternative method of analysis was devised for the examination of the time dependence of the observed deviations. Although the results of this analysis were not used in the development and validation of the model, they are sufficiently interesting to be included here.

Consider a line distribution of pollutant oriented along the y axis and centered at 0:

$$C(x,y,z) = Q_l(x/\sigma_h)S(z/\sigma_z;H/\sigma_z) \qquad (3.46)$$

$$Q_l(x/\sigma_h) = \frac{1}{(2\pi)^{1/2}\sigma_h} \exp\left[-\frac{1}{2}\left(\frac{x}{\sigma_h}\right)^2\right] \qquad (3.47)$$

$$S(z/\sigma_z;H/\sigma_z) = \frac{1}{(2\pi)^{1/2}\sigma_z}\left\{\exp\left[-\frac{1}{2}\left(\frac{z-H}{\sigma_z}\right)^2\right] + \exp\left[-\frac{1}{2}\left(\frac{z+H}{\sigma_z}\right)^2\right]\right\} \qquad (3.48)$$

In Eq. (3.46), Q_l denotes the quantity of pollutant per unit length along the plume and is assumed constant along the plume. Imagine crossing this distribution along a line that is at ground level ($z = 0$) and makes an angle θ with the y axis. The observed concentration distribution along this line will be gaussian with an effective standard deviation σ_{eff} given by:

$$\sigma_{eff} = \sigma_h/\sin\theta \qquad (3.49)$$

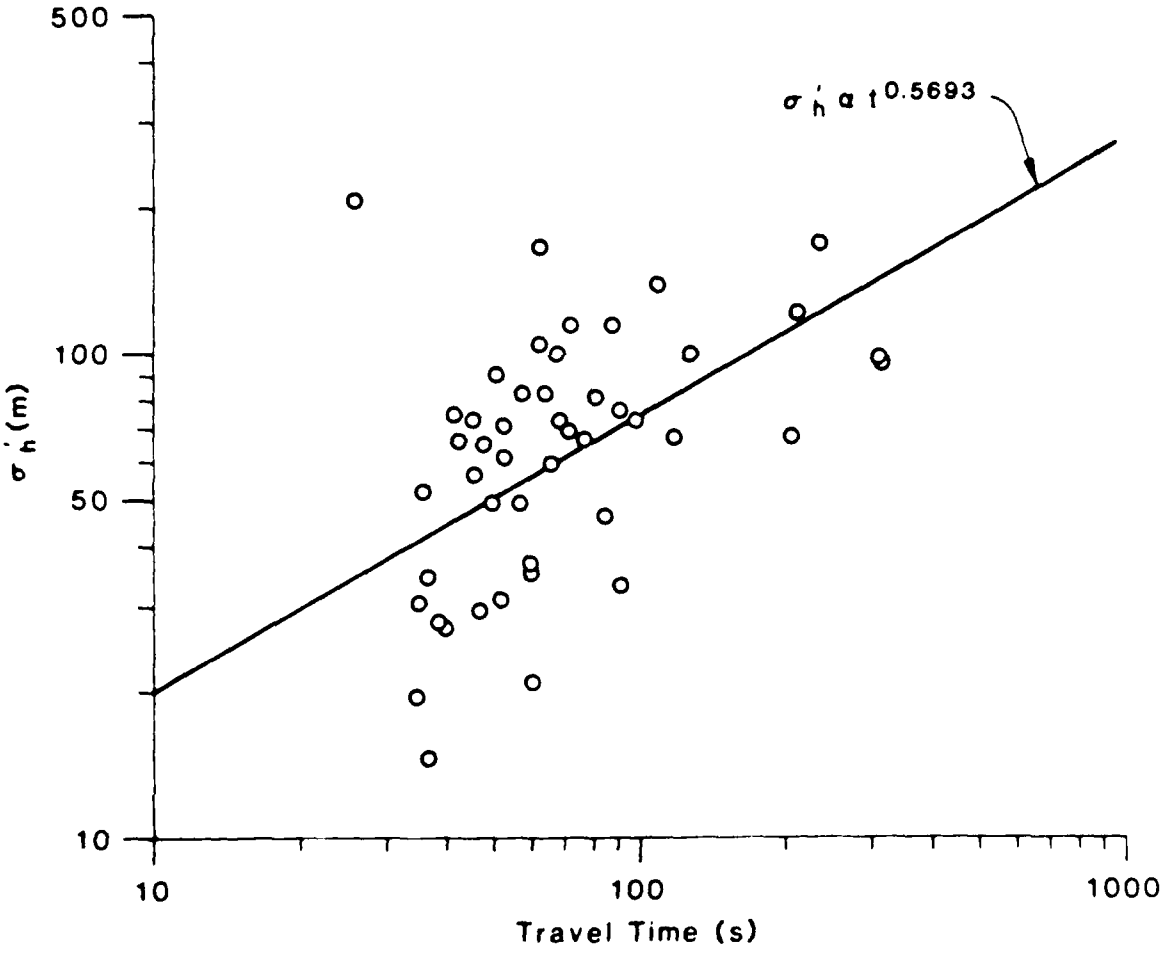

Fig. 3.7 Dependence of Plume Width on Travel Time

the maximum concentration at x = 0 will be given by:

$$C_{max} = \frac{Q_o}{\pi \sigma_z \sigma_h} \exp\left[-\frac{1}{2}\left(\frac{H}{\sigma_z}\right)^2\right] \qquad (3.50)$$

and the integrated dose D by:

$$D = \frac{1}{u \sin\theta} \int_{-\infty}^{\infty} C(x,y,z=0)dx \qquad (3.51)$$

or

$$D = \frac{2\, Q_o}{(2\pi)^{1/2}\, u \sin\theta \sigma_z} \exp\left[-\frac{1}{2}\left(\frac{H}{\sigma_z}\right)^2\right] \qquad (3.52)$$

From these expressions, one finds that:

$$\frac{\sigma_{eff}}{uD} = \left(\frac{\pi}{2}\right)^{1/2} \frac{\sigma_z \sigma_h}{Q_o} \exp\left[+\frac{1}{2}\left(\frac{H}{\sigma_z}\right)^2\right] \qquad (3.53)$$

and

$$\frac{C_{max}\sigma_{eff}}{uD} = (2\pi)^{-1/2} \doteq 0.3989 \qquad (3.54)$$

These results imply that something might be learned about the time dependence of σ_h, σ_z and the effective plume height by plotting the quantity σ_h/uD against travel time, taking σ_h to be an estimate of σ_{eff}. The useful feature of this approach is that the angle θ at which the plume approaches the stationary monitoring site does not appear and need not be known. Essentially, both σ_h and the integrated dose depend on θ in the same way and this fact allows the θ-dependence to be removed.

In applying Eq. 3.53 to aircraft plumes, a problem arises in that the quantity of pollutant per unit length, Q_o, is not strictly constant along the plume, being given by Q/v where Q is the (constant) emission rate and v is the aircraft speed. In addition, the exact portion of the takeoff plume that passes over the monitor can only be poorly estimated although it would presumably depend upon the travel time. About the best that can be done is to plot σ_h/uD versus travel time for specific aircraft types and assume that Q_o is not strongly dependent on travel time.

The results of these computations for NO_x are shown in Fig. 3.8 for both 727 and DC-10 aircraft, along with dashed lines corresponding to power law dependencies with an exponent of 1.2. The consistency of the points with this time dependence is clear. It is tempting to attribute the difference between the two lines (or sets of points) to the difference in emission rates between the two aircraft. The DC-10/727 NO_x emission ratio = 2.3 from the

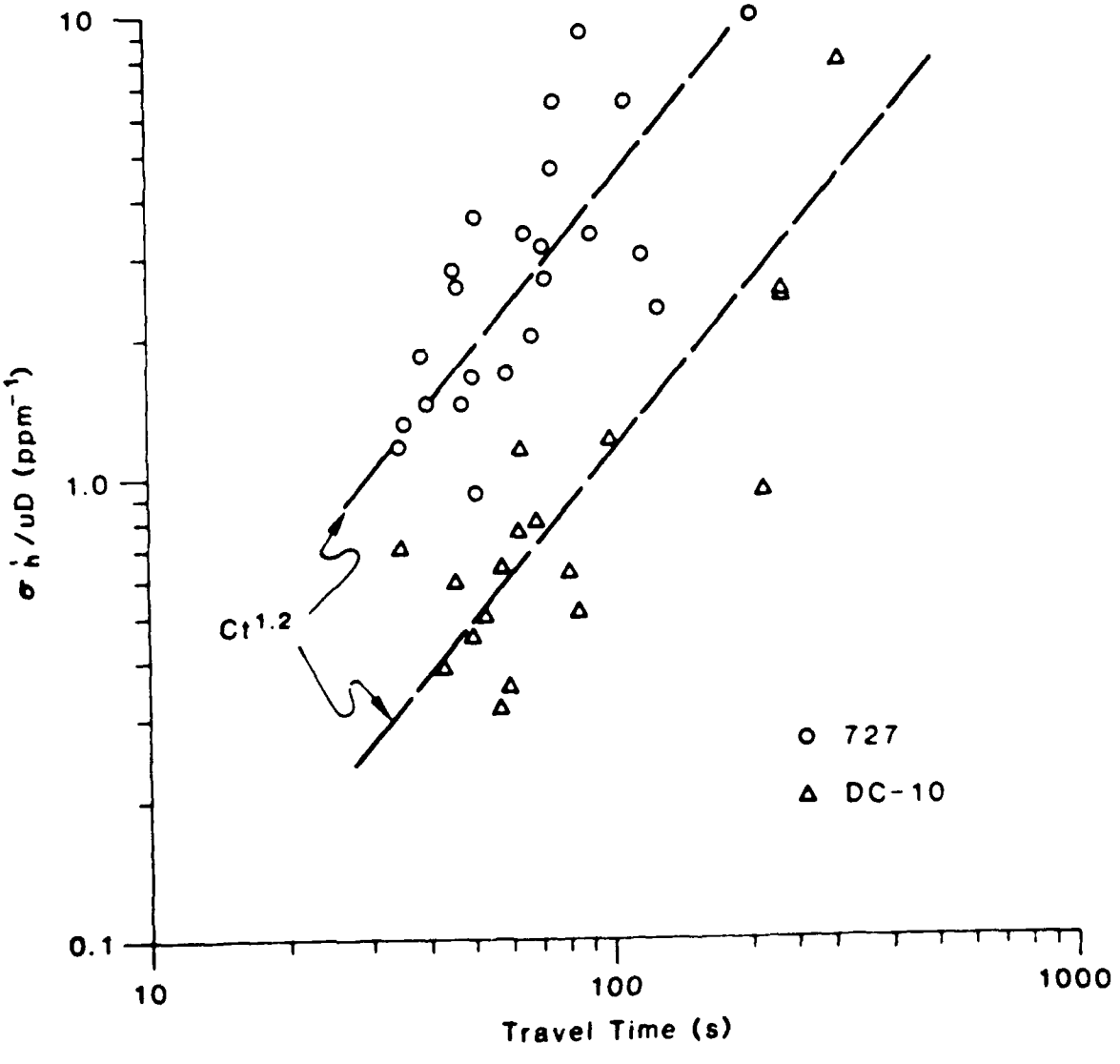

Fig. 3.8 σ_h'/uD versus Travel Time

data in Table 3.2, while the ratio of values taken at any given travel time from Fig. 3.8 is 3.8 ± 2.0 (uncertainty estimated visually from the figure). Thus the numbers are not inconsistent with each other, and this interpretation of the difference between the lines is consistent with the data.

The exponential factor on the right-hand side of Eq. 3.53 is not expected to depend strongly on travel time, and the main dependence on travel time is expected to come from the product $\sigma_z\sigma_h$. If the dependencies of each factor are assumed to be the same, one obtains a time dependence of $t^{0.56}$ for both standard deviations, in (perhaps fortuitously) good agreement with the result of Fig. 3.7.

Equation 3.54 provides an interesting check on the assumption of a Gaussian distribution within aircraft plumes. Everything on the left-hand side of this equation is known, if σ_h is used as an estimate of σ_{eff}. Using the data in Tables 3.3 and 3.4, the average values of the quantity $C_{max}\sigma_h/uD$ for 727 and DC-10 aircraft turned out to be 0.53 ± 0.18 and 0.47 ± 0.17, respectively. The uncertainties represent one-standard-deviation values based on 24 and 18 plumes, 727 plumes no. 1, 2, 5, 12, and 20 being omitted and DC-10 plumes no. 1, 2, and 21 being omitted. The results are not statistically different from the expected value of 0.3989, and the data are therefore reasonably consistent with the Gaussian assumptions.

Determination of $\sigma_z(t)$ and $z_o(t)$. An examination of Eqs. 3.28-3.31 shows that the effects of the dependencies of σ_z and z_o on travel time are closely related to each other and, as a practical matter, must be considered jointly. In addition, due to the absence of pollutant and meteorological data for other monitoring sites, and especially for other downwind distances and heights above ground, the quantities σ_z and z_o could not be uniquely determined in the absence of additional external assumptions regarding their behavior. Given such assumptions, discussed below, the procedure adopted in this work was to estimate the time dependence of σ_z and z_o such that the peak NO_x concentrations predicted by the model were in agreement, on the average, with observed peak concentrations.

The initial step in the analysis was to assume that $\sigma_z(t) = \sigma_h(t)$, that z_o was constant, i.e., there was no plume rise, and to compute the ratios of model to observed peak NO_x concentrations for the analysis plumes. These initial calculations showed that under these assumptions the model overpredicted by a factor of about four for travel times up to 80-90 seconds and underpredicted by a factor of about 0.2 for travel times above about 130 seconds.

The next step was to assume that the plume rise could be described by a modified form of the expression given by Yamartino et al. (1980):

$$\Delta z_o = a(t)H_y(t) \qquad (3.55)$$

$$H_v(t) = h_v t^{p} u^{p-q} \tag{3.56}$$

In these equations, α is a function of time to be determined, $H_y(t)$ is the Yamartino plume rise formula, h_v is an aircraft type-dependent coefficient, and p and q are 2/3 and 1, respectively. In addition, $\sigma_z(t)$ was assumed given by:

$$\sigma_z(t) = \beta(t)\sigma_h(t) \tag{3.57}$$

where $\beta(t)$ is another function of travel time to be determined. The ratio α/β at several travel times was determined by running the model for a range of values of α and β, plotting the ratio R of model to observed peak NO_x concentrations against α for each value of β, for several different plumes spanning a range of travel times, and finally identifying by interpolation the value of α that, for given travel time and value of β, would result in R being equal to unity. It was found that for travel times below about 70 seconds, the optimum ratio α/β was independent of β and its graph was linear on log-log paper, indicating a power-law dependence on the travel time given by:

$$\frac{\alpha}{\beta} = 8.59\ t^{-0.92} \tag{3.58}$$

with a correlation coefficient of $r = -0.99$. For travel times greater than 70 seconds, the optimum ratio decreased with time more rapidly than in Eq. 3.58, and a definite dependence on the value of β was apparent.

At this point, it became necessary to introduce an additional assumption in order to separate the effects of σ_z and z_o. In effect, the assumption adopted was to require $\sigma_z(t)$ to vary with travel time as $t^{1.31}$ for short travel times. From Eqs. 3.57 and 3.45, this implies that for short travel times, $\beta(t)$ must vary as $t^{0.74}$ and, therefore, from Eq. 3.58, $\alpha(t)$ must vary as $t^{-0.18}$. Given these short-time dependencies, the following functional forms were assumed for $\alpha(t)$ and $\beta(t)$:

$$\alpha(t) = \frac{at^{-0.18}}{1 + \left(\frac{t}{t_\alpha}\right)^b} \tag{3.59}$$

$$\beta(t) = \frac{ct^{0.74}}{1 + \left(\frac{t}{t_\beta}\right)^d} \tag{3.60}$$

Thus the short-term time dependence required by the above considerations are followed, but the possibility of different dependencies at longer travel times

is allowed for. Furthermore, the ratio a/c must equal 8.59, from Eq. 3.58, and we make the additional assumption that a is unity, corresponding to the assumption that the coefficient h_y in the Yamartino plume-rise formula is correct for short travel times. These considerations imply that c = 1/8.59 or that c = 0.116.

The values of the remaining parameters, b, d, t_α and t_β, were estimated on a trial-and-error basis because of time and budget constraints. The final expressions for $\alpha(t)$ and $\beta(t)$ that were implemented in the model are:

$$\alpha(t) = \frac{(t/\text{seconds})^{-0.18}}{1 + (t/16.62 \text{ seconds})^{0.64}} \tag{3.61}$$

$$\beta(t) = \frac{0.116(t/\text{seconds})^{0.74}}{1 + (t/7.1 \text{ seconds})^{0.30}} \tag{3.62}$$

The expression for $\alpha(t)$ gives rise to a very broad maximum in $\Delta z_0(t)$ at a travel time of 101.5 seconds. In the model, the plume rise was assumed to remain constant at the maximum value for travel times greater than this. The asymptotic long-travel-time behavior of $\sigma_z(t)$ that results from Eqs. 3.62, 3.57, and 3.45 is a power law with an exponent of 1.0.

The results of a comparison between observed maximum NO_x concentrations and those predicted by the model with dispersion coefficients and plume rise given by Eqs. 3.45, 3.55-3.57, and 3.61-3.62 may be summarized by stating that the average value of the ratio R of predicted peak concentrations to observed peak concentrations is 1.3 ± (1σ) 0.9 (N = 46). However, an examination of the individual results for the various plumes reveals two features that indicate that the predictions could be further improved and that somewhat more optimal descriptions of the dispersion coefficients and plume rise could be found.

The first feature is a residual variation of R with travel time. If the results are aggregated according to whether the travel time is greater or less than 100 seconds, one finds an average ratio for travel times less than 100 seconds of 1.4 ± (1σ) 0.7 (N = 37), and an average value of 0.8 ± (1σ) 1.7 (N = 9) for travel times greater than 100s. The very large standard deviation in the last result is due almost entirely to two 727 points at 3.5 and 2.5, the rest being very much smaller (the largest remaining value is 0.41, the next largest 0.20, and the average of these remaining seven points is only 0.16). Although no firm conclusions can be drawn because of the scatter in the results, the trend towards underprediction at longer travel times seems clear.

The second feature is an apparent difference between aircraft types. If average ratios are computed separately for the two aircraft types involved, one finds that for 727 plumes R = 1.73 ± (1σ) 0.74 (N = 22), and for DC-10 plumes R = 0.90 ± (1σ) 0.28 (N = 15). In these results, plumes having travel

times greater than 100 seconds have been excluded. Although the scatter is such that the regions of uncertainty overlap and no firm statistical conclusions can be drawn, the apparent difference in performance for the two aircraft is sufficiently great as to suggest that it may be real.

On the whole, the model appears to predict peak concentrations at the monitoring site relatively well, with the caveats just discussed. Due to time and budget constraints, additional tuning of the model, including comparisons of predicted and observed NO_x doses, could not be performed although the predictive power of the model would certainly benefit from them.

3.2 MODEL VALIDATION FOR ONE-HOUR PREDICTIONS

The main objective of the model-development and validation phase of the program was a model suitable for the estimation of one-hour average NO_2 concentrations from aircraft. As explained earlier, the approach adopted in this work was to compute the contribution from individual takeoff events and sum the results. This section describes both the manner in which this is done by the model and the validation results.

3.2.1 Multiple-Plume Model Description

In most dispersion models that compute one-hour average concentrations of some pollutant, the assumption is made that the meteorological conditions are constant over the one-hour period for which predictions are to be made. The same assumption was made in this work, and since individual aircraft plumes are assumed to be independent, the contribution from each type of aircraft to a one-hour average concentration may be estimated by computing the contribution from one takeoff event and multiplying by the number of takeoffs by that type of aircraft in an hour. Thus the computational burden may be significantly lessened.

The multiple-plume version of the model computes total aircraft-related NO_x and NO_2 dosages (ppm-s) for one-hour time periods, and obtains the corresponding average concentrations by dividing by 3600 seconds. The number of each type of aircraft that take off in each one-hour period may be provided by the user, or a default distribution may be used that is contained within the model itself and is based upon 10 hours of direct observations of takeoffs on runway 32R at O'Hare International Airport. The default distribution is given in Table 3.5. This distribution is not intended for use at other airports, nor even for other runways at Chicago O'Hare. The frequency distribution is different for each airport and for each runway in a given airport and depends on a number of factors, including the length of the runway and the proximity to the various gates used by different commercial carriers.

Table 3.5 Default Aircraft-Takeoff Frequency Distribution[a]

Aircraft Type	747	737	727	707	DC-9	DC-10	L-1011	Misc.[b]	Total
Average Takeoffs per Hour	0.1	2.0	13.9	2.5	4.4	4.6	0.3	8.5	36.3
Percent of Total	0.28	5.51	38.29	6.89	12.12	12.67	0.83	23.41	100.00

[a]Based upon 10 hours of observations on runway 32R at Chicago O'Hare International Airport.

[b]Misc. includes small private and commercial jets and propeller aircraft.

3.2.2 Multiple-Plume Model Validation

For model validation purposes, 31 distinct one-hour periods with relatively constant wind speed, direction, solar intensity, and ambient ozone concentration were identified. These periods were also chosen so as to provide a range of numbers of takeoffs per hour; the individual aircraft types could not be identified, but the number of distinct jet-aircraft plumes could easily be determined by inspection of the data. The default distribution given in Table 3.5 was used to estimate the number of each type of jet aircraft that took off in each one-hour period. Table 3.6 shows the periods selected, the number of jet plumes observed, the vector mean wind speed ($\bar{V}_{vec}$) and direction ($\bar{\theta}_{vec}$), the wind-velocity variance components perpendicular (σ_t) and parallel (σ_ℓ) to the vector mean wind velocity, the observed and calculated aircraft-related NO_x and NO_2 one-hour dosages, and the average ambient ozone level.

Figures 3.9 and 3.10 represent plots of calculated versus observed hourly aircraft-related dosages for NO_x and NO_2, respectively. Only points for which both calculated and observed dosages are nonzero are shown. As can be seen from the data in Table 3.6, several periods were found for which the calculations indicated no effect. In all of these instances, the wind direction was greater than 307°, corresponding to winds blowing nearly along the runway axis. In these cases the geometry of the runway direction, wind direction and monitoring-site location is such that little or no effect is expected if the plumes travel in straight-line trajectories. These results indicate that meandering or some systematic perturbation of the wind field is causing the plume trajectories to deviate sufficiently from linearity to cause the plumes to affect the monitoring site but to also give rise to wind directions as measured at the monitor to be systematically in error. This points up the inadequacy of monitoring the wind velocity at only one point and attempting to derive trajectories from those measurements, at least in the near-critical geometrical configurations. The same effect can be seen for some of the individual plumes described earlier in Tables 3.3 and 3.4.

The solid lines on Figs. 3.9 and 3.10 represent the results of regression analyses run on the two sets of data, after discarding those points for which the predicted values are less than 1.0 ppm-s. The regression equations that correspond to those lines are:

$$\begin{pmatrix}\text{Calculated}\\ NO_x\ \text{Dose}\\ (\text{ppm-s})\end{pmatrix} = -14.27 + 1.570 \times \begin{pmatrix}\text{Observed}\\ NO_x\ \text{Dose}\\ (\text{ppm-s})\end{pmatrix} \qquad (3.63)$$

with a correlation coefficient of 0.872 ($R^2 = 0.76$), and

$$\begin{pmatrix}\text{Calculated}\\ NO_2\ \text{Dose}\\ (\text{ppm-s})\end{pmatrix} = -1.67 + 1.171 \times \begin{pmatrix}\text{Observed}\\ NO_2\ \text{Dose}\\ (\text{ppm-s})\end{pmatrix} \qquad (3.64)$$

Table 3.6 One-Hour Validation Periods and Results

Date/ Time	No. Takeoffs	$\bar{V}_{vec}$ (m/s)	$\bar{\alpha}_{vec}$ (deg.)	σ_l (m/s)	σ_t (m/s)	Dosages (ppm-s Observed NO_2	Observed NO_x	Calculated NO_2	Calculated NO_x	Average $[O_3]_a$ (ppm)
293/09	22	6.6	293.3	1.213	1.031	21.36	130.70	24.50	180.62	0.015
293/13	18	6.7	301.9	1.852	1.322	23.58	106.07	39.16	185.11	0.031
293/14	28	6.8	299.8	2.099	1.557	29.52	137.58	52.35	267.92	0.030
293/15	24	6.9	293.3	2.028	1.518	38.21	121.81	38.62	191.32	0.033
293/16	10	8.0	295.7	1.802	1.427	18.88	65.32	14.90	75.41	0.030
294/16	9	7.8	302.2	2.054	1.502	21.91	67.96	19.92	84.04	0.033
298/15	10	8.1	267.8	1.764	1.513	4.32	38.59	3.85	55.88	0.003
299/08	20	8.4	301.0	2.003	1.421	29.64	141.38	24.54	179.77	0.015
299/09	9	9.0	305.6	2.212	1.266	12.80	27.43	2.07	12.35	0.018
299/13	28	10.3	302.8	2.380	1.638	33.42	205.52	36.60	206.72	0.022
299/14	28	10.2	303.8	2.240	1.474	36.12	169.17	37.99	216.23	0.021
300/17	20	4.9	300.3	1.515	1.230	33.78	118.55	51.08	243.58	0.025
293/10	30	7.0	299.7	1.422	1.171	36.06	199.78	37.66	275.98	0.015
295/1	09	3.1	308.0	1.279	1.555	14.95	64.43	32.96	97.62	0.033
299/1	16	10.4	307.9	2.482	1.654	21.07	121.04	0.0	0.0	0.022
299/16	24	9.3	310.3	2.388	1.567	30.05	178.03	0.0	0.0	0.023
299/17	25	9.9	312.2	2.483	1.397	33.78	195.62	0.0	0.0	0.022
300/08	22	6.9	315.3	1.927	1.315	14.74	68.72	0.0	0.0	0.025
300/11	28	8.1	322.4	2.224	1.675	41.01	181.94	0.0	0.0	0.025
300/12	16	6.6	320.6	2.104	1.247	26.23	122.13	0.0	0.0	0.026
300/13	11	6.5	314.7	2.279	1.457	14.46	66.01	0.0	0.0	0.027
300/14	29	6.4	307.5	2.149	1.335	41.12	217.83	0.0	0.0	0.026
300/15	20	6.7	308.5	2.196	1.383	39.35	172.81	0.0	0.0	0.028
300/16	20	5.6	315.5	1.772	1.158	32.58	141.10	0.0	0.0	0.028
300/18	35	4.5	291.5	1.523	1.087	54.11	198.07	33.76	379.30	0.006
303/11	29	3.5	314.8	1.318	1.082	62.61	241.17	0.06	0.12	0.023
303/12	19	4.6	329.6	1.380	1.218	29.04	114.63	0.0	0.0	0.030
303/13	16	3.8	325.4	1.520	1.286	23.10	79.85	0.0	0.0	0.030
294/15	8	7.0	307.0	1.929	1.368	18.41	69.62	4.06	13.48	0.033
293/12	14	7.0	309.8	1.937	1.441	25.96	141.59	0.0	0.0	0.030
293/11	21	7.0	305.6	1.641	1.382	24.72	137.02	46.80	230.58	0.025

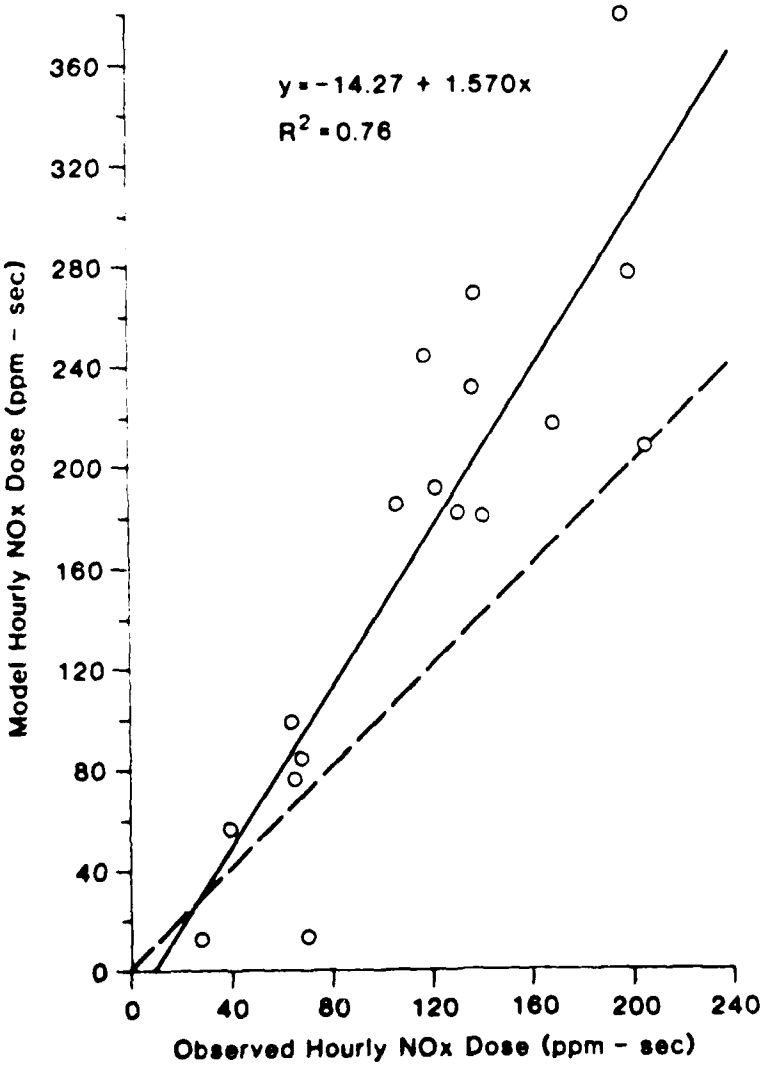

Fig. 3.9 Predicted versus Observed One-Hour NO_x Dosages

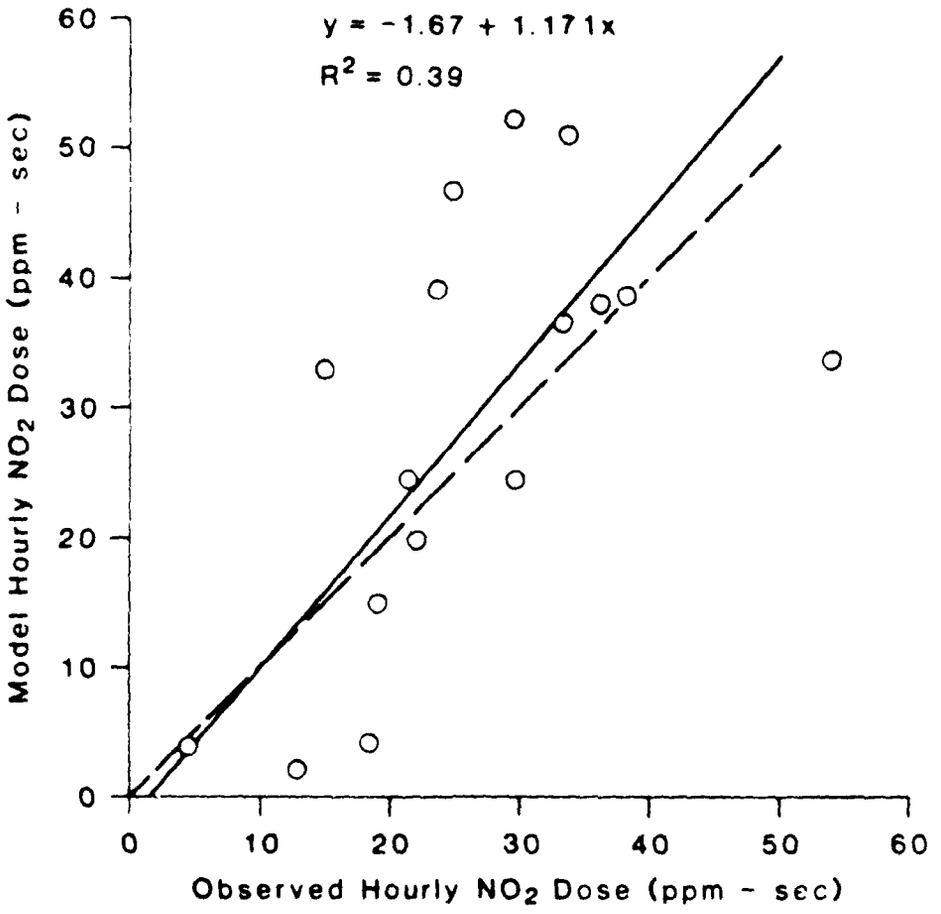

Fig. 3.10 Predicted versus Observed One-Hour NO_2 Dosages

with a correlation coefficient of 0.625 (R^2 = 0.39). In view of the difficulty usually experienced in trying to predict one-hour concentration values for any pollutant from a single source, these results should be considered quite acceptable. The slight overprediction for both NO_x and NO_2 may be due to the incomplete optimization of model parameters discussed previously.

3.3 MODEL APPLICABILITY AND LIMITATIONS

It is convenient to summarize in this section the general features of the model whose formulation, implementation, and validation have been discussed up to this point. The model's limits of applicability and the possibility of extending those limits to include more general situations will also be discussed.

The specific application for which the model was developed is the prediction of the contribution from aircraft takeoff activites to one-hour average NO_2 and NO_x concentrations in the vicinity of the runway involved. The effect of a single aircraft takeoff is simulated by a moving effective source point that generates an initial plume as it moves. The transport and dispersion of that plume is described by a general time-dependent formalism due to Lamb and Seinfeld (1973) in which the concentrations of NO_x and NO_2, uncorrected for the effects of ambient ozone and light intensity, are given by the product of an emission rate and a transport kernel integrated over the history of the source. The effects of the photolysis of NO_2 to produce NO and O_3, and the chemical reaction of NO with O_3 to produce NO_2, are incorporated into the model via the assumption, verified by us as well as by other workers, of the existence of a photostationary state in plumes and polluted atmospheres. The combined effects of many aircraft takeoffs over a one hour period are estimated by assuming that the effect of each is independent of the others, an assumption that is quite reasonable because of their staggered takeoff times from the runway and because of the short residence times of the model predictions at [illegible] within its limits of [illegible], the [illegible] is entirely acceptable.

As discussed [illegible], the [illegible] of the model are very general and are [illegible] to be modified to handle other situations. [illegible] sources, in the sense of several source points [illegible], other types of motion including taxiing and [illegible] could easily be made. The [illegible] this type of model should not be underestimated.

The applicability of the [illegible] is restricted in two ways. The first and most important is the fact that the model has been compared against observations only for a limited range of plume travel times and only at [illegible] runways. Furthermore, as

AD-A148 253 IMPACT OF AIRCRAFT EMISSIONS ON AIR QUALITY IN THE VICINITY OF AIRPORTS V..(U) ARGONNE NATIONAL LAB IL ENERGY AND ENVIRONMENTAL SYSTEMS DIV.. 2 2

UNCLASSIFIED K I BRUBAKER ET AL. APR 84 FAA/EE-84-14 F/G 13/2 NL

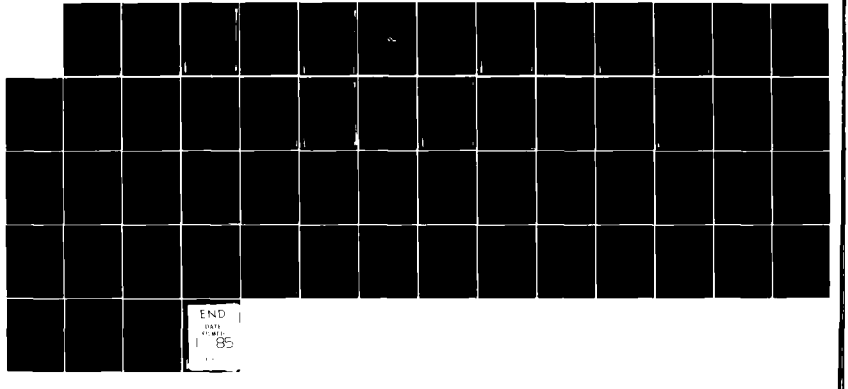

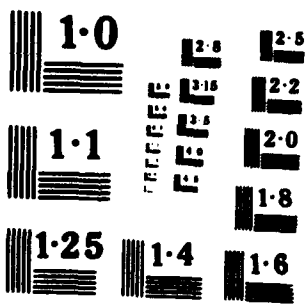
1·0
1·1
1·25
1·4
2·8
3·15
3·5
2·5
2·2
2·0
1·8
1·6

discussed earlier, the model should be regarded as only partially optimized and independent data on plume rise and on the horizontal and vertical rates of plume growth would be of particular value in any further optimization and/or validation work. In general, however, the existing model can be considered applicable to situations in which pollutant concentrations due to aircraft takeoff events are to be estimated at locations in the vicinity of a runway at any major airport or air base.

The second factor restricting the applicability of the model is that only certain types of aircraft, specifically the common types of passenger aircraft used by major commercial carriers, are presently included in the model. Extension to include other types of aircraft, including military aircraft, can easily be accomplished. With regard to one-hour concentrations specifically, the model requires the user to specify the number of takeoffs of each type of aircraft for the hour in question. A default distribution is currently incorporated in the code for use in the event that the specific distribution is not known. This default distribution is suitable only for runway 32R at Chicago O'Hare International Airport, and not for any other runway at O'Hare nor necessarily for runways at other airports or air bases.

4 AIRCRAFT HYDROCARBON-EMISSION CHARACTERIZATION

4.1 INTRODUCTION

Jet aircraft engines, like other sources involving the combustion of an organic fuel, emit hydrocarbons. Total hydrocarbon emission rates of several common jet engines for various aircraft operations are shown in Table 4.1, reproduced from Yamartino et al. (1980a). Clearly, the taxi/idle mode is the predominant source of aircraft hydrocarbon emissions. Table 4.1 does not provide any information on the chemical nature of those hydrocarbons, however, and for many purposes, detailed knowledge of the chemical composition is required. The second major component of the research program discussed in this report is the preliminary characterization of aircraft hydrocarbon emissions.

The motivation for this work is the fact that hydrocarbons are important precursors to the formation of photochemical smog. Certain types of hydrocarbons, notably the unsaturated hydrocarbons (alkenes and aromatics), are more active than others in the generation of photochemical smog (Finlayson-Pitts and Pitts, 1977 and Demerjian et al., 1974), although with very few exceptions all hydrocarbons are currently felt to contribute to some degree. The primary difference between the different types of hydrocarbon is the rate at which smog is generated, rather than the eventual amount. Any assessment of the effects of hydrocarbons must necessarily incorporate information about the actual composition of the emissions. In addition, if the particular composition of jet exhaust is sufficiently unique, it may be possible to determine quantitatively the contribution of aircraft emissions to the organic constituents collected in ambient air at some distance from an airport, and thereby obtain some measure of the relative contribution from aircraft.

The approach adopted in this work was to simultaneously collect air samples at Chicago's O'Hare Airport in the immediate vicinity of taxiing and idling aircraft and at sites that were expected to be free from the influence of aircraft emissions, obtain detailed chemical characterization of those samples, and identify aircraft emissions by comparison of simultaneous taxiway and background samples. Characterization by gas chromatography/mass spectrometry (GC/MS) permits evaluation of the similarities and differences among the samples and allows judgements to be made as to the sources of the various constituents identified in the samples.

4.2 MATERIALS AND METHODS

The air-sampling units used to collect vapor-phase organic compounds from the air at O'Hare Airport are specially modified high-volume air samplers. They consist of explosion-proof vacuum motors, in-line Gilmont flow meters, polymeric resin adsorbents, and 3-in. Teflon filters with an 0.3-

Table 4.1 Hydrocarbon Emission Rates (lb/hr) of Aircraft Engines[a]

Engine Manufacturer and Model	Taxi/ Idle	Landing	Takeoff	Approach	Climbout
Pratt and Whitney, JT9D-7	55.1	34.0	0.8	4.6	1.3
Pratt and Whitney, JT3D-7	124.6	77.0	5.0	6.5	3.3
Rolls Royce, RB-211-22B	100.1	72.2	29.1	32.2	8.3
General Electric, CF6-50C	36.2	21.8	0.2	0.1	0.2
General Electric, CF6-6D	21.8	16.2	8.3	7.0	6.8
Pratt and Whitney, JT8D-17	10.1	6.4	0.5	1.4	0.4
Rolls Royce, RDa7	25.5	17.4	8.8	0.0	2.1
Garrett AiResearch, TPE731-2	4.1	2.7	0.1	1.5	0.1
Pratt and Whitney, PT6A-27	5.8	3.5	0.0	0.5	0.0
General Electric, 700-2D	8.3	5.2	0.3	1.3	0.2
AVCO Lycoming, TIO540 J2B2	1.7	2.0	3.2	1.3	3.4

[a]All emission rates except those for landing are from Pace (1977). The landing emission rates are computed by assuming that the landing operation consists of 60% idle, 24% takeoff thrust (i.e., thrust reversers), and 16% approach thrust (to account for the spool-down/up/down cycle).

micron pore size. The air sample is drawn through the filter, which removes particulate matter, and then through a 120-gram bed of resin that collects the organic compounds.

The resin material used for this study was Rohm & Haas Amberlite XAD-2 resin. The resin was precleaned before use by extracting for four hours at least once in a Soxhlet apparatus, first with ethanol, then hexane, and finally methylene chloride. Sample collection was made at a rate of 30 liters per minute for 90 to 180 minutes. The exposed resin was returned to the laboratory and extracted in a Soxhlet apparatus for 30 minutes using 150 mL methylene chloride. A Kuderna-Danish evaporator was used to concentrate the methylene chloride extract to 1 mL.

The extracts were analyzed using a Hewlett-Packard 5982A GC/MS and a Hewlett-Packard 5934A Data System. The 5930 Hewlett-Packard gas chromatograph was equipped with a split/splitless Grob-type injection system and a 50-m large-bore fused-silica capillary column coated with OV-101. The temperature program selected to provide maximum resolution of the organic constituents started with a 2-minute hold at 20°C, followed by a programmed rate of 2°C/min to 110°C and finally, from 110°C to 270°C at 4°C/min.

4.3 SAMPLING PROTOCOL

A matched pair of sampling units was taken to O'Hare Airport on Jan. 9, 1981. One sampler, designated the downwind sampler, was located adjacent to the taxiway leading to runways 32R and 27R (Fig. 4.1). All aircraft using either of these runways passed the sampler, and emissions from the passing planes plus the normal background air were sampled. The other sampling unit was located across the airport adjacent to runway 9R. Since the prevailing winds were from the west and southwest and since runway 9R was not in use, emissions from aircraft were not expected to be collected by the second sampler. Power for the sampling units was supplied by portable generators. The generators were fueled and operated away from and downwind of the sampling units. Sampling was begun and terminated at prearranged times, so that simultaneous 3-hour samples were taken. A total of approximately 5.4 m^3 of air per unit was sampled. Following collection of the samples, the filters and particulates were discarded.

Several similar sets of samples were obtained on other dates. Experimental difficulties, particularly with respect to the need for careful pre-cleaning of resin that had been used previously, precluded the use of these other sets of samples in this analysis.

4.4 RESULTS AND DISCUSSION

The reconstructed total-ion chromatograms obtained from GC/MS analysis of the two samples are reproduced in Fig. 4.2 along with the chromatogram from

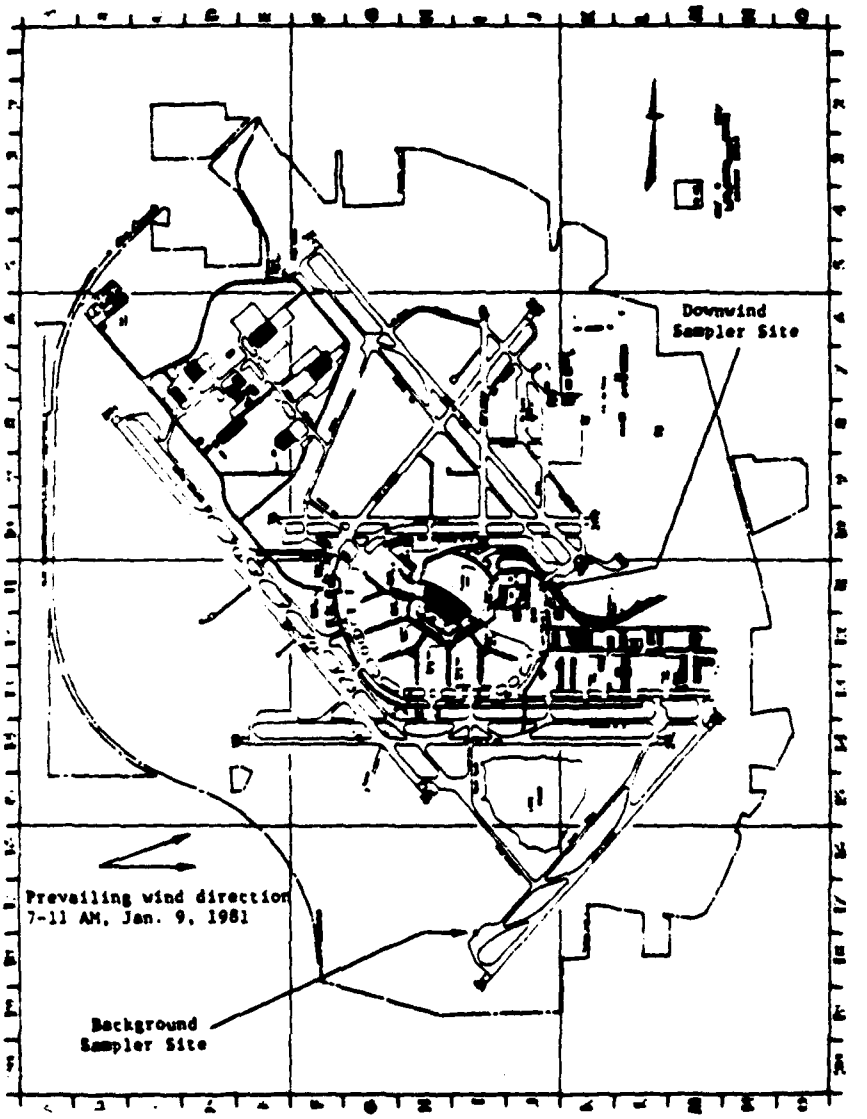

Fig. 4.1 Hydrocarbon Sampling Sites, January 9, 1981

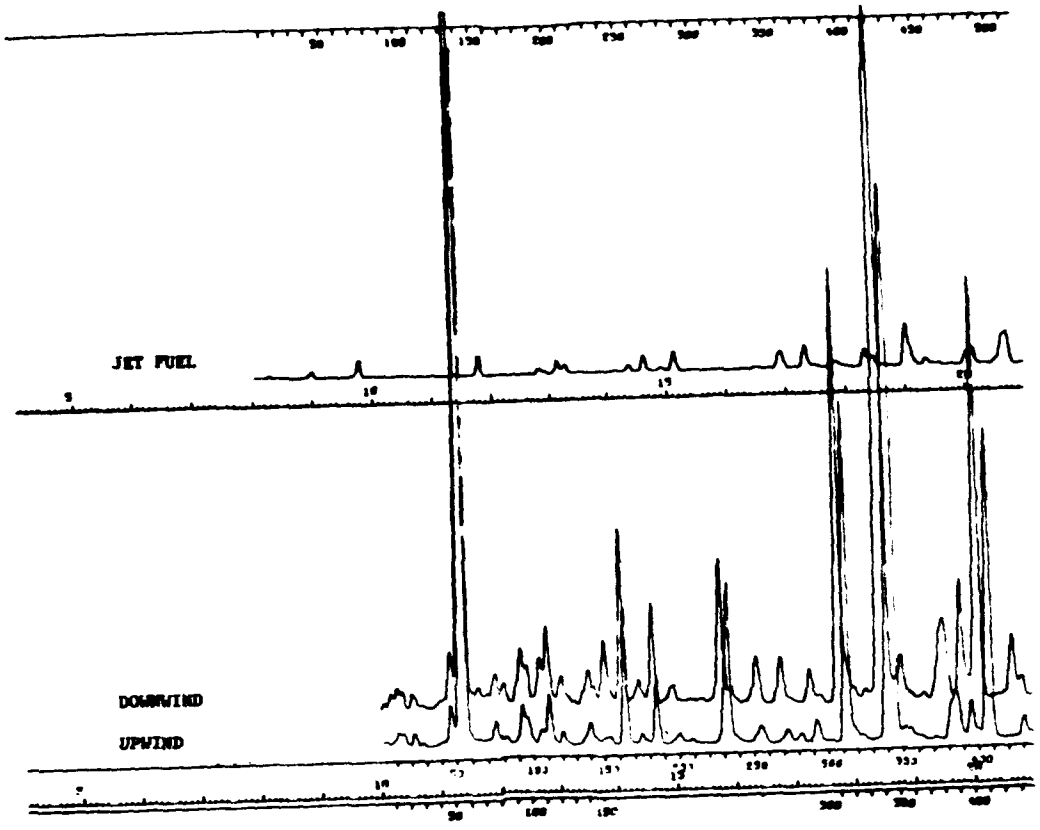

Fig. 4.2 Total-Ion Chromatograms for O'Hare Samples of January 9, 1981, and for a Liquid Jet-Fuel Sample

(The upper trace shown in the figure is the chromatogram for the jet fuel sample, the middle trace is the chromatogram for the downwind (aircraft taxiing/idling) sample, and the lower trace is the chromatogram for the background or ambient air sample.)

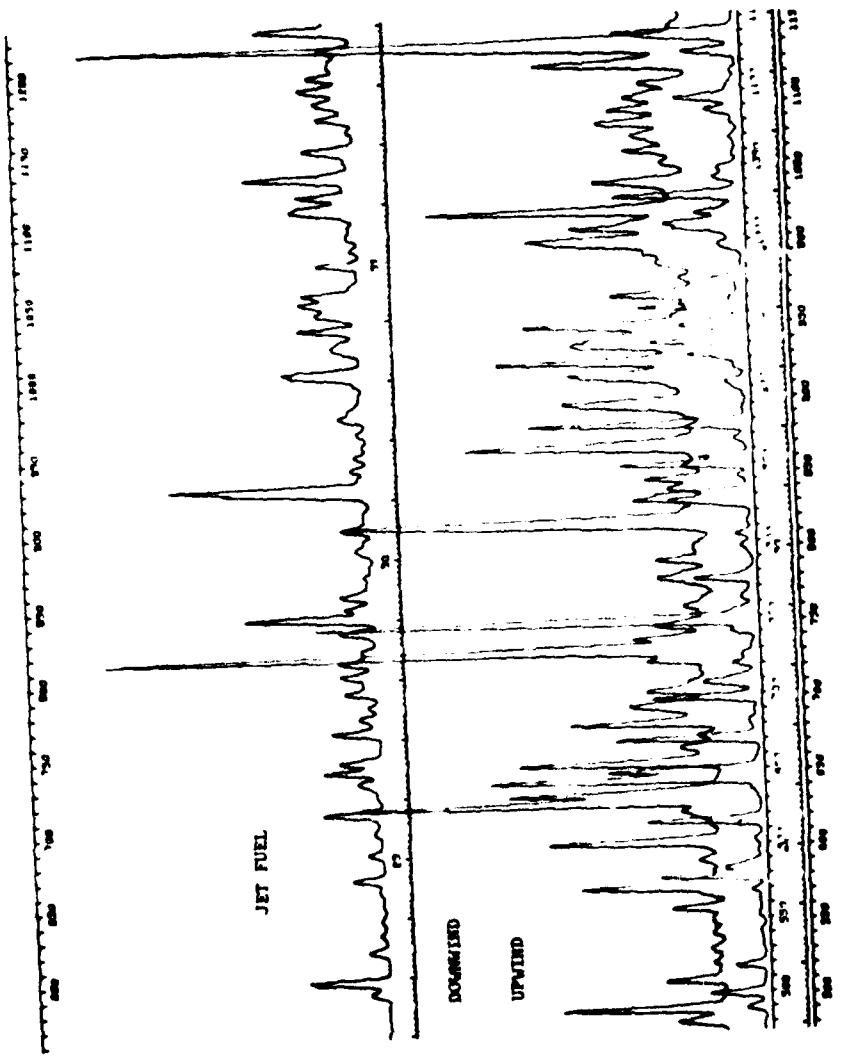

Fig. 4.2 (Cont'd)

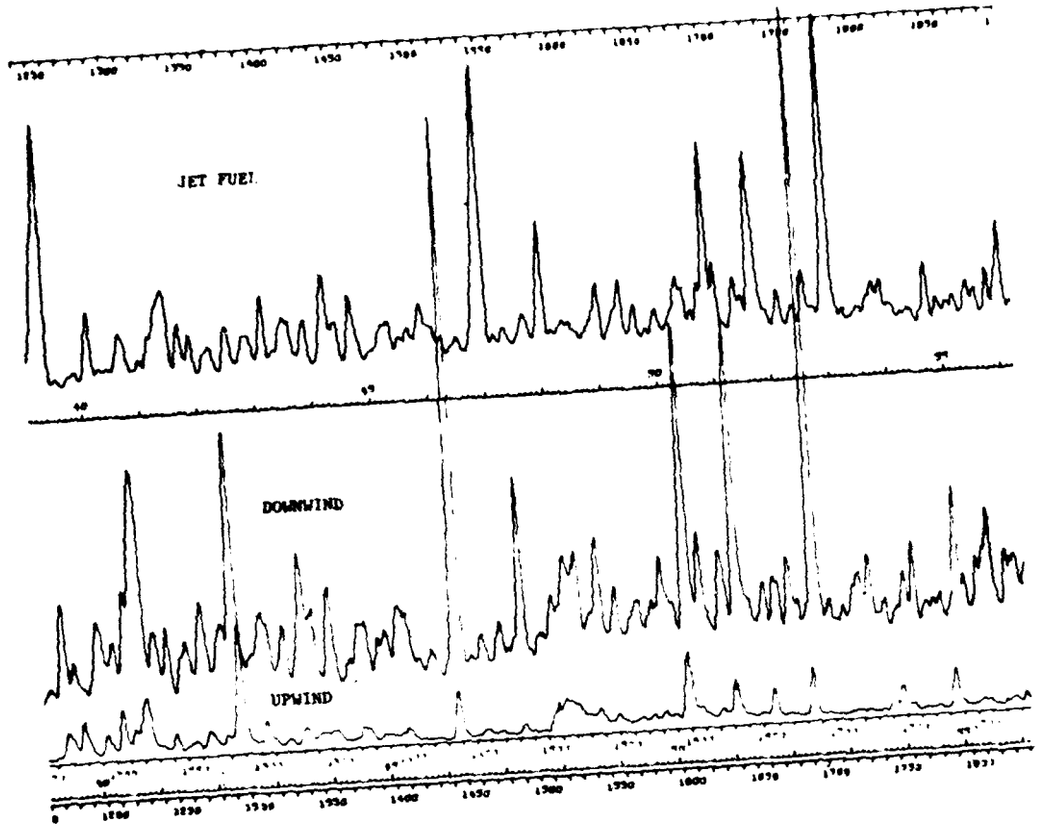

Fig. 4.2 (Cont'd)

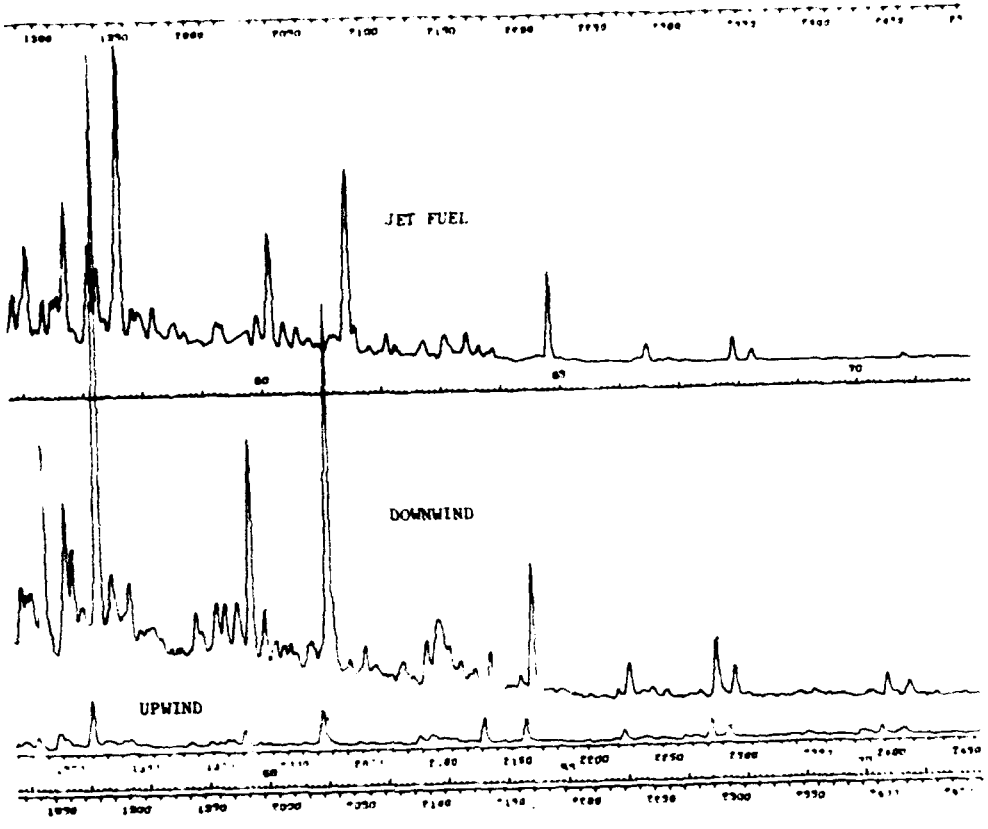

Fig. 4.2 (Cont'd)

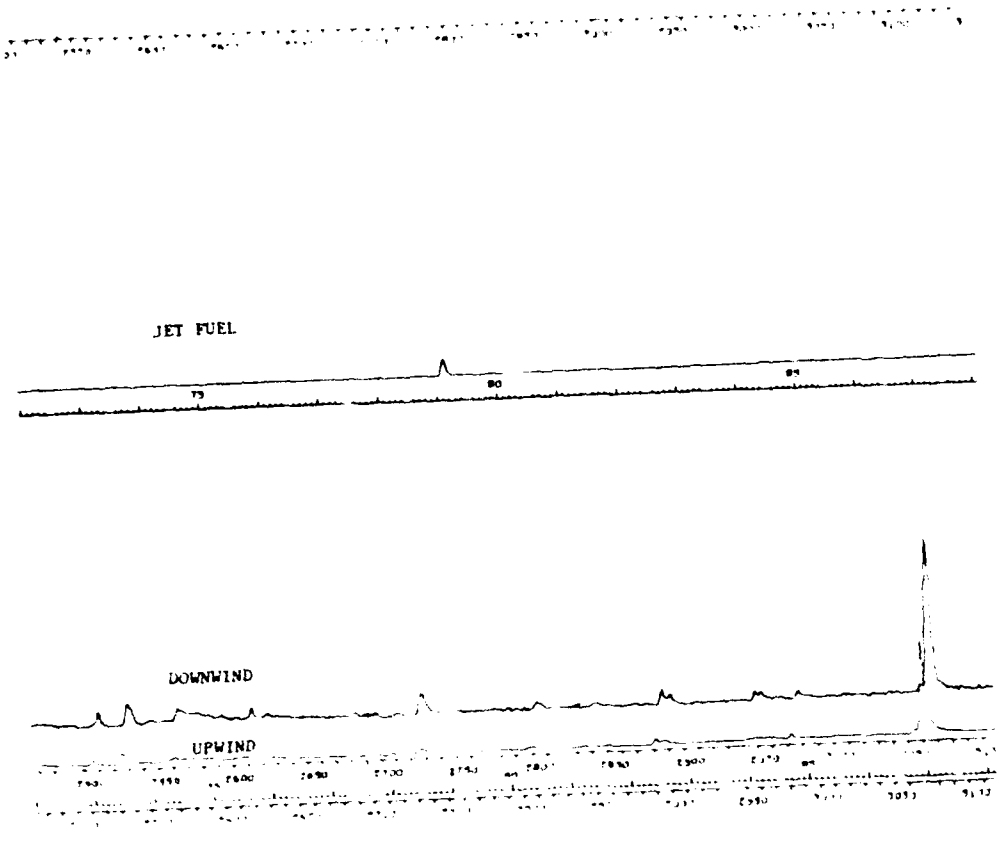

Fig. 4.2 (Cont'd)

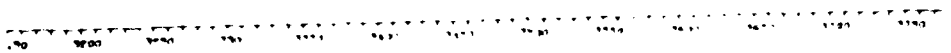

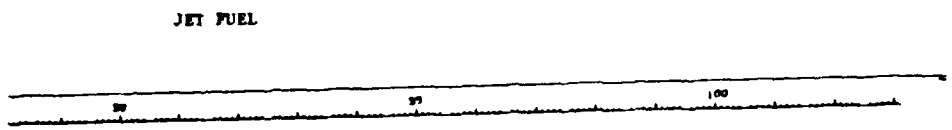

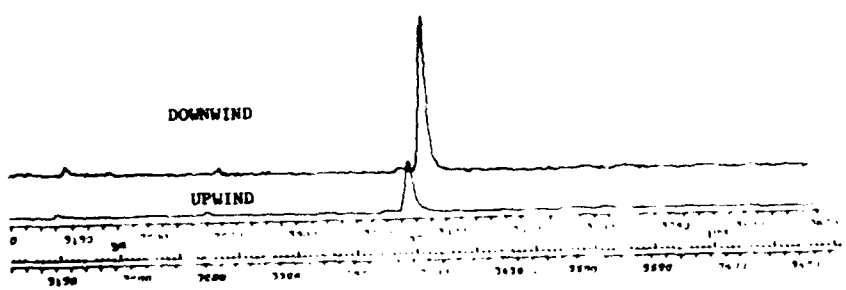

Fig. 4.2 (Cont'd)

a sample of raw jet fuel. Due to slight run-to-run differences, the retention times of the components in the upwind and downwind samples do not match exactly. Larger retention-time differences exist between the components of these samples and those of the jet fuel sample, which was analyzed approximately six months after the others. These differences do not preclude in any way an accurate evaluation of either the physical or chemical similarities and differences between the samples.

Examination of the chromatograms of the upwind and downwind samples reveals that the latter contain significantly more components than the former, and their concentrations as judged by peak height are generally greater. The more volatile components that appear in the early part (10-35 min) of the chromatograms produce identical "patterns" and are of very similar concentrations in the two samples. However, after a retention time of about 35 minutes, the concentration of components in the upwind sample falls off rapidly. The reverse is seen to be true for the downwind sample, and the difference seems to be primarily due to jet fuel in the gas phase, as may be seen by comparing the downwind-sample chromatogram with the chromatogram obtained from the jet fuel sample. The relative component concentrations within the jet fuel sample and the downwind sample appear similar over the range of retention times from 40 to 65 minutes. (The upper trace shown in the figure is the chromatogram for the jet fuel sample, the middle trace is the chromatogram for the downwind (aircraft taxiing/idling) sample, and the lower trace is the chromatogram for the background or ambient air sample.)

The chromatograms shown in Fig. 4.2 may be compared with respect to the absence and/or presence of total ion chromatographic peaks and their intensities (peak heights). In addition, similar peak patterns or fingerprints in the three chromatograms can be identified. A peak pattern, or fingerprint, is a sequence of peaks whose relative intensities are essentially identical in two or more chromatograms. For example, the patterns observed in the downwind sample chromatogram between the retention times of 36.4 to 38.0 min and 41.3 to 46.3 min are also observed in the jet-fuel-sample chromatogram. By contrast, the pattern at 47.5 to 48.5 minutes in the downwind-sample chromatogram is absent in the chromatogram of the jet fuel and is present to only a small extent in the upwind-sample chromatogram.

Comparison of samples by this method does not take into account the fact that different components having identical retention times may be present in these samples. In view of this, a comprehensive characterization of the major components in these samples was conducted. The results are presented in Table 4.2. For simplicity, the retention times of the components in the upwind and jet-fuel-sample chromatograms were normalized to the values obtained for the components in the downwind sample. A summary of the types and number of compounds identified in the three samples is presented in Table 4.3.

Examination of the identities of the compounds found in these three samples indicates they are essentially the same. Differences do exist, but

Table 4.2 Detailed Chemical Characterization of Atmospheric and Jet Fuel Samples

Retention Time (min)	Downwind Sample		Upwind Sample		Jet Fuel Sample		Comments
	Compound Identity	Peak Size	Compound Identity	Peak Size	Compound Identity	Peak Size	
1[illegible].1	C_7-Alkene	m	-		C_7-Alkene	M	
1[illegible].2	C_7-Alkyne	m	-		-		
1[illegible].3	C_7-Alkane	m	-		-		
1[illegible].4	C_7-Alkene	m	-		-		
1[illegible].5	*	m	-		-		
11.2	C_8-Alkene	m	-		-		
11.4	*Toluene*	M	Toluene	M	Toluene	M	
11.7	C_8-Alkene	m	-		-		
12.1	C_8-Alkane	m	C_8-Alkane	m	C_8-Alkane	m	
12.6	C_8-Alkane	tr	C_8-Alkene	tr	-		
12.8	C_8-Alkene	m	C_8-Alkane	m	C_9-Alkene	m	
12.9	-		-		C_9-Alkene	m	
13.1	-		-		C_9-Alkene	m	
13.8	C_8-Alkene	m	C_8-Alkene	tr	C_8-Alkene	m	
14.1	Tetrachlorethane	m	Tetrachloroethane	m	Tetrachloroethane	M	Recognizable pattern on all
14.4	C_8-Alkene	m	C_8-Alkene	m	C_8-Alkene	m	these chromatograms
14.6	C_8-Alkane	m	C_8-Alkane	m	C_8-Alkane	M	
14.6	C_8-Alkane	m	-		-		
15.8	MW 101	m	MW 101	m	-		
16.4	C_2-Cyclohexane	m	C_2-Cyclohexane	m	C_2-Cyclohexane	m	
16.8	C_9-Alkane	m	C_9-Alkane	m	C_8-Alkene	m	
17.2	C_9-Alkane	m	C_9-Alkane	m	-		
17.4	-		C_2-Benzene	m	-		
17.8	Ethyl Benzene	M	Ethyl Benzene	m	C_2-Benzene	M	Pattern distinguishable
18.2	C_9-Alkene	tr	-		C_9-Alkene	m	*also on downwind trace*
18.5	m,p-Xylene	M	m,p-Xylene	m	m,p-Xylene	M	
18.8	C_2-Cyclohexane?	m	-		C_9-Alkane	m	
19.5	C_9-Alkane	m	C_9-Alkane	m	C_9-Alkane	l	
19.8	Styrene	m	Styrene	m	-		
20.1	o-Xylene	M	o-Xylene	M	o-Xylene	M	
20.6	C_9-Alkene	m	C_9-Alkene	m	C_9-Alkene	M	Pattern present in all three
20.8	C_9-Alkene	tr	-		C_9-Alkene	m	
21.2	C_9-Alkane	tr	C_9-Alkene	tr	-		
21.3	-		C_9-Aldehyde or Ketone	m	-		
22.1	C_9-Alkene	m	C_9-Alkene	m	C_9-Alkane	l	
22.3	n-C_9-Alkane	m	C_9-Alkane	m	C_9-Alkane	M	Pattern present in all three
22.8	C_3-Benzene	m	C_3-Benzene	m	C_3-Benzene	l	

Table 4.2 (Cont'd)

Retention Time (min)	Downwind Sample Compound Identity	Peak Size	Upwind Sample Compound Identity	Peak Size	Jet Fuel Sample Compound Identity	Peak Size	Comments
23.1	C_3-Cycloalkane or C_9-Alkene	tr	-		C_9-Alkene	m	
23.3	C_3-Cycloalkene or C_9-Alkyne	tr	-		C_9-Alkene	m	These compounds differ between jet fuel and downwind sample
23.6	C_9-Alkene	tr	-		C_{10}-Alkene	m	
23.8	C_9-Alkene	tr	-		C_{10}-Alkene	m	
24.0	C_9-Alkene	m	C_9-Alkene	tr	C_{10}-Alkene	M	
24.4	Benzaldehyde	m	Benzaldehyde	tr	-		
24.5	-		$C_{10}H_{16}$	m	C_{10}-Alkane	m	
24.8	C_9-Alkene	tr	-		-		
25.1	C_3-Benzene	m	C_3-Benzene	m	C_3-Benzene	l	Present in all three
25.3	C_9-Alkene	tr	-		-		
25.6	C_9-Alkene	tr	-		C_{10}-Alkene	m	
25.8	n-Propylbenzene	M	n-Propylbenzene	M	n-Propylbenzene	m	
25.9	C_3-Benzene	m	C_3-Benzene	m	C_{10}-Alkene	m	
26.4	1,3,5-Trimethyl-benzene	m	1,3,5-Trimethyl-benzene	m	C_3-Benzene	m	
26.7	C_{10}-Alkene	m	-		C_{10}-Alkene	m	
26.8	-		-		C_4-Cycloalkene	m	
27.1	C_3-Benzene	m	C_3-Benzene	m	C_3-Benzene	m	
27.4	C_{10}-Alkane	m	C_{10}-Alkane	m	-		
27.6	C_{10}-Alkene	m	-		C_{10}-Alkane		
27.7	-		C_{10}-Alkane	m	C_{10}-Alkene	m	
27.8	-		C_{10}-Alkane	tr	-		
28.1	Benzofuran	m	-		-		
28.2	-		C_{10}-Alkane	tr	C_{10}-Alkane	m	
28.3	C_3-Benzene	M	C_3-Benzene	M	C_3-Benzene	M	
28.5	C_{10}-Alkene	m	-		C_{10}-Alkene	m	
28.7	C_{10}-Alkene	m	C_{10}-Alkene	tr	C_{10}-Alkene	m	
29.0	C_{10}-Alkene	m	-		-		
29.0	Dichlorobenzene	m	Dichlorobenzene	m			Not in jet fuel
29.5	C_{10}-Alkene	m	-		C_{10}-Alkene	m	
29.8	C_{10}-Alkene	m	-		-		
29.8	C_4-Benzene	m	C_4-Benzene	tr	C_4-Benzene	m	
30.4	n-C_{10}-Alkane	M	n-C_{10}-Alkane	m	-		C_{10}-Alkane absent in jet fuel
30.4	C_3-Benzene	M	C_3-Benzene	m	-		
30.8	C_4-Benzene	m	-		C_4-Benzene	l	

Table 4.2 (Cont'd)

Retention Time (min)	Downwind Sample		Upwind Sample		Jet Fuel Sample		Comments
	Compound Identity	Peak Size	Compound Identity	Peak Size	Compound Identity	Peak Size	
31.0	C_4-Benzene	m	C_4-Benzene	m	C_4-Benzene	m	
31.2	Indan	m	Indan	tr	-		
31.6	C_{10}-Alkene	tr	C_{10}-Alkene	tr	-		
31.7	C_{10}-Terpene	l	C_{10}-Terpene	l	-		
32.1	C_{10}-Alkene	tr	-		C_{10}-Alkene	m	
32.4	C_{10}-Alkane	m	C_{10}-Alkane	m	C_4-Cycloalkane		
32.6	-		-		C_{10}-Alkene	m	
32.7	-		-		C_{11}-Alkane	m	
32.9	C_4-Benzene	m	C_4-Benzene	m	-		
33.2	C_4-Benzene	m	C_4-Benzene	m	C_{11}-Alkene	m	C_4-Benzenes present in upwind
33.4	C_4-Benzene	m	C_4-Benzene	m	C_4-Benzene	m	and downwind samples as a
33.8	C_4-Benzene	m	C_4-Benzene	m	C_4-Benzene	m	group are not present in
34.3	C_4-Benzene	m	C_4-Benzene	m	-		jet-fuel sample
34.5	C_{11}-Alkene	tr	-		C_4-Benzene	m	
34.8	C_{11}-Alkene	tr	Oxygenated aliphatic	tr	-		
35.2	C_4-Benzene	m	C_4-Benzene	m	-		
35.5	C_1-Indan	m	C_1-Indan	m	C_4-Benzene	m	
35.8	C_4-Benzene	m	C_4-Benzene	m			
36.1	-		Oxygenated aliphatic	tr	C_{11}-Alkane	m	
36.1	-		-		C_4-Benzene	m	
36.2	C_{11}-Alkane	m	C_{11}-Alkane	m			
36.5	C_{11}-Alkene	tr	-		C_{11}-Alkane	m	
36.5	C_1-Indan	tr	-		-		Obvious "fingerprint" seen
36.7	C_{11}-Alkene	m	-		-		in downwind sample has
37.0	C_{11}-Alkene	m	-		C_{10}-Alkene	m	different components from
37.2	C_5-Benzene	m	C_5-Benzene	m	C_{10}-Alkene	m	those in the jet-fuel sample
37.4	C_5-Benzene	m	C_5-Benzene	m	C_5-Benzene	m	
37.6	C_5-Benzene	m	-		C_5-Benzene	m	
37.6	C_{11}-Alkene	m	-		-		
37.9	C_5-Benzene	m	-		-		
38.2	C_2-Benzaldehyde	m	C_5-Benzene	m	C_5-Benzene	m	Pattern recognizable in all
38.5	n-C_{11}-Alkane	M	C_{11}-Alkane	m	C_{11}-Alkane	l	three samples
39.2	$C_{11}H_{20}O$?	m	$C_{11}H_{20}O$?	m			
39.6	C_1-Indan	m	C_1-Indan	m	C_1-Decalin	m	
40.0	C_5-Benzene	m	C_5-Benzene	m	-		

Table 4.2 (Cont'd)

Retention Time (min)	Downwind Sample Compound Identity	Peak Size	Upwind Sample Compound Identity	Peak Size	Jet Fuel Sample Compound Identity	Peak Size	Comments
40.3	C_1-Indan	m	C_1-Indan	m	-		
40.5	C_5-Benzene	m	C_5-Benzene	m	-		Enhanced in downwind sample
40.7	C_5-Benzene	M	C_5-Benzene	m	C_5-Benzene	m	
41.0	$C_{11}H_{20}$?	m	-		C_1-Indan	m	
41.3	C_5-Benzene	m	C_5-Benzene	m	C_5-Benzene	m	
41.5	C_{12}-Alkene	m	-		C_{12}-Alkene	m	
41.6	C_5-Benzene	m	C_5-Benzene	tr			
41.9	C_5-Benzene	m	C_5-Benzene	m	C_5-Benzene	m	
42.2	C_5-Benzene	m	-		C_5-Benzene	m	
42.4	Napththalene	M	Naphthalene	m	Naphthalene	m	
42.8	C_5-Benzene	m	C_5-Benzene	m	C_5-Benzene	m	
42.9	-		-		C_{12}-Alkane	m	
43.0	C_{12}-Alkane	m	-		-		
43.2	C_{12}-Alkane	m	-		C_{12}-Alkane	m	
43.3	-		C_{11}-Alkene	tr	-		
43.5	-		C_2-Indan	tr	-		
43.8	-		C_{11}-Alkane	tr	-		
43.9	C_{12}-Alkane	m	-		C_{12}-Alkane	m	
43.7	C_2-Indan	tr	-		C_2-Indan	tr	
43.7	C_2-Decalin	tr	-		C_2-Decalin	m	
44.1	C_{12}-Alkane	m	-		C_{12}-Alkane	m	
44.4	C_6-Benzene	m	C_6-Benzene	tr	C_6-Benzene	m	
44.6	C_2-Decalin	m	C_5-Benzene	tr	C_{12}-Alkene?	m	
44.9	C_2-Decalin	tr	-		C_2-Tetralin?	tr	
45.0	C_{12}-Alkene	m	-		C_{12}-Alkene	tr	
45.2	C_2-Indan	m	-		C_2-Indan	m	
45.3	C_6-Benzene	m	C_5-Benzene	tr	C_6-Benzene	m	
45.3	-		-		C_2-Indan	m	
45.4	C_{12}-Alkene	tr	-		C_{12}-Alkene	tr	
45.6	C_{12}-Alkane	m	-		-		
45.8	C_2-Indan	tr	-		C_2-Indan	tr	
45.8	C_6-Benzene	tr	-		C_6-Benzene	tr	
46.3	n-C_{12}-Alkane	M	n-C_{12}-Alkane	m	n-C_{12}-Alkane	M	
46.7	C_2-Indan	m	-		-		
46.7	C_6-Benzene	m	-		C_6-Benzene	m	
47.0	C_6-Benzene	m	-		C_6-Benzene	m	
47.0	C_2-Decalin	m	-		C_2-Decalin	m	

Table 4.2 (Cont'd)

Retention Time (min)	Downwind Sample Compound Identity	Peak Size	Upwind Sample Compound Identity	Peak Size	Jet Fuel Sample Compound Identity	Peak Size	Comments
47.6	C_{13}-Alkane	l	C_{13}-Alkane	tr	C_{13}-Alkane	m	
47.6	C_6-Benzene	tr	-		-		
47.7	C_2-Decalin	tr	-		-		
47.7	C_1-Indan	tr	-		-		
47.9	C_2-Indan	m	-		-		
48.2	C_6-Benzene	tr	-		-		
48.4	C_{12}-Cycloalkane	m	-		C_{12}-cyclo-alkane	m	
48.8	C_2-Indan	m	-		C_2-Indan	m	
49.0	C_6-Benzene	m	-		C_6-Benzene	m	
49.3	C_3-Decalin	m	-		C_3-Decalin	tr	
49.3	C_6-Benzene	m	-		C_6-Benzene	tr	
49.7	C_7-Benzene	tr	-		C_{13}-Alkane	m	
49.9	C_{13}-Alkyne	m	-		-		
50.0	C_6-Benzene	tr	-		-		
50.2	-		-		C_{13}-Alkene	m	
50.3	2-Methyl Naphthalene	M	2-Methyl Naphthalene	m	2-Methyl Naphthalene	m	
50.4	-		-		C_{13}-Alkane	m	
50.5	C_{13}-Alkyne	m	-		-		
50.7	-		-		C_{13}-Alkyne	m	
50.9	C?-Alk?	m	-		-		
51.0	-		-		C_3-Indan	tr	
51.0	-		-		C_{14}-Alkane	tr	
51.1	C_{13}-Alkyne	M	1-Methyl Naphthalene	m	Methyl Naphthalene	m	
51.6	C_{13}-Alkene	m	?		C_{13}-Alkene	m	
51.8	C_{13}-Alkene	m	-		C_{13}-Alkene	m	
52.1	C_{13}-Alkene	m	-		C_{13}-Alkene	m	
52.1	C_3-Indan	m	-		C_3-Indan	m	
52.4	n-C_{13}-Alkane	M	-		n-C_{13}-Alkane	M	
52.7	C_{13}-Alkene	m	-		-		
53.0	C_{13}-Alkene	tr	-		-		
53.2	C_{13}-Alkane	tr	-		-		
53.3	C_3-Indan	m	-		C_3-Indan	tr	
53.5	C_{13}-Alkene	m	-		C_{14}-Alkene	tr	
53.7	C_3-Decalin	m	-	-			

Table 4.2 (Cont'd)

Retention Time (min)	Downwind Sample Compound Identity	Peak Size	Upwind Sample Compound Identity	Peak Size	Jet Fuel Sample Compound Identity	Peak Size	Comments
54.4	C_{13}-Cycloalkane	m	-		C_{13} Cyclo-alkane	m	
54.5	C_4-Tetralin	tr			C_4-Tetralin	tr	
54.6	C_4-Decalin	tr			C_4-Decalin	tr	
54.7	Biphenyl	tr			Biphenyl	tr	
55.	$C^?$-Alk$^?$ne	m			C_{14}-Alkane	tr	
55.1	$C^?$-Alk$^?$ne	tr			$C^?$-Alk$^?$ne	tr	
55.4	C_{13}-Alkane	tr			$C^?$-Alk$^?$ne	tr	
55.5	C_2-Naphthalene	tr			-		
55.6	C_{13}-Alkyne	m			C_{15}-Alkyne	m	
55.9	C_{14}-Alkyne	tr	-		-		
56.1	C_2-Naphthalene	tr	C_{14}-Alkane		C_2-Naphthalene	m	
56.2	$C^?$-Alk$^?$ne	tr	-		$C^?$-Alk$^?$ne	m	
56.4	C_2-Naphthalene	m	C_2-Naphthalene	m	C_2-Naphthalene	m	
56.7	C_2-Naphthalene	m	C_2-Naphthalene	tr	C_2-Naphthalene	m	
57.0	n-C_{14}-Alkane	m	n-C_{14}-Alkane	m	n-C_{14}-Alkane	M	
57.4	C_2-Naphthalene	m	-		C_2-Naphthalene	tr	
57.7	C_5-Decalin		-		C_{15}-Alkane	m	
58.1	-		-		C_2-Naphthalene	m	
58.3	n-C_{15}-Alkane	M	n-C_{15}-Alkane	m	n-C_{15}-Alkane	m	
58.7	Fluorene	m	-		-		

Peak size key:

M: major component (large peak intensity)
l: large component (moderate peak intensity)
m: minor component (small peak intensity)
tr: trace component

Table 4.3 Summary of Number of Identified Compounds by Hydrocarbon Type

Hydrocarbon Type	Sample		
	Jet Fuel	Downwind	Upwind
Saturated	27	29	21
Unsaturated	39	53	14
Cycloalkanes	4	6	1
Substituted Benzenes	36	45	35
Chlorinated Hydrocarbons	1	2	2
Indans	10	15	5
Tetralins	2	1	0
Decalins	4	9	0
Naphthalenes	8	7	5
Total	130	167	83

many are due to the relatively low concentrations of components (especially in the downwind sample) that were therefore not readily detected by the instrument. Thus, while 167 compounds were tentatively identified in the downwind sample, only half that number were found in the upwind sample. Computerized analysis of the jet-fuel-sample data indicated a total of about 450 compounds. However, only 130 were present in sufficient concentration to be easily identified by manual methods. Some differences were apparent between the downwind sample and the jet fuel sample. In particular, the peak pattern already indicated at 36.4 to 38.0 min in these samples is produced by different compounds, which demonstrates that using only peak patterns to ascertain chemical similarities can lead to incorrect evaluations. The percentages of the total number of major compounds identified that correspond to photochemically active unsaturated hydrocarbons (32%) and benzenes (27%) in the downwind sample are identical to those in the jet fuel sample. In the upwind sample, the corresponding percentages are 17 and 42%, respectively. Calculation of the peak intensities of the compounds in the jet fuel indicates that it consists of 39% unsaturated ring compounds (substituted benzenes, indans, naphthalenes, tetralins), 51% saturated hydrocarbons (alkanes, decalins, cycloalkanes), and 10% unsaturated hydrocarbons (alkenes) by weight. Two chlorinated hydrocarbons were identified in the samples. Surprisingly, tetrachloroethane was not only found in the upwind and downwind samples, but also in the jet-fuel sample. Dichlorobenzene was found only in the upwind and downwind samples.

4.5 CONCLUSIONS

The site of the upwind sampler (adjacent to runway 9P, Fig. 4.1) was selected to preclude the collection of aircraft emissions and provide an idea of the background content of the air prior to contamination by aircraft emissions. The fact that the early part (10-35 min) of the upwind-sample chromatogram appears to contain the same relative concentration of volatile components as the downwind-sample chromatogram is therefore not unusual and is attributable to hydrocarbons present in the background air. However, most of these lighter components are also present in the jet fuel sample with similar peak patterns, indicating that additional sampling is necessary to resolve their origin.

There is no doubt as to the source of the components with elution times of approximately 40-65 min in the downwind sample, since the peak patterns are nearly identical to those present in the jet-fuel-sample chromatogram. The identification of jet fuel as a major component is further substantiated by the similar percentages of the total number of major compounds identified in the two samples. The downwind sample contains a high percentage of unsaturated hydrocarbons and benzenes that apparently originate from the unburned jet fuel. Thus, this jet fuel appears to have a greater potential to cause photochemical smog than would a fuel consisting primarily of saturated hydrocarbons.

5 AIRCRAFT EMISSION EFFECTS ON PHOTOCHEMICAL SMOG

As indicated in the previous section, the principal motivation for studying hydrocarbon emissions from aircraft is the fact that hydrocarbons are precursors to the formation of photochemical smog. A detailed quantitative assessment of these effects for any particular airport necessarily involves a very significant expenditure of time and effort, substantially greater than that required for a comparable assessment for some unreactive pollutant. A summary of what is involved is given in Sec. 5.1 as part of a qualitative assessment based upon currently available information. Section 5.2 contains a disucssion of further research required in order to quantify the effect.

5.1 DISCUSSION

Assessing the impact of aircraft emissions on photochemical smog formation is complicated by several factors that do not exist in the case of an unreactive pollutant. The ozone criteria document (USEPA, 1978a) contains an extensive discussion of the current state of our understanding of the origin of ozone and other substances in the atmosphere that together comprise photochemical smog. Ozone itself results from the photolysis of NO_2, as described in Secs. 2.2.1 and 3.1.3, and the photostationary state between O_3, NO, and NO_2 does exist in urban atmospheres to a reasonable degree of approximation. The presence of trace amounts of various hydrocarbons in addition to oxides of nitrogen results in other manifestations of photochemical smog, including, for example, the production of additional ozone above the amount initially present and the production of a host of other substances, such as aldehydes, ketones, organic nitrates, and PAN (peroxyacetylnitrate) and its analogs, all of which result from oxidation of the hydrocarbons (Finlayson-Pitts and Pitts, 1977; USEPA, 1978a). The amount of ozone generated, the time needed to generate it, and the nature of the other reaction products depend upon, among other things, the specific chemical types of hydrocarbon present and their concentrations. The chemistry involved is quite complex, and certain aspects, such as the mechanisms by which higher-molecular-weight hydrocarbons are oxidized, are poorly or incompletely understood.

Elevated ozone levels and other photochemical-smog manifestations are present in plumes downwind from urbanized areas ("urban plumes"). These plumes are detectable at distances comparable to the total distance that pollutants can be transported by the wind over the course of a day. In addition, ozone and other substances can persist overnight and be ready to initiate further photochemical reactions the next day, with the result that photochemical smog episodes can persist for several days at a time within a multistate area over which the emissions and their reaction products have been distributed. This large-scale multiday aspect of the photochemical smog problem was only recognized within the last decade.

From this brief description, it should be clear that quantitatively characterizing the effect on ozone levels of a certain subset of precursor emissions, such as those due to aircraft, is a formidable task. Even if the more limited objective of achieving such a characterization within a specific urban plume or airshed on a single specific day were adopted, the amount of effort that is required is clearly substantial. In particular, even assuming that one or more appropriate computer models are available, the complexity of the chemistry requires that a very extensive and detailed emissions inventory be prepared, including not only aircraft sources but also all other sources both stationary and mobile that may contribute significantly, and including not only emissions of NO and NO_2 but also those of CO (carbon monoxide) and especially also those of various chemical classes of hydrocarbon (usually at least four classes are used: alkanes, alkenes, aromatics and aldehydes, although in some cases it may be desirable or even necessary to subdivide these still further). In addition, the computer model must incorporate a sufficiently detailed description of the chemical reaction kinetics, which itself requires that the various reactions and their rate coefficients be understood and known; of particular relevance here is our result that aircraft hydrocarbon emissions are composed to a large extent of unburned jet fuel, which consists of higher-molecular-weight hydrocarbons than those emitted by automobiles, for example. Most photochemical models incorporate a simplified description of the chemical kinetics associated with the lighter hydrocarbons emitted by autos and therefore may not be suitable in this application. The meteorological data requirements, even for a single-day simulation for a particular urban area, are also quite substantial for most photochemical models. Boundary and initial conditions must also be taken into account, and require the availability of suitable air-quality data. Finally, the computational burden and facility requirements are significant for most existing photochemical models. Thus, although the situation is not hopeless, the resource requirements for a modeling assessment of the impact of aircraft emissions on photochemical smog are substantially beyond the scope of this research effort.

It is possible, however, to utilize here several published studies of various kinds in order to discuss the potential impact of such emissions. In particular, the results of previous modeling studies, emission summaries, and smog-chamber studies all provide relevant information, although a quantitative assessment for a particular area cannot be made without the kind of effort described above.

Several modeling studies have been published that address the question of aircraft effects, including those of Frame (1978), Duewer and Walton (1978), and Swan and Lee (1980). Of these, the Duewer and Walton paper is the most useful. Frame's modeling approach does not appear to be suitable for the problem at hand, and no useful results are included in his brief paper. The work by Swan and Lee represents a "very preliminary" attempt to use a meteorological planetary-boundary-layer model for the purpose of making air quality predictions in the San Francisco Bay area and, according to the authors, no quantitative conclusions should be drawn.

Duewer and Walton used one version of the Livermore Regional Air Quality model (LIRAQ) to examine the effects of doubling or halving the emissions from commercial-aircraft activities in the San Francisco Bay area. A considerably more detailed chemical-reaction system was used than in the other two works mentioned above, and yet the hydrocarbon reactions are more typical of light than of heavy hydrocarbons. Duewer and Walton also suggest that the neglect of natural hydrocarbon emissions in this inventory may represent a substantial omission. Aircraft emissions comprise 2.3% of the basic (1975) inventory with respect to both NO_x and HC (hydrocarbons). Calculations were carried out using meteorological data for one specific day, chosen because both observational data and previous modeling results had indicated the conditions to be particularly suitable for ozone formation. In addition to the 1975 inventory, a projected 1985 inventory was also used as a basis for examining the sensitivity of ozone levels to aircraft emissions.

Significant local effects on the concentrations of primary pollutants, aldehydes, and NO_2 were predicted in the vicinity of major airports. This result is certainly understandable, since in the corresponding emission-model grid cells, aircraft emissions account for more than 50% of the NO_x and Hc emissions. Local reductions in ozone levels were also predicted, resulting from scavenging of ozone by reaction with NO. For the 1975-inventory calculation, ozone concentration increases of a few (up to 3) ppb were predicted downwind of the major airports when aircraft emissions were doubled. The effect appeared to be a nearly linear function of the relative change in aircraft emissions. For the 1985 inventory, increasing aircraft emissions resulted in a reduction in ozone levels over most of the area covered by the model. Significant ozone increases were predicted only for a few downwind stations, mostly in the northeastern part of the modeled region. This difference is attributed to two significant differences between the 1975 and 1985 inventories. First, the ratio of aircraft hydrocarbon emissions to aircraft NO_x emissions declined from 1.42 for 1975 to 0.90 for 1985, and second, a similar change occurred in the overall Hc/NO_x emission ration, from 1.45 to 1.07. It is known in general that the Hc/NO_x emission ratio is a significant factor in determining the ultimate amount of ozone produced.

Two remarks seem to be in order concerning these results: (1) It appears that Duewer and Walton did not do a calculation for 1985 in which the aircraft HC/NO_x emission ratio was maintained at its 1975 value. This calculation would have simulated the effect of imposing no additional emission controls on aircraft. (2) The fact that increases in ozone at downwind sites were in fact predicted may imply that the time required for maximum ozone formation may simply have been lengthened by the change in the HC/NO_x ratio and the corresponding downwind distance is such that it lies outside the modeled domain. In this respect, a model that can follow a plume for some distance downwind might have been a more suitable tool for making this kind of assessment. Overall, the effect of aircraft emissions does not seem large according to the results of Duewer and Walton, but the issue cannot be regarded as settled.

Another useful source of information is the published emission summaries that compare aircraft and other emissions at various levels of aggregation. Although a comprehensive review of such sources of information has not been made, a partial compilation of recent results appears in Tables 5.1, 5.2, and 5.3. Table 5.1 summarizes aircraft hydrocarbon and NO_x emissions at a few selected airports and air bases, expressed as percentages of the total hydrocarbon and NO_x emissions at the airport or air base. These results indicate that on the local level, aircraft emissions at major metropolitan airports account for between 70% and 95% of the total for both hydrocarbons and NO_x. The situation is mixed at air bases, with aircraft accounting for the vast majority of emissions at Williams AFB but for a significantly lower percentage at the other air bases. Table 5.2 gives the total annual hydrocarbon and NO_x emissions for selected airports and air bases. The total aircraft emissions at these selected sites vary over nearly two orders of magnitude, although the major commercial airports each give rise to at least several hundred metric tons per year of both pollutants. It is interesting to note that aircraft hydrocarbon emissions from Chicago O'Hare alone are greater than the combined total for all aircraft included in Duewer and Walton's modeling study, and the NO_x emissions are only slightly less than those for San Francisco. In this context it would have been interesting to see the results of a calculation for San Francisco in which all aircraft emisssions were assumed to arise from a single airport.

Table 5.3 gives aircraft emissions as percentages of total AQCR (Air Quality Control Region) emissions from all sources. Generally speaking, aircraft account for up to 3% of both hydrocarbon and NO_x emissions. At this level of aggregation, however, the results may be somewhat misleading in the sense that not all the emissions within an area as large as an AQCR will affect pollutant concentrations at the same locations. In assessing the effect of aircraft emissions, one must keep in mind that only those locations downwind of an airport or air base will be affected on a given day. The aircraft emissions from a given airport or air base should be compared with only that part of the other emissions that have an effect at the same locations. In addition, one has to keep in mind that the downwind distance from a source is an important factor in determining pollutant concentrations. Clearly, an emission comparison such as is given in Table 5.3 should be considered as a qualitative indicator only. It might also be mentioned here that nationwide, aircraft account for 1.2% of the hydrocarbon and 0.6% of the NO_x emissions (Naugle and Fox, 1981).

A third useful indicator of potential aircraft effects on photochemical smog is a recent report by Pitts and co-workers at the California Statewide Air Pollution Research Center containing the results of an extensive series of outdoor smog-chamber experiments in which various types of jet aircraft fuel were characterized with respect to their ozone-forming potential (Carter et al., 1981). This research represents the only investigation known to us that has looked explicitly at photochemical effects arising from the specific hydrocarbon mixtures that comprise several commonly used jet fuels. The

Table 5.1 Aircraft Emissions as Percentages of the Airport/Air Base Totals

Airport Air Base	NO_x	HC	Reference
Atlanta	75	69	Naugle and Fox (1981)
Atlanta	77*	78*	Naugle and Fox (1981)
Dulles International	84	72	Shelar (1978)
Dulles International	91*	84*	Sandys (1978)
Minneapolis	93*	87*	Sandys (1978)
Tinker AFB	45*	69*	Sandys (1978)
Davis Monthon AFB	31*	36*	Sandys (1978)
Williams AFB	86*	98*	Sandys (1978)

*Percentage of aircraft and vehicular emissions only; other sources ignored.

Table 5.2 Annual Aircraft Hydrocarbon and NO_x Emissions at Selected Airports/Air Bases

Airport/Air Base	Aircraft Emissions (metric tons/year) NO_x	HC	Reference
Dulles International	642	881	Sandys (1978); Shelar (1978)
Minneapolis	464	637	Sandys (1978)
Chicago O'Hare	4138	8674	Daley and Naugle (1978)
San Francisco*	4818	8220	Duewer and Walton (1978)
Tinker AFB	360	92	Sandys (1978)
Davis-Monthon AFB	54	30	Sandys (1978)
Williams AFB	1400	120	Sandys (1978)

*Combined totals for three major bay-area commercial airports (San Francisco, San Jose, and Oakland), three military airfields (Alameda Naval Air Station, Moffett Field, and Hamilton AFB) and several general aviation airports. Commercial aircraft emissions comprise about two-thirds of each total.

Table 5.3 Aircraft Emissions as Percentages of AQCR Totals

AQCR	Airport	NO_x	HC	Reference
Atlanta	all	3.2	3.1	Naugle and Fox (1981)
	ATL	2.3	2.1	Patten (1978)
DC	all	-	-	
	DCA	0.6	0.2	Patten (1978)
Los Angeles	all	0.81	1.30	Jordan and Broderick (1978)
	LAX	0.5	0.5	Patten (1978)
NY-NJ-Conn	all	0.50	0.70	Jordan and Broderick (1978)
	JFK	0.3	0.7	Patten (1978)
Chicago	all	0.59	0.70	Jordan and Broderick (1978)
	ORD	0.6	1.0	Patten (1978)
San Francisco	all	1.20	1.60	Jordan and Broderick (1978)
	all	1.9	2.2	Duewer and Walton (1978)

results have special significance from the point of view of this report, since the major conclusion arrived at on the basis of the measurements described in Sec. 4 was that the composition of hydrocarbon emissions from queuing aircraft is essentially the same as that of unburned jet fuel. Thus many of the smog-chamber results may be taken over more or less directly into the atmosphere. However, the smog-chamber experiments do not in fact simulate faithfully all the features of atmospheric chemistry, for several reasons (nor do Pitts and co-workers claim that they do). In particular, the effects of hydrocarbons emitted by other sources, especially automobiles, are not included, nor are the overall effects of dilution and fresh NO_x injections. Also, it is known that smog-chamber walls act as a free radical source under irradiation with sunlight or UV light, and these chamber effects are not very well understood. Nevertheless, the results of Carter et al. are very useful for understanding the qualitative effects that the rather-high-molecular-weight hydrocarbons in jet fuel have on the formation of smog, especially relative to other fuels, and represent a starting point in the research work needed to understand the photochemistry of NO_x-jet fuel mixtures.

Rather than discuss all the results and conclusions arrived at by Carter et al., we refer the reader to their report. In the context of this discussion, the two results of greatest significance are (1) that the reactivity of a hydrocarbon fuel, consisting of a mixture of alkanes and aromatics, with respect to the rate at which ozone is generated, increases with increasing aromatic content, and (2) that the total amount of ozone that can be formed may not differ greatly from fuel to fuel. In addition to several types of jet fuel, unleaded gasoline and diesel No. 2 were examined, and both were found to be more reactive with respect to ozone formation rate than any of the jet fuels examined. The reactivities correlated well with aromatic content except for those fuels consisting almost entirely of various polycyclic C_{10} to C_{14} isomers. Such fuels are high-energy fuels developed for use in various military applications, and all result in only slow formation of ozone.

The second result cited above indicates, however, that given enough time, even the unreactive hydrocarbons can ultimately cause the formation of as much, if not more, ozone than can the reactive fuels. Carter et al. point out in addition that the conditions under which optimum ozone formation occurs differ from fuel to fuel because of the effect of nighttime ozone and NO_x removal. They also note that the types of experiments that were conducted are not particularly suitable for determining maximum ozone yields, especially for relatively unreactive fuels. Carter et al. go on to say that diesel No. 2 clearly forms less ozone, and that it is probable that unleaded gasoline may also form somewhat less ozone than the other fuels. The implication seems to be, although it is not stated in so many words, that the jet fuels examined all probably form more ozone, albeit after a longer period of time, than does unleaded gasoline and that this is clearly the case for diesel No. 2. In other words, aircraft hydrocarbon emissions may give rise to less ozone than do other emissions on the day of the emission, but they have the potential to

generate an equal, if not a greater, amount of ozone than others in multiday episodic situations.

5.2 FURTHER RESEARCH REQUIREMENTS

Progress must be made in at least two areas before the impact of aircraft hydrocarbon and NO_x emissions on photochemical smog production can begin to be quantified. The first area is that of our knowledge of emission rates and composition. Additional studies should be carried out in order to (a) verify or refute our observation that the composition of hydrocarbon emissions from queuing and taxiing aircraft is essentially that of raw jet fuel, and (b) quantify the emission rates of several classes of hydrocarbon, including alkanes, alkenes, aromatics, and oxygenated hydrocarbons such as aldehydes. It may be desirable to consider subclasses as well, the main criterion being similarity of chemical behavior in the generation of photochemical smog. It is understood that some of this work is already being done by other research groups.

The second area in which progress is needed is that of understanding the various chemical reactions that hydrocarbons of the type in jet fuel and in jet-engine emissions undergo in the atmosphere. As discussed in the previous section, a good beginning has been made in this respect, but more work is needed in order to develop a reaction mechanism that could be incorporated into a photochemical smog model. For a detailed list of recommendations along these lines, see the report by Carter et al. (1981). Experiments involving mixtures of jet fuel and other hydrocarbons representative of automotive emissions would be useful in elucidating the interaction of aircraft emissions with urban photochemical smog.

The research goals just mentioned will take some time to achieve, and enough information exists now to allow the development of a preliminary reaction mechanism for heavier hydrocarbons that could be used in a photochemical modeling study. We recommend that, concurrent with the fundamental chemical kinetic studies, such a preliminary mechanism be developed and incorporated into a model and that the resulting model be exercised to obtain estimates of the actual effect of aircraft emissions on photochemical smog for single-day simulations. This type of initial quantitative assessment would be valuable in providing timely information to FAA and USAF on such impacts and may also indicate the need for specific experimental or observational studies to provide data in areas where they are lacking.

6 SUMMARY, CONCLUSIONS AND RECOMMENDATIONS

6.1 NITROGEN DIOXIDE EFFECTS AND MODELING OF TAKEOFF EMISSIONS

A combined field-measurement and model-development program has been carried out to investigate aircraft contributions to ambient NO_2 and NO_x levels. The field measurements were made at one location near a busy runway at Chicago's O'Hare International Airport over a period of approximately two and a half months in the fall of 1980, with a complete set of measurements of all variables being taken once every second throughout the entire period. A large data base has thereby been compiled, suitable not only for the purposes of the work reported here but for other possible studies involving jet-aircraft takeoff events. General data reduction and processing routines have been developed that facilitate the use of this data base.

Much of the analysis discussed in Sections 2 and 3 could not have been made without the high sampling rate utilized in this study. In addition to allowing detailed plume concentration profiles to be determined, the high sampling rate allowed reasonably accurate corrections to be made for instrument/sampling system effects such as arise from finite response times and relative time lags in concentration measurements. In our opinion, the gain in resolution obtained by including these procedures was significant. It is strongly recommended that in any future field monitoring studies of a similar nature, similar efforts be made. In addition, the high desirability of redundancy in the monitoring instrumentation was pointed up when problems were encountered in the dynamic calibration system used in calibrating one of the NO_x instruments. The presence of another NO_x instrument using a different calibration procedure turned a serious and program-threatening problem into an annoying but solvable difficulty.

Several notable results arose from the measured data themselves, independent of any modeling assumptions. Most of these results were obtained as part of a general effort to independently check several assumptions that were incorporated into the model being developed.

The ambient air measurements of NO, NO_x, and O_3 were checked for consistency with the assumption of a photostationary state in the ambient atmosphere. Although a totally independent verification could not be made because of the lack of direct measurements of the NO_2 photodissociation rate coefficient k_A, the data were found to be consistent with the photostationary-state assumption, as expected from other studies. Equally as important for the model-validation phase of the program, an empirical expression with which k_A could be estimated from pyranometer data was developed. The expression so derived was consistent with similar results reported in the literature. The consistency of the results of the analysis of ambient data and the development of a method for estimating k_A with other results reported in the literature served also as a valuable check on the data collection, reduction, and processing procedures.

The assumption of a photostationary state within aircraft plumes was also made in the NO_2 model, and an important result of the field program was the verification of this assumption by two different techniques. The first method involved examining the quantity $\Phi = [NO][O_3]/K[NO_2]$ and its possible dependence on the NO_x concentration. No significant dependence was found, implying similar values both within and without aircraft plumes. In addition, the median value of this quantity was near unity, the value expected from the photostationary-state assumption. Problems can arise with this technique, however, primarily related to (1) the estimation of $[NO_2]$, which must be done by taking the difference of $[NO_x]$ and $[NO]$, and (2) the facts that Φ is intrinsically positive and its expected value is unity. Measurement errors in Φ can never amount to less than -1.0 but can be greater than zero by virtually any amount. Consequently, the results using this method can be biased towards values greater than one.

The second method of verification was designed to avoid these difficulties and consisted of computing the average value of the quantity $D = ([NO]/[NO_x]) - K/([O_3] + K)$ for concentrations measured at the peaks of fifty individual plumes chosen for analysis. The computed average value was well within one standard deviation of the expected value of zero, thereby confirming again the photostationary-state assumption for aircraft plumes.

The ratio of NO_2 to NO_x in direct emissions by jet aircraft was estimated from NO, NO_x, and O_3 measurements at the peaks of the plumes referred to above, in combination with the corresponding ambient measurements. The value found for the ratio of NO to NO_x was $0.93 \pm (1\sigma)0.08$, implying an emission ratio of 7% for NO_2/NO_x. This result was found to be independent of aircraft type, although only Boeing 727s and McDonnell-Douglas DC-10s were considered. The value obtained in this work agreed closely with other estimates in the literature, but represented a totally independent check because of the utilization of measurements involving actual aircraft plumes rather than direct engine-emission measurements.

The primary goal of the study was to investigate aircraft effects on local NO_2 concentrations. Two mechanisms exist whereby aircraft emissions affect NO_2 levels: direct NO_2 emissions and chemical reaction of direct NO emissions with ozone in the ambient air to form NO_2. By measuring NO, NO_x, and O_3 within a number of plumes, it proved to be possible to evaluate the relative importance of these two mechanisms and its dependence on the travel time of a plume since emission. The fraction f of the measured peak NO_2 concentration that is due to the NO + O_3 reaction is given by $f = ([O_3]_a - [O_3]_p)/[NO_2]_p$, where subscripts p and a denote peak plume and ambient values, respectively. Our results showed that for aircraft plumes, f is approximately 0.3 at a travel time of 40 s, and approximately 0.7 at 80 s. Furthermore, f is expected to lie between 0.9 and 1.0 after approximately 120 s and to approach the limiting value of 1.0 for longer travel times. These results were found for rather low ambient ozone levels; the relative importance of chemical reaction is expected to increase with increasing ozone concentration

for any given travel time. These results were independent of aircraft type, only 727s and DC-10s being considered.

Finally, observed NO_2 and NO_x aircraft-related one-hour dosages were found to be linear functions of the number of takeoffs per hour, as expected. Of the 31 one-hour periods examined, the highest aircraft-related NO_x dosage was 250 ppm-s, corresponding to a one-hour average concentration of 69 ppb, and the highest aircraft-related NO_2 dosage was 64 ppm-s, corresponding to a one-hour concentration of 18 ppb. The linear relationship between hourly dosage and number of takeoffs supports the approach adopted in the model, which involves computing the dose due to a single aircraft of each type and multiplying by the number of takeoffs of each. The slope of the line of a plot of dose versus takeoffs per hour is expected to depend somewhat on the particular mixture of aircraft types involved in addition to the location of the observer. The most prevalent aircraft on the runway used in this study were 727s and DC-10s; relatively few Boeing 747s were observed, for example, and a 747 has 35% more NO_x emissions than a DC-10 and 214% more than a 727. The possibility exists, therefore, for significantly higher NO_2 and NO_x concentrations to be produced with a different aircraft mix and, for NO_2, with higher ambient ozone levels.

The mathematical model, which was developed and implemented in a FORTRAN computer program, incorporates a very general, time-dependent formulation suitable for evaluating effects from several sources, each undergoing an arbitrary set of motions. The current version of the computer program incorporates only a description of the motion of aircraft during takeoff, and handles only one takeoff event at a time, although the generalization to other modes of activity involving other movements could be made with relative ease. The current model predicts both single-plume and one-hour average concentrations of NO_x and NO_2, although again with relatively minor changes other pollutants such as CO or particulate matter could be handled as well.

The validation of the model proceeded in two steps. Initially, the width and depth of an individual aircraft plume were expected to grow proportionally to $t^{1.2}$ (Gifford, 1977), where t is the travel time. An examination of the width of approximately fifty plumes indicated however that the (horizontal) standard deviation σ_h varied as $At^{0.57}$ rather than the higher rate expected from other published results, although considerable scatter exists in these data and it would be highly desirable to examine more data in order to get a better statistical basis for such an estimate. The appropriate modification was made to the model, and the coefficient A was adjusted so that model predictions were on the average in agreement with observations of σ_h.

Based on the experience with plume widths, it was decided to attempt to determine both the plume height and the (vertical) standard deviation σ_z as functions of travel time. Due to the functional form of the expressions used in the model, plume rise and vertical dispersion must be considered jointly. Also, since measurements were made at only one location and height, a unique

determination was impossible and several additional assumptions had to be made, particularly with respect to the functional form used to express the time dependence and to the expected behavior in certain limiting cases. The adjustment of the values of several parameters that appear in the equations was carried out by trial and error in such a way as to cause the model predictions of peak NO_x concentrations to agree on the average with observed peak NO_x concentrations. This approach was fairly successful for travel times up to about 100 s, but beyond this the model still systematically underpredicts peak values. Due to budget and time constraints, a more general optimization procedure making use of substantially more data could not be developed, although in our opinion a significantly better parameterization would result from a more extensive effort in this regard. As things now stand, the optimization of the single-plume model should be regarded as only partially complete.

Another aspect of this situation is that additional independent experimental determinations of plume rise and both horizontal and vertical growth as functions of travel time are needed. The method of assessment used here, that of optimizing parameters within the context of a particular dispersion model, is not as satisfactory from a scientific point of view as that of incorporating independently derived expressions.

In addition, several cases were found of individual plumes for which the back trajectories computed by the method discussed in Sec. 3.1.6 did not intersect the runway, and indeed could be rather far from it. Similar situations were found for a number of the one-hour periods examined in Sec. 3.2.1. Systematic deviations from straight-line trajectories are suspected as the cause of this behavior; in other words, the wind field in the vicinity of runway 32R may not be sufficiently homogeneous for the straightforward approach used in this work, which considers mean trajectories to be straight. A possible reason for the apparent lack of homogeneity is the presence of several Air Force alert hangars near the monitoring site. These hangars are sufficiently large and are located in approximately the right place to cause the observed behavior. It may be possible to correct for this effect, although no such correction was attempted in this study.

The results of the validation of the multiple-plume version of the model for the prediction of one-hour dosages and the corresponding one-hour average concentrations were satisfactory, considering the difficulties discussed above. Graphs of predicted and observed NO_x and NO_2 dosages yielded acceptable regression lines, and the agreement would be expected to improve if the single-plume description were improved as suggested above. On the whole, the model currently tends to overpredict one-hour NO_2 concentrations by about 17% and one-hour NO_x concentrations by about 57%.

It must be pointed out that the validation carried out thus far is appropriate for locations relatively close to the aircraft that are taking off and for correspondingly short travel times. Confidence in the model predictions necessarily declines as the travel time is increased. Additional

validation studies involving greater distances and travel times are needed to firmly establish the validity of the model at these distances. Additional optimization of the single-plume model and/or independent determinations of plume rise and dispersion should precede any new field program for model validation, however.

6.2 HYDROCARBON-EMISSION COMPOSITION

The technique utilized in this study to investigate the composition of hydrocarbons in the exhaust of jet aircraft consisted of the collection of sets of ambient samples using a resin to adsorb hydrocarbons from air drawn through it and subsequent analysis using gas chromatography/mass spectrometry. Each set consisted of two samples, one taken upwind of and one taken downwind of busy taxiways upon which queues of aircraft often form while awaiting clearance for takeoff. The exhaust composition was inferred by examining the differences between the samples.

A total of four different sets of samples were collected for the purposes of this study, and one sample of commercial jet fuel was also obtained for analysis. Due to experimental difficulties, only one set of samples proved to be suitable for study and only the results of that analysis is discussed in this report.

One unambiguous conclusion that may be drawn from the analysis is that unburned jet fuel constitutes a major portion of the downwind sample that was examined. Although the downwind sampler was positioned to maximize the collection of exhaust gases from queuing aircraft, on that particular day the upwind sampler had to be positioned on the other side of the airport and differences between the two samples cannot be unambiguously attributed to aircraft-exhaust emissions. It is possible that evaporative emissions from fueling or other operations were a significant contributor; even fuel spilled on the wings of the aircraft and evaporating into the air as the aircraft prepared to take off may have contributed. The identification of a significant contribution from unburned fuel seems clear, however, from a comparison of the gas chromatograms from the two ambient samples with that from the sample of jet fuel. Patterns that are distinctive in the fuel show up strongly in the downwind sample but not in the upwind sample, and mass-spectrometric analysis verifies the identity of the constitutents giving rise to corresponding peaks in the vast majority of cases.

Detailed analysis of the jet fuel sample reveals a high percentage of aromatic and unsaturated aliphatic compounds, approximately 50% by weight. Aromatics and unsaturated compounds in general are known to be significant contributors to the production of photochemical smog. The conclusion is that the fuel examined at least has the potential to have a significant impact on smog levels, depending on the overall emission rate at the airport.

Considerably more work needs to be done to draw any firm conclusions about the composition and effects of aircraft hydrocarbon emissions, and the small effort described here can only be regarded as very preliminary. It would be of considerable interest simply to characterize a large number of commercial jet fuels in order to quantify the differences in their compositions. It is also necessary to obtain sets of samples in which aircraft exhaust clearly represents the major cause of any differences between upwind and downwind samples. With regard to the possibility of identifying the aircraft contribution to an ambient sample collected downwind of an airport, more work needs to be done in simply determining chromatographic "signatures" for aircraft exhaust as well as for other common hydrocarbon sources. No clear reason why this identification cannot in principle be made has been uncovered.

6.3 EFFECTS ON PHOTOCHEMICAL SMOG

The basis does not yet exist from which to draw firm quantitative conclusions about the effect of aircraft emissions on the generation of photochemical smog. Modeling studies to date do not incorporate an adequate understanding of the atmospheric chemistry of the heavier hydrocarbons in jet fuel or jet aircraft emissions, nor have they been used to simulate a sufficiently long atmospheric residence time. Many questions regarding how a model should handle multiday situations remain to be answered. Emission summaries provide interesting comparisons of the relative magnitudes of aircraft and other emissions but cannot be used to generate a quantitative measure of their effects. Recent smog-chamber experiments represent a good beginning to the work that needs to be done to achieve an understanding of the chemistry involved, but as yet have not provided all of the needed information.

Additional emission measurements are needed to quantify the emission rates of various types of hydrocarbons, including aldehydes, and to provide additional information on the composition of the hydrocarbon emissions. Further kinetic studies are essential to elucidate the atmospheric chemistry of the hydrocarbons involved. Work should be initiated on the development of a suitable chemical reaction mechanism and on its incorporation into a model in order that preliminary estimates of aircraft effects may be provided and specific areas of uncertainty identified concurrently with the pursuit of more fundamental research goals.

REFERENCES

Abramovich, G.N., (1963), The Theory of Turbulent Jets, The MIT Press, Cambridge, Mass.

Bahe, F.C., U. Schurath, and K.H. Becker, (1980), The Frequency of NO_2 Photolysis at Ground Level as Recorded by a Continuous Actinometer, Atm. Env. 14:711-718.

Bauer, E., (1978), On the Discrete Aspect of Pollution Jets from Aircraft Takeoffs, in Sundararaman (1978), p. 78.

Bilger, R.W., (1978), The Effect of Admixing Fresh Emissions on the Photostationary State Relationship in Photochemical Smog, Atm. Env. 12:1109-1118.

Bowen, B.M., and C.R. Stearns, (1977), On the Depletion of Ambient Ozone by a Rural Coal-Fired Power Plant Near Portage, Wisconsin, paper presented at 4th Joint Conference on Sensing of Environmental Pollutants, New Orleans, La., Nov. 6-11, 1977.

Briggs, G.A., (1969), Plume Rise, Office of Information Services, U.S. Atomic Energy Commission; available as TID-25075 from NTIS, U.S. Dept. of Commerce, Springfield, Va. 22151.

Briggs, G.A., (1975), Plume Rise Predictions, in D.A. Haugen, ed., Lectures on Air Pollution and Environmental Impact Analyses, American Meteorological Society, Boston, Mass., pp. 59-111.

Burch, D.E., R.C. Bean, and F.J. Gates, (1974), NO_2 Actinometer for Field Use, Report No. EPA-650/4-74-036, Office of Research and Development, U.S. Environmental Protection Agency, Washington, D.C. 20460.

Calvert, J.G., (1976), Test of the Theory of Ozone Generation in Los Angeles Atmosphere, Env. Sci. Tech. 10:248-256.

Carter, W.P.L., P.S. Ripley, C.G. Smith, and J.N. Pitts, (1981), Atmopsheric Chemistry of Hydrocarbon Fuels, Report No. ESL-TR-81-53 of the Engineering and Services Laboratory, Air Force Engineering and Services Center, Tyndall AFB, Fla. 32403.

Daley, P.S., and D.F. Naugle, (1978), Measurement and Analysis of Airport Emissions, in Sundararaman (1978), pp. 2-9.

Davis, M.R., and H. Winarto, (1980), Jet Diffusion from a Circular Nozzle Above a Solid Plane, J. Fluid Mech. 101:201-221.

REFERENCE (Cont'd)

Demerjian, K.L., J.A. Kerr, and J.G. Calvert, (1974), The Mechanism of Photochemical Smog Formation, Adv. Env. Sci. Tech. 4:1-262.

Duewer, W.H., and J.J. Walton, (1978), Potential Effects of Commercial Aviation on Region-Wide Air Quality in the San Francisco Bay Area, in Sundararaman (1978), pp. 88-102.

Eastman, J.A., and D.H. Stedman, (1980), Variations in the Ambient Ozone Concentration During the 26 February 1979 Solar Eclipse, Atm. Env. 14:731-732.

Finlayson-Pitts, B.J., and J.N. Pitts, (1977), The Chemical Basis of Air Quality: Kinetics and Mechanisms of Photochemical Air Pollution and Application to Control Strategies, Adv. Env. Sci. Tech. 7:75-162.

Frame, G.B., (1978), Simulation of Airport Air Quality by Box Photochemical and Gaussian Models, J. Air Pollution Control Assoc. 28:155-157.

Gifford, F., (1977), Tropospheric Relative Diffusion Observations, J. Appl. Met. 16:311-313.

Hampson, R.F., (1980), Chemical Kinetic and Photochemical Data Sheets for Atmospheric Reactions, Report No. FAA-EE-80-17, High Altitude Pollution Program, Office of Environment and Energy, Federal Aviation Administration, U.S. Dept. of Transportation, Washington, D.C. 20591.

Harvey, R.B., D.H. Stedman, and W. Chameides, (1977), Determination of the Absolute Rate of Solar Photolysis of NO_2, J. Air Pollution Control Assoc. 27:663-666.

Hegg, D., P.V. Hobbs, and L.F. Radke, (1976), Reactions of Nitrogen Oxides, Ozone and Sulfur in Power Plant Plumes, Electric Power Research Institute Report no. EPRI EA-270, EPRI, 3412 Hillview Ave., Palo Alto, Calif. 94304.

Hegg, D., P.V. Hobbs, L.F. Radke, and H. Harrison, (1977), Reactions of Ozone and Nitrogen Oxides in Power Plant Plumes, Atm. Env. 11:521-526.

Hinze, J.O., (1975), Turbulence, 2nd ed., McGraw-Hill Book Co., New York.

Hudson, R.D., and E.I. Reed, (1979), The Stratosphere: Present and Future, NASA Reference Publication 1049, National Aeronautics and Space Administration.

Jackson, J.O., D.H. Stedman, R.G. Smith, L.H. Hecker, and P.O. Warner, (1975), Direct NO_2 Photolysis Rate Monitor, Rev. Sci. Instr. 46:376-378.

REFERENCE (Cont'd)

Jordan, B.C., and A.J. Broderick, (1978), Emissions of Oxides of Nitrogen from Aircraft, in Sundararaman (1978), pp. 10-19; also J. Air Poll. Control Assoc. 29:119-124 (1979).

of Oxides of Nitrogen and Nitric Acid in Clean Air, J. Geophys. Res. 85:7417-7425.

Kewley, D.J., (1980), The Effect upon the Photostationary State Relationship When Clean Air and Photochemical Smog Mix, Atm. Env. 14:1445-1448.

Lamb, R.G., and J.H. Seinfeld, (1973), Mathematical Modeling of Urban Air Pollution - General Theory, Env. Sci. Tech. 7:253-261.

Leighton, P.A., (1961), Photochemistry of Air Pollution, Academic Press, New York.

Linz, P., (1972), Algorithm 427; Fourier Cosine Integral [D1], Comm. ACM 15:358-360.

Naugle, D.F., and D.L. Fox, (1981), Aircraft and Air Pollution, Env. Sci. Tech. 15:391-395.

O'Brien, R.J., (1974), Photostationary State in Photochemical Smog Studies, Env. Sci. Tech. 8:579-583.

Pace, R.G., (1977), Aircraft Emissions Factors, U.S. Environmental Protection Agency Technical Support Report.

Patten, C.W., (1978), FAA Airport Emissions Data Base -- Development and Application, in Sundararaman (1978), pp. 205-212.

Peters, L.K., and L.W. Richards, (1977), Extension of Atmospheric Dispersion Models to Incorporate Fast Reversible Reactions, Atm. Env. 11:101-108.

Pratt and Whitney, (1972), Collection and Assessment of Aircraft Emissions Baseline Data - Turbine Engines, Report No. P&WA 4339, Pratt and Whitney Aircraft Group, East Hartford, Conn.

Ritter, J.A., D.H. Stedman, and T.J. Kelly, (1979), Ground-level Measurements of Nitric Oxide, Nitrogen Dioxide and Ozone in Rural Air, Chapter 20 in D. Grosjean (ed.), Nitrogenous Air Pollutants - Chemical and Biological Implications, Ann Arbor Science Pub., Inc., Ann Arbor, Mich..

REFERENCE (Cont'd)

Sandys, R.C., (1978), Modeling Mobile Ground-Source Emissions at Air Bases and Airports, in Sundararaman (1978), pp. 45-49.

Segal, H.M., (1981), Aircraft Pollution in the Vicinity of Airports, paper presented at the American Institute of Aeronautics and Astronautics 19th Aerospace Science Meeting, St. Louis, Mo., Jan. 12-15, 1981.

Seinfeld, J.H., (1977), correspondence, Env. Sci. Tech. 11:1218-1219.

Shelar, E., (1978), Air Quality Characteristics at Dulles International Airport for 1976, 1980, 1985, and 1995, in Sundararaman (1978), pp. 165-169.

Spicer, C.W., G.M. Sverdrup and M.R. Kuhlman, (1981), Smog Chamber Studies of NO_x Chemistry in Power Plant Plumes, Atm. Env. 15:2353-2365.

Stedman, D.H., and J.O. Jackson, (1975), The Photostationary State in Photochemical Smog, Int. J. Chem. Kinetics Symposium No. 1; Proceedings of the Symposium on Chemical Kinetics Data for the Lower and Upper Atmosphere, Benson, S.W., D.M. Golden, and J.R. Barker, eds., John Wiley and Sons, New York.

Stedman, D.H., W. Chameides, and J.O. Jackson, (1975), Comparison of Experimental and Computed Values for $j(NO_2)$, Geophys. Res. Lett. 2:22-24.

Sundararaman, N., (ed.), (1978) Proceedings of Air Quality and Aviation: an International Conference, Report No. FAA-EE-78-26, Office of Environment and Energy, Federal Aviation Administration, U.S. Dept. of Transportation, Washington, D.C. 20591.

Sverdrup, G.M., C.W. Spicer and M.R. Kuhlman, (1982), Nitrogen Oxide Transformations in Power Plant Plumes, Electric Power Research Institute Report No. EPRI EA-2217, 3412 Hillview Ave., Palo Alto, Calif. 94304.

Swan, P.R., and I.Y. Lee, (1980), Meteorological and Air Pollution Modeling for an Urban Airport, J. Appl. Met. 19:534-544.

Tank, W.G., and B.K. Hodder, (1978), Engine Exhaust Plume Growth in the Airport Environment, in Sundararaman (1978), pp. 153-164.

Tennekes, H., and J.L. Lumley, (1972), A First Course in Turbulence, The MIT Press, Cambridge, Mass.

Thuillier, R.H., and W. Vieze, (1978), Air Quality Analysis in Support of a Short-Term Ambient Air Quality Standard for Nitrogen Dioxide, Final report to U.S. Environmental Protection Agency under contract EPA 68-62-2835 with SRI

REFERENCE (Cont'd)

International, Menlo Park, Calif. Cited in J.R. Martinez and K.C. Nitz, Analysis of High NO_2 Concentrations in California, 1975-1977, Report No. EPA-A50/4-79-034a, U.S. Environmental Protection Agency, Research Triangle Park, N.C.. 27711, Aug. 1979.

USEPA, (1978a), Air Quality Criteria for Ozone and Other Photochemical Oxidants, Report No. EPA-600/8-78-004, U.S. Environmental Protection Agency, Washington, D.C. 20460.

USEPA, (1978b), Workbook for Comparison of Air Quality Models, Report No. EPA-450/2-78-028a, b, U.S. Environmental Protection Agency, Research Triangle Park, N.C. 27711.

Wang, I.T., D.M. Rote, and L.A. Conley, (1974), Airport Vicinity Air Pollution Study - Model Application and Validation and Air Quality Impact Analysis at Washington National Airport, Report No. FAA-RD-7A-132, Federal Aviation Administration, U.S. Dept. of Transportation, Washington, D.C. 20590.

Wang, I.T., L.A. Conley, and D.M. Rote, (1975), Airport Vicinity Air Pollution Model User Guide, Report No. FAA-RD-T5-230, Federal Aviation Administration, U.S. Dept. of Transportation, Washington, D.C. 20590.

White, W.H., (1977), NO_x-O_3 Photochemistry in Power Plant Plumes: Comparison of Theory with Observation, Env. Sci. Tech. 11:995-1000.

World Health Organization, (1977), Environmental Health Criteria 4: Oxides of Nitrogen, Geneva, Switzerland.

Yamartino, R.J., D.G. Smith, S.A. Bremer, D. Heinhold, D. Lamich, and B. Taylor, (1980a,b), Impact of Aircraft Emissions on Air Quality in the Vicinity of Airports, Vols. I and II, Report Nos. FAA-EE-80-09A, B, Office of Environment and Energy, Federal Aviation Administration, U.S. Dept. of Transportation, Washington, D.C. 20591.

Zafonte, L., P.L. Rieger, and J.R. Holmes, (1977), Nitrogen Dioxide Photolysis in the Los Angeles Atmosphere, Env. Sci. Tech. 11:483:487.

APPENDIX 1

$NO-NO_2-O_3$ CHEMICAL DYNAMICS IN HOMOGENEOUS MIXTURES

It is possible to describe exactly the evolution of a spatially homogeneous system containing a mixture of NO, NO_2, and O_3 in air under the assumption that the only chemical reactions that take place are

$$NO_2 + O_2 \xrightarrow{h\nu} NO + O_3 \qquad (A)$$

and

$$NO + O_3 \longrightarrow NO_2 + O_2 \qquad (B)$$

The purpose of this appendix is to derive the relevant mathematical expressions and to examine certain limiting cases, among them the approach to a photostationary state.

For notational convenience, denote the concentrations (number densities) of NO_2 by x, of NO by y and of O_3 by z, and denote their respective initial values by subscript o's. Denote the difference $x - x_o$ by ξ; then the stoichiometry of reactions A and B implies that $y_o - y = \xi = z_o - z$, and that $\xi = 0$ at time $t = 0$. These relations imply that at any time $t \geq 0$, x, y and z are given by:

$$x(t) = x_o + \xi(t) \qquad (A1.1a)$$

$$y(t) = y_o - \xi(t) \qquad (A1.1b)$$

$$z(t) = z_o - \xi(t) \qquad (A1.1c)$$

Assuming that reactions A and B are the only reactions that apply, the total rate of change of the NO_2 concentration is

$$\frac{dx}{dt} = -k_A x + k_B yz \qquad (A1.2)$$

where k_A and k_B are the rate coefficients for reactions A and B. Substituting in Eq. A1.2 for x, y, and z yields a differential equation for ξ:

$$\frac{d\xi}{dt} = a - \beta\xi + k_B\xi^2 \qquad (A1.3)$$

in which:

$$a = -k_A x_o + k_B y_o z_o \tag{A1.4a}$$

and

$$\beta = k_A + k_B(y_o + z_o) \tag{A1.4b}$$

Clearly, $\beta \geq 0$ and a can have either sign or be zero. Equation A1.3 may be integrated to give $\xi(t)$ in terms of the rate coefficients and initial concentrations; substitution into Eqs. A1.1a-c) then gives each concentration as a function of time. The result of integrating Eq. A1.3 is:

$$\xi(t) = \left(\frac{\beta - \lambda}{2k_B}\right) \frac{[1 - \exp(-\lambda t)]}{\left[1 - \left(\frac{\beta - \lambda}{\beta + \lambda}\right)\exp(-\lambda t)\right]} \tag{A1.5}$$

in which:

$$\lambda = (\beta^2 - 4ak_B)^{1/2} \tag{A1.6}$$

It can be shown that λ is always greater than or equal to zero. For some purposes, it is convenient to have an alternate expression, obtained by substitution:

$$\mu = \lambda/\beta \text{ and } \sigma = \beta t \tag{A1.7}$$

$$\xi(t) = \left(\frac{\beta}{2k_B}\right)(1-\mu) \frac{[1 - \exp(-\mu\sigma)]}{\left[1 - \left(\frac{1 - \mu}{1 + \mu}\right) \exp(-\mu\sigma)\right]} \tag{A1.8}$$

The expression for $\xi(t)$, Eq. A1.5 or Eq. A1.8, provides the complete solution to the problem under the assumptions given above and the tacit assumption that k_A and k_B are not time-dependent. Several limiting cases are of special interest, however.

The value of the parameter μ characterizes the initial conditions, and certain values are of particular interest. For example, the value $\mu = 1$ results in $\xi(t)$ being zero for all t. Physically, this corresponds to a system already in a stationary state at the beginning, so that no change is observed in the various concentrations. This interpretation is most easily seen from an alternate expression for μ:

$$\mu = \left[1 - \left(\frac{2k_B}{\beta}\right)^2 \left(y_o z_o - K x_o\right)\right]^{1/2} \tag{A1.9}$$

in which K denotes the ratio k_A/k_B. If the initial rate of NO_2 loss due to photolysis ($k_A x_o$) exactly balances the initial rate of NO_2 production due to

reaction B ($k_B y_o z_o$), the initial state is already stationary and no change occurs. Clearly, if these two expressions are equal, $\mu = 1$ from Eq. A1.9.

From the definition and properties of λ and β, it is seen that $\mu \geq 0$. As Eq. A1.9 indicates, values less than unity correspond to initial situations that are deficient in NO_2 ($Kx_o < y_o z_o$), and values greater than unity correspond to initial situations in which there is excess NO_2 ($Kx_o > y_o z_o$). The limiting case $\mu = 0$ is somewhat pathological in that both numerator and denominator in Eq. A1.8 approach zero. Accordingly, care must be taken in evaluating the limit, but when this is done the expression for $\xi(t)$ becomes:

$$\xi(t) = \left(\frac{\beta}{2k_B}\right)\left(\frac{1}{1 + 2/\sigma}\right) \qquad (\mu = 0) \tag{A1.10}$$

Physically, this corresponds to the initial situation in which $y_o = z_o$ (equal initial concentrations of NO and O_3) and in which $k_A = 0$ (zero ambient light intensity, and therefore no NO_2 photolysis). This is most easily seen by observing that these are the only conditions under which λ, and therefore μ, can be zero. A special case of this situation is that in which both y_o and z_o are zero, in which case $\beta = 0$ also and $\xi(t) = 0$ for all t. This corresponds to the initial presence of NO_2 only, and in the absence of light, the system remains unchanged.

The other limiting case of special interest is that in which t approaches infinity. The limiting value, denoted by ξ_{ss} in anticipation of its identification as a steady state value, is given by:

$$\xi_{ss} = \left(\frac{\beta}{2k_B}\right)(1 - \mu) \tag{A1.11}$$

for all possible values of β and μ. Substitution of this value into Eq. A1.3, followed by a small amount of algebraic manipulation, shows that for $\xi = \xi_{ss}$, $d\xi/dt = 0$ and no substantial change occurs, i.e., a stationary state exists in which the production and loss rates of all substances are zero and in which the concentrations are related by:

$$\frac{yz}{x} = \frac{[NO][O_3]}{[NO_2]} = K \tag{A1.12}$$

as can be seen from Eq. A1.2.

The rate at which the system approaches a stationary state is of considerable practical interest. It can be shown from Eq. A1.8 that after a sufficiently long time [with $\xi(\infty) = \lim\xi(t) = \xi_{ss}$]:

$$\frac{\xi(\infty) - \xi(t)}{\xi(\infty)} \longrightarrow A(\mu)\, e^{-\lambda t} \qquad (\mu > 0) \tag{A1.13a}$$

where $A(\mu)$ is a coefficient dependent on μ, and

$$\frac{\xi(\infty) - \xi(t)}{\xi(\infty)} \longrightarrow 1 + \frac{1}{2}\beta t^{-1} \qquad (\mu = 0) \tag{A1.13b}$$

Thus, for $\mu > 0$ the stationary state is eventually approached exponentially with a time constant (relaxation time) of $\tau = \lambda^{-1}$. For $\mu = 0$, a time constant or relaxation time in the usual sense cannot be defined, since the approach to stationary state is never exponential. Equation A1.6 provides an expression for τ^{-1} in terms of the initial conditions. Alternate expressions for λ or τ^{-1} are:

$$\lambda = \tau^{-1} = \beta - 2k_B\xi_{ss} \tag{A1.14a}$$

and

$$\lambda = \tau^{-1} = k_A + k_B(y_{ss} + z_{ss}) \tag{A1.14b}$$

Expression A1.14b is the one cited in Sec. 3.1.3 of this report. A plot of τ versus $(y_{ss} + z_{ss})$ was given in Fig. 3.4.

APPENDIX 2

DIFFERENT METHODS OF AVERAGING AND COMPUTING VARIANCES OF WIND VELOCITY VECTORS

Given a horizontal wind velocity vector $\vec{V}$, denote the (standard meteorological convention) wind direction angle by θ and the wind speed by V, the magnitude of $\vec{V}$. Define a coordinate system in which the positive x-axis is directed towards the east and the positive y-axis towards the north. Then the components of $\vec{V}$ are given by:

$$V_x = - V \sin \theta \tag{A2.1}$$

$$V_y = - V \cos \theta \tag{A2.2}$$

Assume that a sequence of values of θ and V has been measured, θ_i, V_i for i=1 to N, and that it is desired to compute a mean and variance about the mean. At least two different procedures may be employed. The first and simplest is to compute the scalar mean wind speed and direction by averaging the speeds and directions independently of each other; denoting these scalar averages by $\overline{V}$ and $\overline{\theta}$, we have for $\overline{V}$ the equation:

$$\overline{V} = \frac{1}{N} \sum_{i=1}^{N} V_i \tag{A2.3}$$

The mean wind direction is obtained by averaging the x and y components of a unit vector in the direction θ_i and by obtaining $\overline{\theta}$ from the average components. Denoting the average x- and y-components by $\overline{u}_x$ and $\overline{u}_y$, we have:

$$\overline{u}_x = \frac{1}{N} \sum_{i} (-\sin\theta_i) \tag{A2.4}$$

$$\overline{u}_y = \frac{1}{N} \sum_{i} (-\cos\theta_u) \tag{A2.5}$$

$$\overline{\theta} = \tan^{-1}(\overline{u}_x/\overline{u}_y). \tag{A2.6}$$

The corresponding variances are obtained in the usual way:

$$\sigma_V^2 = \frac{1}{N} \sum_{i} (V_i - \overline{V})^2 \tag{A2.7}$$

$$\sigma_\theta^2 = \frac{1}{N} \sum_{i} (\theta_i - \overline{\theta})^2 \tag{A2.8}$$

where $\theta_i - \bar{\theta}$ must be adjusted, by addition or subtraction of 360°, so that it lies in the range from -180° to +180°.

The second procedure is far more suitable for use in the analysis of air-pollutant transport and dispersion because it takes proper account of the vectorial nature of the wind velocity. The average velocity vector $\langle\vec{V}\rangle$ is defined by:

$$\langle\vec{V}\rangle = \frac{1}{N} \sum_i \vec{V}_i \tag{A2.9}$$

so that the corresponding x- and y-components may be computed from the measurements as follows:

$$\langle\vec{V}\rangle_x = \frac{1}{N} \sum_i (-V_i \sin\theta_i) \tag{A2.10}$$

$$\langle\vec{V}\rangle_y = \frac{1}{N} \sum_i (-V_i \cos\theta_i) \tag{A2.11}$$

The vector mean wind speed $\bar{V}_{vec}$ is by *definition* the *magnitude* of $\langle\vec{V}\rangle$, and is given by:

$$\bar{V}_{vec} = \left[\langle\vec{V}\rangle_x^2 + \langle\vec{V}\rangle_y^2\right]^{1/2} \tag{A2.12}$$

The vector mean wind direction $\bar{\theta}_{vec}$ is by definition the direction of $\langle\vec{V}\rangle$, and is given by:

$$\bar{\theta} = \tan^{-1}\left[\langle\vec{V}\rangle_x \,/\, \langle\vec{V}\rangle_y\right] \tag{A2.13}$$

The concept of variance in the case of a vector quantity is similar to that in the scalar case except that the square of the difference between an individual value and the mean is replaced by the scalar (dot) product with itself of the difference between an individual vector and the mean vector. The vector difference is given by:

$$\Delta\vec{V}_i = \vec{V}_i - \langle\vec{V}\rangle \tag{A2.14}$$

and the total variance σ_T^2 may be computed from:

$$\sigma_T^2 = \frac{1}{N} \sum_i \Delta\vec{V}_i \cdot \Delta\vec{V}_i$$

$$= \frac{1}{N} \sum_i |\Delta V_i|^2$$

$$= \frac{1}{N} \sum_i \left[\left(V_{ix} - \langle \hat{V} \rangle_x \right)^2 + \left(V_{iy} - \langle \hat{V} \rangle_y \right)^2 \right] \tag{A2.15}$$

It is useful to resolve σ_T^2 into components associated with variations in velocity parallel and perpendicular to the mean velocity. Figure A2.1 illustrates the situation. In that figure, $(\Delta V_i)_\parallel$ and $(\Delta V_i)_\parallel$ denote components of $\Delta \hat{V}_i$ parallel and perpendicular to $\langle \hat{V} \rangle$, respectively, and $\hat{\imath}_\parallel$ and $\hat{\imath}_\perp$ denote unit vectors parallel and perpendicular to $\langle \hat{V} \rangle$ so that $\hat{\imath}_\parallel$, $\hat{\imath}_\perp$ and $\hat{k}$ (a unit vector in the vertical direction) together comprise a right-handed Cartesian coordinate system. The parallel and perpendicular components are given by:

$$(\Delta V_i)_\parallel = |\Delta \hat{V}_i| \cos\phi \tag{A2.16}$$

$$(\Delta V_i)_\perp = |\Delta \hat{V}_i| \sin\phi \tag{A2.17}$$

The perpendicular component is also given by the alternate expression

$$(\Delta V_i)_\perp = V_i \sin(\theta_i - \bar{\theta}_{vec}) \tag{A2.18}$$

$$= (V_i \sin\theta_i)\cos\bar{\theta}_{vec} - (V_i \cos\theta_i)\sin\bar{\theta}_{vec} \tag{A2.19}$$

The total variance may be written:

$$\sigma_T^2 = \frac{1}{N} \sum_i (\Delta V_i)_\parallel^2 + \frac{1}{N} \sum_i (\Delta V_i)_\perp^2$$

$$= \sigma_\parallel^2 + \sigma_\perp^2 \tag{A2.20}$$

since $\hat{\imath}_\parallel$ and $\hat{\imath}_\perp$ are perpendicular. Expansion of $(\Delta V_i)_\perp^2$ using Eq. A2.19 and substitution into the definition of $\sigma_\perp^2$ yields:

$$\sigma_\perp^2 = \cos^2\bar{\theta}_{vec} \cdot \frac{1}{N} \sum_i (V_i \sin\theta_i)^2$$

$$- 2\cos\bar{\theta}_{vec} \cdot \frac{1}{N} \sum_i (V_i^2 \sin\theta_i \cos\theta_i)$$

$$+ \sin^2\bar{\theta}_{vec} \cdot \frac{1}{N} \sum_i (V_i \cos\theta_i)^2 \tag{A2.21}$$

The total variance may also be written, from Eq. A2.15:

$$\sigma_T^2 = \frac{1}{N} \sum_i (V_{ix}^2 + V_{iy}^2) - (\langle \hat{V} \rangle_x^2 + \langle \hat{V} \rangle_y^2)$$

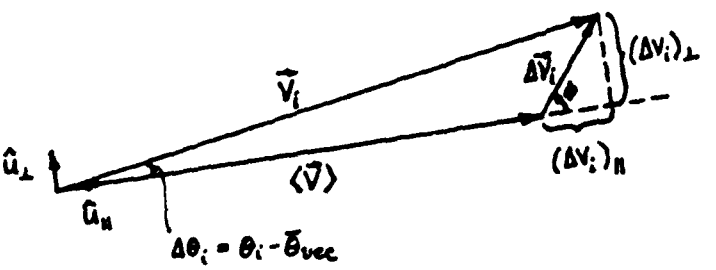

Fig. A2.1 Vectors Used in the Computation of Variances

or

$$\sigma_T^2 = \frac{1}{n} \sum_i v_i^2 - \vec{v}_{vec}^2 \qquad \text{(A2.22)}$$

Consequently, by evaluating in one pass through the data the sums of the quantities v_i^2, $V_i\cos\theta_i$, $V_i\sin\theta_i$, $(V_i\cos\theta_i)^2$, $(V_i\sin\theta_i)^2$, and $V_i^2\sin\theta_i\cos\theta_i$, the vector mean speed and direction as well as σ_1^2 and σ_2^2 σ_T^2 may be evaluated, and σ_1^2 may be obtained as the difference between σ_T^2 and σ_1^2.

APPENDIX 3

INSTRUMENT RESPONSE EFFECTS

If variations in the value of some measured quantity occur over time intervals shorter than or comparable to the response time of the instrumentation used in the measurements, the output of that instrumentation will not faithfully reproduce the input. For some purposes, it is necessary to understand under what conditions such effects can become important and to know how to make the appropriate corrections. This appendix contains a brief introductory discussion of some of the simpler aspects of this issue; for more detailed information, the references given at the end of the appendix, or other texts dealing with communication theory, may be consulted. Kanasewich (1975) discusses the subject from the particular point of view of its application to geophysical measurements.

Denote the input signal to a measurement device by x(t) and the output (the response of the device to the input signal) by y(t). Then, if the response is linear, y(t) is, in general, given by:

$$y(t) = \int_0^\infty w(t')\, x(t - t')dt' \tag{A3.1}$$

in which w(t) denotes the instrument response function and is simply the instrument response to a unit impulse (Dirac delta function) input. The response function may be found in principle if the response to a unit step input is known; a unit step input is defined by:

$$x_{us}(t) = \begin{cases} 0 \text{ for } t < 0 \\ 1 \text{ for } t > 0 \end{cases} \tag{A3.2}$$

For example, if the response to a unit step is known to be exponential:

$$y_{us}(t) = 1 - \exp(-t/\tau) \tag{A3.3}$$

then:

$$1 - \exp(-t/\tau) = \int_0^\infty w(t')x_{us}(t - t')\, dt'$$

Differentiating both sides with respect to t and using the fact that $d[x_{us}(t - t')]/dt = \delta(t - t')$ results in:

$$\frac{1}{\tau}\exp(-t/\tau) = \frac{1}{\tau}\int_0^\infty w(t')\ \delta(t - t')dt' = w(t) \qquad \text{(A3.4)}$$

using the properties of $\delta(t - t')$ and assuming that $t > 0$.

Due to causality, we must require $w(t) = 0$ for $t < 0$; i.e. the effect cannot precede the cause. Thus, the response function for such an instrument is:

$$w(t) = \begin{cases} \frac{1}{\tau}\exp(-t/\tau) & t > 0 \\ 0 & t < 0 \end{cases} \qquad \text{(A3.5)}$$

Throughout the rest of this brief discussion, it will be assumed that the response of any device under consideration is exponential.

The total, time-integrated signal is often of interest also, and it is desirable to require the time-integrated output to equal the time-integrated input, even if the individual values are not equal:

$$\int_{-\infty}^{\infty} y(t)dt = \int_{-\infty}^{\infty} x(t)dt \qquad \text{(A3.6)}$$

Integration of Eq. A3.1 shows that in order to satisfy this relation, we must require that the response function is normalized so that its integral is unity:

$$\int_0^\infty w(t)dt = 1 \qquad \text{(A3.7)}$$

This requirement is satisfied by the form given in Eq. A3.5.

Using Eqs. A3.1 and A3.5, the instrument response to a variety of special input signals can be calculated.

1. Gaussian pulse.

$$x(t) = \frac{1}{\sqrt{2\pi}\sigma}\exp\left[-\frac{1}{2}\left(\frac{t - t_o}{\sigma}\right)^2\right] \qquad \text{(A3.8)}$$

$$y(t) = \frac{1}{2\tau}\left[\exp\frac{1}{2}\left(\frac{\sigma}{\tau}\right)^2 - \frac{t - t_o}{\tau}\right]\operatorname{erfc}\left[\frac{\sigma}{\sqrt{2}\tau} - \frac{t - t_o}{\sqrt{2}\sigma}\right] \qquad \text{(A3.9)}$$

with the error function erf(z) and complementary error function erfc(z) defined by:

$$\text{erfc}(z) = 1 - \text{erf}(z)$$

$$\text{erf}(z) = \frac{2}{\sqrt{\pi}} \int_0^z \exp(-t^2)dt$$

Denote $\zeta = \frac{t - t_o}{\sqrt{2}\sigma}$, $\alpha = \frac{\sigma}{\sqrt{2}\tau}$, and $Y(\zeta) = \sqrt{2\pi}\sigma y(t)$; then:

$$Y(\zeta) = \sqrt{\pi}\alpha\exp[(\alpha - \zeta)^2 - \zeta^2]\text{erfc}[\alpha - \zeta] \qquad \text{(A3.10)}$$

Figure A3.1 shows a plot of $Y(\zeta)$ versus ζ for various values of α. As the figure shows, visible distortion of the input signal (which is the same as the output signal for the limiting value $\alpha = \infty$) begins to occur for α about equal to five, or for signals with standard deviations σ about equal to $5\sqrt{2}\tau$, or 7.07τ. For narrower signals, the distortion becomes more pronounced. As implied above, the distortion is in principle unimportant if a time-averaged signal is the significant quantity, rather than the details of the shape of the pulse, since Eq. A3.6 is satisfied (assuming the interval of integration is much larger than σ).

2. Diffuse unit step increase.

$$x(t) = \frac{1}{2}\left[1 + \text{erf}\left(\frac{t - t_o}{\sqrt{2}\sigma}\right)\right] = \frac{1}{2}\left[1 + \text{erf}(\zeta)\right] \qquad \text{(A3.11)}$$

Note that in the limit as σ approaches zero, $x(t)$ as given in Eq. A3.11 approaches the unit step input $x_{us}(t - t_o)$; the quantity σ parameterizes the "diffuseness" of the step.

$$y(t) = \frac{1}{2}\left[1 + \text{erf}(\zeta) - \frac{1}{\sqrt{\pi}\alpha} Y(\zeta)\right] \qquad \text{(A3.12)}$$

where $Y(\zeta)$ is the function introduced in the previous example, and $\alpha = \sigma/\sqrt{2}\tau$ as before.

3. Diffuse unit step decrease.

$x(t) = 1 -$ (case 2 input)

or

$$x(t) = \frac{1}{2}\left[1 - \text{erf}(\zeta)\right] \qquad \text{(A3.13)}$$

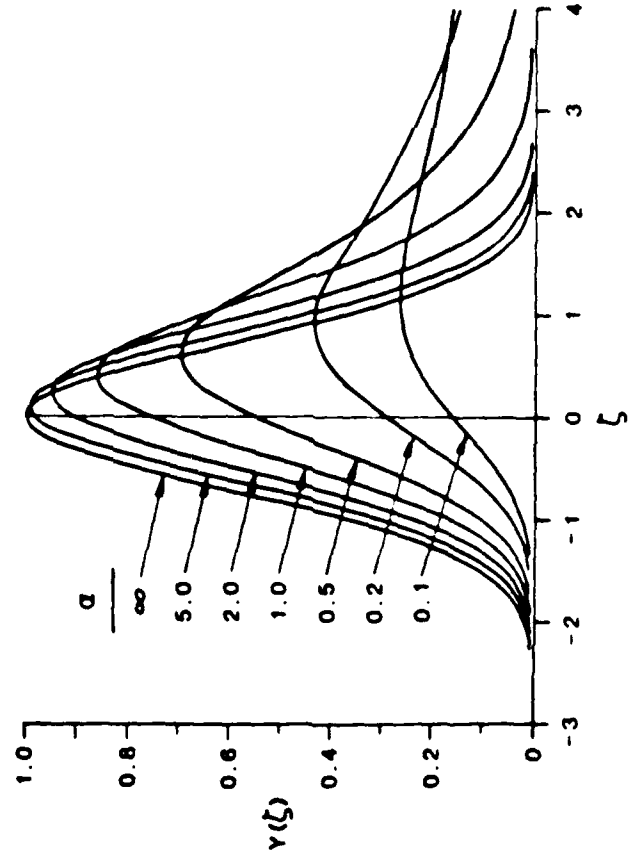

Fig. A3.1 Instrument Response to a Gaussian Pulse Input

Then $y(t) = 1 - (\text{case 2 output})$

or

$$y(t) = \frac{1}{2}\left[1 - \text{erf}(\zeta) + \frac{1}{\sqrt{\pi}\alpha}\, Y(\zeta)\right] \tag{A3.14}$$

The expressions given in Eqs. A3.12 and A3.14, multiplied by scale factors y_∞ and $y_{-\infty}$ and augmented by a baseline value y_o, were used in the analysis of the instrument response experiments described in Sec. 2.1.2 (see Eqs. 2.4 and 2.5 in that section).

It is desirable to have a method for correcting measured data for instrument response effects when such effects are significant. We will be concerned only with the usual case in which discrete measurements made at uniform time intervals are available and are to be corrected. Denote the times at which measurements were made by t_i, the time interval by δt, and the corresponding data values by y_i. In general, y_i is given by:

$$y_i = \int_{-\infty}^{\infty} w(t')\, x(t_i - t')dt' \tag{A3.15}$$

where the lower integration limit has been extended to $-\infty$, a valid manipulation since $w(t) = 0$ for $t < 0$. An important point is that the values of $x(t)$ for <u>all</u> times earlier than t_i contribute to y_i. However, the usual formalism associated with the analysis of time sequences deals with expressions for y_i of the form:

$$y_i = \sum_k w_k x_{i-k} \tag{A3.16}$$

which refers to input signal values at discrete instants of time. Equation A3.15 may be put into a form that resembles Eq. A3.16 by breaking the integration interval up into segments of length δt centered on the points t_i, which are given by:

$$t_i = t_o + i\delta t \tag{A3.17}$$

After some manipulation, the expression for y_i given by Eq. A3.15 becomes:

$$y_i = \delta t \sum_k w(k\delta t)\tilde{x}_{i-k} \tag{A3.18}$$

where $\tilde{x}_{i-k}$ is defined by:

$$\tilde{x}_{i-k} = \frac{1}{2}\int_{-1}^{+1}\left[\frac{w(k\delta t + \zeta\delta t/2)}{w(k\delta t)}\right]\left(t_{i-k} - \zeta\frac{\delta t}{2}\right)d\zeta \qquad \text{(A3.19)}$$

and represents a weighted average of x(t) in the interval centered on t_{i-k}. For an exponential response (and only an exponential response), the quantity in square brackets in Eq. A3.19 is independent of the index k, and x_{i-k} is in fact a well-defined average value very nearly equal to the arithmetic average for small values of $\delta t/\tau$. Assuming an exponential response, y_i is given by:

$$y_i = \sum_k w_k \tilde{x}_{i-k} \qquad \text{(A3.20)}$$

with

$$w_k = \left(\frac{\delta t}{\tau}\right)\exp\left(-k\frac{\delta t}{\tau}\right) \qquad \text{(A3.21)}$$

and

$$\tilde{x}_{i-k} = \frac{1}{2}\int_{-1}^{+1}\exp\left(-\frac{1}{2}\frac{\delta t}{\tau}\zeta\right)\left(t_{i-k} - \zeta\frac{\delta t}{2}\right)d\zeta \qquad \text{(A3.22)}$$

If x(t) is constant in the interval around t_{i-k}, then it is easy to show that $\tilde{x}_{i-k}$ differs from that constant value by a factor depending only on the value of the ratio $\delta t/\tau$:

$$\frac{\tilde{x}_{i-k}}{x_{i-k}} = \frac{2\tau}{\delta t}\sinh\left(\frac{\delta t}{2\tau}\right) \qquad \text{(A3.23)}$$

The value of the right-hand side is 1.000 exactly for $\delta t/\tau = 0$, 1.010 for $\delta t/\tau = 0.5$, 1.042 for $\delta t/\tau = 1.0$ and 1.175 for $\delta t/\tau = 2.0$.

The above discussion shows that one can obtain only average values of x(t) over the sampling interval δt. Given the measurements y_i and knowledge of the response function, it is possible to determine the values $\tilde{x}_{i-k}$ by inverting Eq. A3.20. Reference should be made to Kanasewich (1975) or an equivalent text for a discussion of the various procedures available to carry out this task. One in effect writes $\tilde{x}_k$ as a linear combination of the y_i and determines the coefficients in such a way as to either satisfy Eq. A3.20 exactly or to minimize the error involved. In the case of exponential response, the result is actually very simple compared to that for any other realistic response function, and is given by:

$$\tilde{x}_k = \left(\frac{\tau}{\delta t}\right)[y_k - y_{k-1}\exp(-\delta t/\tau)] \qquad \text{(A3.24)}$$

Equation A3.24 was used to correct the digitized data from the O'Hare study for instrument response effects using the response times given in Table 2.2, Sec. 2.1.2, and the sampling interval of (very nearly) one second.

APPENDIX 3 REFERENCES

Blackman, R.B., and J.W. Tukey, (1958), The Measurement of Power Spectra, Dover Publications, Inc., New York.

Kanasewich, E.R., (1975), Time Sequence Analysis in Geophysics, The University of Alberta Press, Edmonton, Alberta, Canada.

Nahi, N.E., (1969), Estimation Theory and Applications, John Wiley and Sons, New York.

U.S. GOVERNMENT PRINTING OFFICE 1984 0-461-016/10094


DAT
FILM